Division of Engineering Mechanics

STANFORD UNIVERSITY

Technical Report No. 178

VISCOUS, HYPERSONIC FLOW AROUND A BLUNT BODY

By

J. E. Kaiser and I. Flügge-Lotz

January 1968

Research sponsored by the
Air Force Office of Scientific Research
Office of Aerospace Research under
AFOSR Contract No. 49 AF(638)1385

DIVISION OF ENGINEERING MECHANICS

STANFORD UNIVERSITY, STANFORD CALIFORNIA

Division of Engineering Mechanics

STANFORD UNIVERSITY

Technical Report No. 178

VISCOUS, HYPERSONIC FLOW AROUND A BLUNT BODY

By

J. E. Kaiser and I. Flügge-Lotz

January 1968

Research sponsored by the
Air Force Office of Scientific Research
Office of Aerospace Research under
AFOSR Contract No. 49 AF(638)1385

TABLE OF CONTENTS

LIST OF ILLUSTRATIONS

LIST OF ILLUSTRATIONS (continued)

LIST OF ILLUSTRATIONS (continued)

NOMENCLATURE

a	Dimensionless nose radius, $\frac{a^*}{a^*} = 1$
a_1	Slip constant defined by equation (2.10)
A, B, C, D	Matrix coefficients of the difference equation (4.4)
$A1_N$, $B1_N$, $C1_N$, $D1_N$, $E1_N$, $F1_N$, $G1_N$	Coefficients of the difference equation (4.3a), defined in Appendix A
$A2_N$, $B2_N$, $C2_N$, $D2_N$, $E2_N$, $F2_N$, $G2_N$	Coefficients of the difference equation (4.3b), defined in Appendix A
A_I, B_I, C_I	Coefficients in equation (4.14b) and defined in Appendix B
A_v, B_v, D_v, A_p, B_p, D_p	Coefficients in equations (4.20a) and (4.20b)
b	Ratio of the body temperature to the inviscid stagnation temperature, $T_b/T_{stag.}$
b_o, b_2, ...	Coefficients of an expansion of b, equation (3.22)
c	Dimensionless speed of sound, normalized with respect to U^*_∞
c_1	Temperature-jump constant defined by equation (2.11)
C^*_p	Specific heat at constant pressure
f	Vector function defined in equation (3.16)
$f_1, f_2, \ldots, f_{13}$	Components of f, defined by equations (3.17), (3.20), and (3.21)
F, G	Typical variables in the shock layer
h	Weighting factor used in equation (4.16)
i	Number of components of the column vector w

NOMENCLATURE (continued)

I	An integral defined by equation (4.14a)
j	An integer that equals 0 for plane flow and 1 for axisymmetric flow
m	Designation of mesh points at $s = m\Delta s$; see figure 4.1
M_∞	Free-stream Mach number
n	Dimensionless coordinate normal to the body surface, $\frac{n^*}{\epsilon a^*}$
N	Designation of mesh points at $n = N\Delta n$; see figure 4.1
N_s	Designation of the mesh point immediately inside the shock; see equation (4.9)
p	Dimensionless pressure, $\frac{p}{\rho_\infty^* U_\infty^{*2}}$
$p_0, p_2, p_4, \cdots$	Coefficients of an expansion of p, equation (3.1c)
q	Dimensionless heat-transfer rate, $\frac{q^*}{\rho_\infty^* U_\infty^{*3}}$, defined by equation (2.23)
$q_0, q_2, \cdots$	Coefficients of an expansion of q, equations (3.15)
r	Dimensionless distance of the body surface from the axis of symmetry, $\frac{r^*}{a^*}$, figure 2.1
R	In Appendix B only, a function equal to $2^{j-1}\Delta n\rho\,(r + \epsilon n \sin\theta)^j$
Re_s	Shock Reynolds number, $\frac{\rho_\infty^* U_\infty^* a^*}{\mu_{sh}^*}$

NOMENCLATURE (continued)

s	Dimensionless coordinate along the body surface, $\frac{s^*}{a^*}$
T	Dimensionless temperature, $\frac{T^*}{U_\infty^{*2}/C_p^*}$.
$T_0, T_2, \cdots$	Coefficients of an expansion of T, equation (3.1d)
u	Dimensionless velocity component in the s-direction, $\frac{u^*}{U_\infty^*}$
$u_1, u_3, \cdots$	Coefficients of an expansion of u, equation (3.1a)
U_∞^*	Free-stream velocity
v	Dimensionless velocity component in the n-direction, $\frac{v^*}{\epsilon U_\infty^*}$
$v_0, v_2, \cdots$	Coefficients of an expansion of v, equation (3.1b)
w	Vector variable used in Chapter IV
y	Vector variable defined in equation (3.16)
α	Function equal to $(r+\epsilon n \sin\theta)^j$ and used in section D, Chapter IV
α_s	Designates location of shock between two grid points; see equation (4.9)
β	Function equal to $1+\epsilon\kappa n$ and used in section D, Chapter IV
γ	Ratio of specific heats
$\bar{\Delta}$	Dimensionless shock standoff distance $\frac{\bar{\Delta}^*}{\epsilon a^*}$
$\Delta_0, \Delta_2, \cdots$	Coefficients of an expansion of $\bar{\Delta}$, equation (3.3a)

NOMENCLATURE (continued)

Δs, Δn	Dimensionless distances between grid lines, see figure 4.1
$\Delta\xi$, $\Delta\eta$	Dimensionless distances along the arcs 3-2 and 3-1 of figure 4.5, respectively
ϵ	Hypersonic similarity parameter defined by equation (2.1)
η	Characteristic coordinate, Chapter IV, Section D
θ	Body surface angle, measured from a plane normal to the axis of symmetry; see figure 2.1
κ	Dimensionless curvature of the body surface, $\kappa^* a^*$
λ_1, λ_2	Slopes of the characteristic curves, defined by equation (4.17)
μ	Dimensionless viscosity coefficient, $\frac{\mu^*(T^*)}{\mu_r^*}$; assumed to be a function of the temperature only
μ_r^*	Reference viscosity, evaluated at $T^* = U_\infty^{*2}/c_p^*$, i.e. $\mu^*(U_\infty^{*2}/c_p^*)$
ρ	Dimensionless density, $\frac{\rho^*}{\rho_\infty^*}$
ρ_0, ρ_2, ...	Coefficients of an expansion of ρ, equation (3.1e)
σ	Prandtl number
τ	Dimensionless shear stress, $\frac{\tau^*}{\rho_\infty^* U_\infty^{*2}}$, defined by equation (2.22)
τ_1, τ_3, ...	Coefficients of an expansion of τ, equations (3.14)
ϕ	Shock angle, measured from a plane normal to the axis of symmetry; see figure 2.1

$1'$ $3'\cdots$	Coefficients of an expansion of ϕ , ϕ equation (3.3b)
ω	Exponent in the viscosity law $\mu \approx T^{\omega}$

Subscripts:

b	Condition at the body surface
B.L.	First-order boundary-layer result
m,N	Designates a function evaluated at the mesh point $(s,n) = (m\Delta s, N\Delta n)$, figure 4.1
sh	Condition immediately behind a shock that is normal to the direction of the free-stream velocity
stag.	Inviscid stagnation value; total condition in the free stream
Δ	Condition immediately behind the shock
∞	Condition in the free stream

Superscripts:

(1)	Value computed from the first-truncation problem of Chapter III
(2)	Value computed from the second-truncation problem in Chapter III
*	Denotes a dimensional quantity
'	Denotes ordinary differentiation with respect to the given argument

Other Notations:

A coordinate used as a subscript denotes partial differentiation with respect to the coordinate.

Chapter I

INTRODUCTION

The low-density, high-speed flow of a viscous fluid around a blunt body presents a wide variety of problems that have attracted considerable attention. One such area of interest is concerned with the effects of a rarefaction of the fluid at high altitudes. This rarefaction can lead to a wide range of flow conditions -- from continuum flow at low altitudes to free-molecular flow at very high altitudes. The transition region between these two limits has been subdivided into various flow regimes depending on the degree of rarefaction of the fluid. These regimes have been described by Hayes and Probstein [18][1], Probstein [27], and Cheng [2]. These regimes are not sharply defined, and most investigations have been concerned with a penetration of the transition region from either the continuum or free-molecule end. The present investigation will be concerned with just such a penetration from the continuum end.

In the basic continuum approach, valid for large Reynolds numbers, the flow between the detached shock and the body is divided into two regions: an outer region in which the viscous forces are negligible extends across most of the shock layer; and a narrow inner region that can be treated by Prandtl's boundary-layer theory contains all the effects of viscosity. At high altitudes where the Reynolds number is

[1] The numbers enclosed in brackets refer to the list of references at the end of the paper.

not large, the viscous layer thickens and the classical boundary-layer theory is no longer adequate. This flow regime -- in which the viscous layer is too thick to be treated by classical boundary-layer theory but is still smaller than the shock-layer thickness, and in which the effect of a thickening of the shock is not appreciable -- is the region treated in this paper.

The Navier-Stokes equations, modified by appropriate slip and temperature-jump conditions at the boundaries, form the basis of such a study. The study of these equations for low-density flow has been the object of numerous investigations, and several methods of approach have been developed. Of primary interest for the present investigation are the second-order boundary-layer theory, the method of local similarity (and a generalization -- the method of series truncation), and the thin-shock-layer analysis of H.K. Cheng [1,2,3].

The classical boundary-layer theory of Prandtl yields asymptotic solutions, valid at large Reynolds number, to the Navier-Stokes equations. The analysis of secondary boundary-layer effects, which become important at lower Reynolds numbers, has been obtained by application of the method of matched asymptotic expansions to the Navier-Stokes equations. The resulting second-order boundary-layer theory, which has been developed most systematically by Van Dyke [32], represents an extension of continuum results toward the regime of rarefied flow. The secondary effects which are analysed in this manner are the effects of the curvature of the body, the slip and temperature-jump conditions at the boundary, the vorticity in the outer flow, and

the perturbation of the outer flow by the displacement thickness of the first-order boundary layer. A discussion of the development of second-order boundary-layer theory up to 1962 is contained in reference 33. In addition, extensive computation of the second-order boundary-layer effects have been carried out by Davis and Flügge-Lotz [12] and Fannelöp and Flügge-Lotz [13], using an implicit finite-difference method.

This second-order boundary-layer theory has yielded results of considerable interest, but some practical difficulties remain in its application. Its use requires the solution of a series of inter-related problems, each of which is simpler in concept than the basic problem defined by the Navier-Stokes equations. However, despite the apparent simplicity of the inviscid, outer flow (on which the boundary-layer solutions are based), the available methods of solution for the inviscid flow are frequently inadequate. The simpler, analytical methods of solution often encounter convergence difficulties [37], and even the more elaborate numerical procedures may lead to results of insufficient reliability [25]. Due to the difficulty of obtaining such inviscid solutions, many investigators have used various approximations to determine the second-order outer flow due to displacement thickness, and this affects the accuracy of their results.

As an alternative, Davis and Flügge-Lotz proposed that the flow be represented by a simplified form of the Navier-Stokes equations that would be uniformly valid throughout the shock layer. The equations would contain only those terms that contribute to the first- or

second-order boundary-layer equations or to the first- or second-order outer, inviscid flow. Thus the equations are valid in the same flow regime as the second-order boundary-layer theory, but they present a unified treatment of the entire shock layer. The feature of these simplified equations that makes their solutions more feasible than the solution of the entire Navier-Stokes equations is that all the characteristic surfaces of the simplified equations are real. This feature arises the possibility of solving the equations as an initial-value problem[1], and the purpose of the present investigation is to examine methods of analysis that lead to such a solution. Two general methods of analysis are considered. First, we obtain solutions of the equations that are valid in the stagnation region of the flow. Second, we examine the use of implicit finite-difference methods to solve the equations as an initial-value problem using the solutions at the axis as initial data.

The method of local similarity has been widely employed in the study of low-density flow in the neighborhood of the axis of symmetry of a blunt body. In this method, an assumed similitude is used to effect a separation of variables, and the equations are then integrated along the stagnation streamline. In addition, as a numerical convenience, the basic differential equations are often simplified by the introduction

---

[2] The problem is more accurately described as an initial-boundary-value problem. These two descriptions are used somewhat interchangeably in this paper, but this should not present any difficulty.

of additional approximations. The approximations which have been most commonly used are a constant-density flow, e.g. Probstein and Kemp [28], and the thin-shock-layer model, e.g. Ho and Probstein [19]. The assumption of local similitude is based on the existence of a spherical symmetry in the geometry of the flow boundaries, and the thin-shock-layer concept is frequently used as justification for this latter assumption.

A second method that may be used to obtain solutions at the axis is the method of series truncations. The flow variables are expanded into series centered at the axis. In order to obtain solutions to the resulting equations, it is necessary to terminate, or truncate, the series after a finite number of terms. Since the one-term truncation is equivalent to the method of local similarity, the series-truncation method may be considered to be a generalization of the method of local similarity. Thus the two-term (and higher) truncations can be used to test the validity of the local-similitude concept. One previous application of series-truncation methods to the viscous blunt-body problem has been made, by H.C. Kao [21], and he concluded that the local-similitude assumption was accurate. However, Kao required that the body and the shock be concentric, and thus the underlying assumption of spherical symmetry was left untested. The validity of local similitude will be re-examined when the series-truncation analysis is used to obtain solutions of the simplified shock-layer equations at the axis. It will be found that the boundary condition that is imposed on the wall temperature plays a critical role in this examination and, in general, the local-similitude analysis can lead to substantial errors.

In the investigation of finite-difference methods, the thin-shock-layer analysis of H.K. Cheng [1,2,3] serves as a standard reference. In his investigation, the Navier-Stokes equations are reduced, under the thin-shock-layer assumption, to a system of parabolic partial differential equations. These equations are then solved by an implicit finite-difference procedure. The equations to be investigated in the subsequent chapters contain several factors which will make the finite-difference analysis more difficult than the thin-shock-layer analysis. These complications are associated with the description of the inviscid pressure field and of the shock location when the thin-shock-layer assumptions are removed. These factors have been investigated by Davis and Chyu [11] for a constant-density shock layer, and they found that it was necessary to retain some features of the thin-shock-layer model. The extension of the analysis of Davis and Chyu to flows of variable density will be considered here, as well as two other methods used on implicit finite-difference procedures.

In the investigation that has been outlined above, the problem is formulated as a direct one -- that is, the body shape is given and the shock shape is calculated. The alternative method of computing the body shape from a known shock shape has been the basis of numerous studies of the blunt-body problem. This inverse blunt-body problem generally leads to a considerable reduction of the computational difficulties but requires several computations if a particular body shape is to be obtained. It is clearly shown in the following chapters that the shapes of the shock and the body, relative to one another, are quite

dependent upon the boundary conditions that are imposed at the body surface for the flow of a viscous, heat-conducting fluid. This feature is very important to the use of the series-truncation or local-similarity methods -- although the inverse blunt-body problem would reduce the computational difficulties, it would do so at the cost of leaving some ambiguity as to what problem has been solved. Hence, the direct blunt-body problem, despite the inherent computational difficulties that are associated with it, is considered to be more appropriate for the present investigation than the inverse problem is.

In the above discussion, only those references of immediate concern to the analysis of the following chapters have been cited. For a more complete account of the work done on the blunt-body problem, the reader is referred to the reviews by Probstein [27], Van Dyke [33], and Cheng [2,3].

Chapter II

FORMULATION OF THE PROBLEM

The problem considered in this work is that of the flow about a blunt body, which is assumed to be everywhere convex and to have a continuous slope. The flow may be either axisymmetric or plane symmetric although only axisymmetric flows are considered in the application of the equations to specific problems. A simplified form of the Navier-Stokes equations is presented that is uniformly valid throughout the entire shock layer. The nature of these equations is examined, and, for comparison, some of the features of the equations used in several thin-shock-layer investigations are discussed.

A. Coordinate System

A blunt body lies in a flow field that has a constant free-stream velocity, U_∞^*, parallel to the body axis and a density and temperature given by ρ_∞^* and T_∞^* respectively. The body surface is located a distance r^* from the axis of symmetry and is inclined at an angle $\frac{\pi}{2} - \theta$ to the axis as shown in figure 2.1. The body has a longitudinal curvature given by κ^* and a nose radius of a^*. The coordinates, s^* and n^*, measure the arc length along the surface of the body and the distance normal to it. The velocity of the fluid is resolved into components, u^* and v^*, parallel to s^* and n^* respectively. A shock of zero thickness is located at a distance $\bar{\Delta}^*$ from the body. The angle between the shock and a plane normal to the axis is denoted by ϕ.

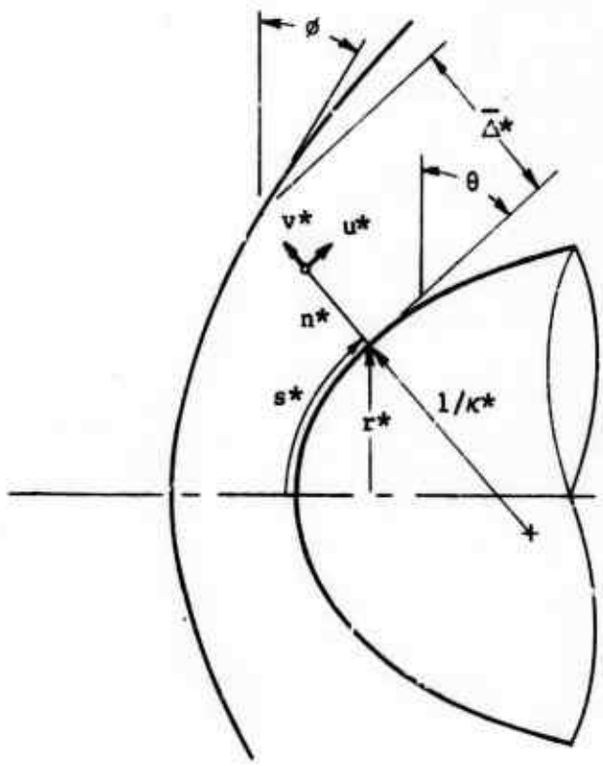

B. Non-dimensional Variables

Dimensionless variables are introduced by referring all lengths to a^*, velocities to U_∞^*, the density to ρ_∞^*, pressure to $\rho_\infty^* U_\infty^{*2}$, temperature to U_∞^{*2}/C_p^*, and viscosity to μ_r^* --its value at the reference temperature U_∞^{*2}/C_p^*.[1] With such a choice of reference values, the variables all remain bounded in the hypersonic limit, $M_\infty \to \infty$. In addition, the normal coordinate and normal velocity are stretched by a factor $1/\epsilon$ where

$$\epsilon = \left[\frac{\mu_r^*}{\rho_\infty^* U_\infty^* a^*} \right]^{1/2} \qquad (2.1)$$

[1] Starred symbols denote dimensional quantities and unstarred symbols denote dimensionless quantities.

The normal coordinate, n, and the normal velocity, v, are identical in form to those used in boundary-layer theory. This form was chosen simply as a convenience for the numerical solution of the equations. Since the viscous effects are confined to a region of order ϵ near the body, the use of the stretched, boundary-layer variables guarantees that the region of large velocity gradients does not become excessively thin as ϵ becomes small. However, the use of this form of the variables is not essential to the method of solution developed here.

C. Shock-layer Equations

The Navier-Stokes equations can be written in the orthogonal, curvilinear coordinate system described above (see, for example, reference 32). The quantity ϵ, defined by equation (2.1), and referred to as the viscous, hypersonic similarity parameter, appears in the momentum and energy equations when the dimensionless variables of section B are introduced. In the hypersonic limit, it is the only similarity parameter that appears in the formulation of the problem. The equation for the similarity parameter may be rewritten in terms of the free-stream Mach number and Reynolds number by using the relation

$$\frac{U_\infty^{*2}}{C_p^*} = (\gamma-1)\, M_\infty^2\, T_\infty^*$$

If a power law is used for the viscosity, $\mu^* \propto T^{*\omega}$, then

$$\epsilon = (\gamma-1)^{\omega/2}\, \frac{M_\infty^\omega}{\sqrt{Re_\infty}}$$

In this form, it can be seen that ϵ is a measure of the ratio of the

mean free path in the shock layer to the thickness of the shock layer [18, p.378]. Thus, ϵ aerves as a measure of the degree of rarefaction of the flow in the shock layer. Further, the quantity ϵ is the perturbation parameter used to systematically expand the Navier-Stokes equations into the equations of boundary-layer theory [32]. Thus the second-order boundary-layer theory represents an extension of the continuum flow equations toward the regime of rarified flow. Adequate numerical techniques for the solution of the first- and second-order boundary-layer equations exist (e.g., Flügge-Lotz and Blottner [14], Davis and Flügge-Lotz [12], Clutter and Smith [5]), but there is still some difficulty associated with the application of boundary-layer theory. In particular, it requires the solution of a series of interrelated problems, two of which (the basic inviscid flow and the inviscid flow due to the displacement thickness) involve solving elliptic partial differential equations in regions in which the locations of the boundaries are unknown.

Numerous methods have been developed to solve this inviscid flow problem. Perry and Pasiuk requested solutions to a few standard problems from various agencies which have developed numerical procedures based on some of these methods. This survey included solutions obtained from both direct and inverse methods and from integral-relation methods, finite-difference methods, series-truncation procedures, and a time-dependent method. A brief comparison of the results of this survey is presented in refcrence 25 . Several of the solutions predicted surface pressures that are in excellent agreement with experimental data; but,

in general, considerable disparity exists in the results.

Thus it appears that accurate results to the inviscid flow problem can be obtained with sufficient numerical skill, but these results must then be used in an entirely different numerical procedure to obtain the first-order boundary-layer results. Then, before all the second-order boundary-layer effects can be computed, the inviscid flow due to the displacement thickness effect of the boundary layer must be obtained either by solving the inviscid flow problem again or by using some approximation (c.f. ref. 12). Thus the application of higher-order boundary-layer theory is complicated by the necessity of solving several different sets of equations which require different methods of solution.

As an alternative, Davis and Flügge-Lotz [12] proposed representing the entire shock layer by one set of equations, a simplified form of the Navier-Stokes equations that would be uniformly valid throughout the shock layer and would contain all the viscous effects that are contained in the boundary-layer equations. Although a solution to this set of equations may require the use of elaborate numerical techniques, only one application of the numerical methods is needed. This paper represents an investigation of this alternative procedure proposed by Davis and Flügge-Lotz. To obtain the desired equations, only those terms of the Navier-Stokes equations that contribute to the first- or second-order boundary-layer equations or contribute to the first- or second-order outer, inviscid flow are retained. Thus the modified equations are uniformly valid to order ϵ throughout the shock layer. The shock-layer equations that are obtained in this manner are

Continuity

$$[(r + \epsilon n \sin\theta)^j \rho u]_s + [(1 + \kappa \epsilon n)(r + \epsilon n \sin\theta)^j \rho v]_n = 0 \tag{2.2}$$

Tangential Momentum

$$\rho\left(\frac{u}{1 + \kappa \epsilon n} u_s + v u_n + \frac{\epsilon \kappa}{1 + \kappa \epsilon n} u v\right) + \frac{p_s}{1 + \kappa \epsilon n} = \mu u_{nn} +$$

$$\mu' (u_n - \epsilon \kappa n) T_n + \epsilon\mu \left(\kappa + \frac{j \sin\theta}{r}\right) u_n \tag{2.3}$$

Normal Momentum

$$\epsilon\rho\left(\frac{\epsilon u}{1 + \kappa \epsilon n} v_s + \epsilon v v_n - \frac{\kappa}{1 + \kappa \epsilon n} u^2\right) + p_n = 0 \tag{2.4}$$

Energy

$$\rho\left(\frac{u}{1 + \kappa \epsilon n} T_s + v T_n\right) - \left(\frac{u}{1 + \kappa \epsilon n} p_s + v p_n\right) =$$

$$\sigma^{-1}\left[\mu T_{nn} + \mu' T_n^2 + \epsilon\mu\left(\kappa + \frac{j \sin\theta}{r}\right) T_n\right]$$

$$+ \mu u_n (u_n - 2 \epsilon \kappa u) \tag{2.5}$$

The subscripts s and n denote partial differentiation with respect to the s and n coordinates, respectively. The quantity j is equal to 0 for plane flow and equal to 1 for axisymmetric flow.

In equation (2.5) the Prandtl number, σ, has been assumed to be a constant, but this assumption is not essential to the use of the methods of analysis investigated in later chapters.

The thermodynamic state relation is taken to be as simple as possible in order to facilitate computations. Thus a perfect gas with constant specific heats is assumed. Hence,

State

$$p = \frac{\gamma-1}{\gamma} \rho T \tag{2.6}$$

This assumption represents a limitation on the applicability of the results of this work. For some flow conditions, it is necessary to consider the real gas effects arising from the molecular structure of the gas or from chemical reactions among the various components of the gas. In addition, the reaction times for such molecular processes become significant for some problems, and in such a case it is necessary to account for the fact that the chemical state of the gas may not be in equilibrium. However, it is desired in this work to concentrate on the difficulties arising solely from the hydrodynamic aspects of the flow, and therefore all complications due to the chemical nature of the gas have been ignored. To the above equations must be added an equation which gives the viscosity as a function of the temperature:

$$\mu = \mu(T) \tag{2.7}$$

Although equations (2.2)-(2.7) have been chosen simply as an attempt to have a somewhat simpler formulation of the problem than is afforded by the boundary-layer theory, there is one aspect of the flow in which the current formulation of the problem may be superior to that of boundary-layer theory. Recently Weinbaum and Garvine [40] have investigated the nature of the pressure field in compressible boundary-layer theory. They assert that under certain flow conditions there are three distinct regions requiring description in a viscous flow problem with large Reynolds number. Near a solid boundary, the usual boundary layer exists where the normal pressure gradient is negligible and the viscous effects predominate. Far from the boundary, there is the usual inviscid region. However, they state that when $M_e \kappa_e > 1$[1] there is an intermediate region where the effects of viscosity are considerable and where the normal pressure gradient cannot be neglected. Thus, they propose the existence of a transition region between the boundary layer and the inviscid flow. Under such conditions, the matching of the boundary-layer solution and the inviscid solution as done in the development of higher-order boundary-layer theory may not be valid.[2]

It should be noted that this proposed intermediate region between the boundary layer and the inviscid flow would not occur in the subsonic portion of the flow around a blunt body. However, Davis and Flügge-Lotz

[1] The subscript e refers to a streamline at the outer edge of the viscous layer.

[2] It has also been suggested [38] that this is a "strong-interaction" phenomenon, which properly lies outside the scope of boundary-layer theory.

[12] report that in the flow around a sphere the normal velocity found from the second-order boundary-layer theory grows extremely rapidly (compared with the first-order normal velocity) after the inviscid sonic line is passed. Davis attributed this to a breakdown of boundary-layer theory as the boundary-layer separation point is approached. Fannelöp and Flügge-Lotz [13] report a similar result for flow around a circular cylinder.[1] However, Fannelöp suggests that the result is not a manifestation of the physical singularity that occurs at separation but that it is a singularity due to a limitation of the mathematical theory. Further, he suggests that the limitation is related to an inadequate description of the streamline curvature.

The normal pressure gradient is proportional to $\rho \kappa u^2$ in second-order boundary-layer theory. This represents the centrifugal force which occurs in a flow field whose streamlines have the same local curvature as the body. Fannelöp points to this similarity to the thin-shock layer model and suggests that the difficulty could be analogous to the occurrence of the zero-pressure point [18, p. 82] in thin-shock-layer theory. This is not inconsistent with the analysis of Weinbaum and Garvine since the interaction of the normal pressure gradient and local variations in the streamline curvature (represented by the terms proportional to $u v_s$ and $v v_n$ in the normal momentum equation) plays an essential role in their analysis. The set of equations (2.2)-(2.7) possesses a complete description of the interaction of the pressure and the local streamline curvature and therefore should not encounter this difficulty.

[1] For non-circular bodies for which $\kappa < 1$ downstream of the sonic line, no difficulties were reported in either reference 12 or 13.

Weinbaum and Garvine also adopt the equations proposed by Davis and Flügge-Lotz, and they propose a method of solution. Weinbaum [39] has applied this method to solve for the flow in a laminar wake. The use of this method to solve the blunt-body problem is investigated in Chapter IV.

D. Characteristics of the Equations

It is interesting to examine the characteristics of the set of equations (2.2)-(2.7). The characteristics fall into two categories. Most of the characteristics coincide and are described by[1]

$$s = \text{constant} \tag{2.8}$$

Although the classifications of hyperbolic, parabolic, and elliptic are not strictly applicable to such higher-order equations, these characteristics may be thought of as being parabolic in nature. This set of characteristics can be traced to the tangential momentum equation and the energy equation. Thus these two equations, which describe the behavior of u and T (u_{nn} and T_{nn} occur only in these two equations), are still essentially parabolic just as they are in boundary-layer theory; but now the pressure gradient is not a known function but is determined together with v from the interaction of the continuity and normal momentum equations. The remaining characteristics are described by

$$\frac{\epsilon}{1 + \epsilon \kappa n} \frac{dn}{ds} = \frac{\epsilon v}{u} \pm \sqrt{\frac{p}{\rho}} \frac{1}{u} = \frac{\epsilon v}{u} \pm \frac{c}{\sqrt{\gamma}\, u} \tag{2.9}$$

[1] The equation describing the characteristic surfaces for a set of nonlinear partial differential equations may be obtained from reference 26 , page 32.

That is, there are two additional characteristics whose slopes differ from that of a streamline by an amount $\pm \frac{1}{\sqrt{\gamma}} \frac{c}{u}$. Thus the behavior of the normal momentum and continuity equations is essentially hyperbolic. Despite the difficulty of dealing with a system of such mixed character, it would appear that the equations should be well suited for an initial-value problem.

Since we know that the subsonic, inviscid flow region of the shock layer is elliptic in character, it is necessary to inquire as to how or whether this "parabolic-hyperbolic" set of equations can adequately describe the flow in a region in which some upstream influence should occur. Weinbaum [40] has reported that these equations are stable as an initial-value problem when applied to laminar-wake flows. However, even though the modified equations are not of an elliptic nature and thus may be numerically stable in an initial-value problem, one would not expect the inherent elliptic character of the blunt-body problem to be absent. The manner in which an upstream influence can occur is not readily apparent, and the answer to this must be deferred until the methods of solution are investigated.

E. Thin-Shock-Layer Investigations

Numerous investigations of the viscous blunt-body problem have utilized the concept of a thin shock layer. Such analyses have much in common with the analysis of this paper. In particular, one set of equations is used to describe the entire viscous shock layer. A few of these investigations are discussed below in order to point out some similarities and differences from the present investigation.

H. K. Cheng has extensively investigated this flow model in a series of papers [1, 2, 3]. The thin-shock-layer equations are an asymptotic description of the shock layer for small density ratio, $\frac{\rho_\infty}{\rho_{sh}}$. Cheng uses the first-order equations that result from an order of magnitude analysis for small $\frac{\rho_\infty}{\rho_{sh}}$. These equations are parabolic in nature (all of the characteristics coincide) and, in fact, are identical to the boundary-layer equations except that the normal pressure gradient is proportional to $\rho \kappa u^2$. This enables Cheng to solve the equations with an implicit finite-difference scheme which starts at the axis of symmetry and marches downstream. This property of the equations is quite desirable since implicit finite-difference methods have been well developed and lead to an accurate solution over as large a region as is desired. Cheng does not assume an infinitesimally thin shock but uses a modified set of the Rankine-Hugoniot conditions to account for transport effects at the shock. These relations are similar to those proposed by Sedov, Michailova and Chernyi [29]. One important simplification in the boundary conditions results from the use of the thin-shock-layer concept. To the order of the approximation considered by Cheng, there is no distinction between the location of the shock interface and the body surface. This appears in most of the analyses based on the thin shock layer as an assumption that the body and shock are concentric ($\phi = \theta$). This simplifies the analysis considerably but, of course, influences the accuracy of the results. Despite the simple nature of this flow model, Cheng obtains reasonable agreement with the results of other investigations.

However, since several terms of $O(\epsilon)$[1], including the slip and temperature jump effects, are missing from his formulation, there is some doubt as to the accuracy of the solutions at the low Reynolds numbers that were considered. Cheng avoids any potential difficulty due to the occurrence of a zero-pressure point by considering only flow around such bodies as paraboloids and hyperboloids. However, as discussed in the previous section, it would be desirable to have a more complete description of the pressure field.

Other investigations have retained more terms of the equations than Cheng did. This provides a more accurate description of the shock layer at low Reynolds numbers but increases the difficulty of obtaining accurate solutions since the equations are no longer parabolic. The method of solution usually employed in such investigations is to reduce the equations to ordinary differential equations by assuming the functional dependence of the variables with the s-coordinate. Examples of such analyses are those of Ho and Probstein [19], Shih and Krupp [30], and L. Goldberg [17].

The investigation of Ho and Probstein removed the constant density assumption which had characterized many prior investigations, and many subsequent investigations have followed the same basic approach. Ho and Probstein emphasize that the thin-shock-layer approximation is not essential to their investigation but is used only to make the numerical analysis simpler. This is true of most of the thin-shock-layer investi-

---

[1] A function $f(\xi)$ is $O(\xi)$--of order ξ--if the limit of $f(\xi)/\xi$ exists as $\xi \to 0$.

gations since the equations are generally not reduced to the parabolic system used by Cheng. Even though the use of the thin-shock-layer equations is not essential to these investigations, the consistent assumption that the body and shock are concentric is very important. These investigations assume that the solution has a locally similar character in the stagnation region. This assumption is based on the existence of spherical or cylindrical symmetry when the body and shock are concentric. H. C. Kao [21] has tested the validity of the local similarity concept by solving the Navier-Stokes equations by the method of series truncations. Kao concluded that the similarity solutions were quite accurate. However, it should be noted that Kao also assumed that the body and shock were concentric. Thus the underlying assumption of spherical symmetry was left untested. This question is examined in Chapter III when the method of series truncation is considered.

The investigetion of Goldberg [17] is similar to that of Ho and Probstein but uses a somewhat more elaborate flow model. In particular, Goldberg modifies the shock conditions in a manner similar to that proposed by Sedov, et al. However, the basic assumption that the shock interface and the body are concentric remains.

W. C. L. Shih and R. S. Krupp [30] have also used the thin-shock-layer assumption to simplify the Navier-Stokes equations but have not assumed that the shock slope is known. In addition the method of analysis is somewhat modified in order to obtain the values of the variables at a specified number of positions downstream of the axis of symmetry. Their analysis also provides for the systematic improvement of the degree

of approximation. In each of the above investigations, except that of H. K. Cheng, the terms proportional to $\rho u v_s$ and $\rho v v_n$ have been retained in the normal momentum equation. Thus a complete description of the inviscid pressure field is afforded. However, these investigations retain a different set of viscous terms than has been retained in equations (2.2)-(2.7). In particular the term $(\mu\, v_n)_n$ is retained in the normal momentum equation. This term has considerable influence on the character of the equations. Shih and Krupp state that such a system of equations is parabolic. Davis and Flügge-Lotz had also suggested the possibility of reducing the equations to parabolic form by including the $(\mu\, v_n)_n$ term in the normal momentum equation. However, the inclusion of this term results in the streamlines being characteristics, and it is not clear that the equations should be classified as parabolic in such a case. Since the streamlines become parallel to the body as $n \to 0$, the body surface will be a characteristic surface for such a set of equations. Thus by the definition of characteristics, one cannot solve for the highest-ordered derivatives normal to the body, given all other flow quantities on the body, unless the specified boundary conditions satisfy a compatibility condition along the boundary. If the boundary conditions do have this special form, then there is no guarantee of the uniqueness of the solution.[1] This fact is very important to any method of analysis that reduces the problem to one of solving ordinary differential equations along lines normal to the body. (This point will be illustrated in Chapter III.) Shih and Krupp modify their equations by neglecting

[1] Discussions of these points may be found in reference 16, especially sections 4.1, 2.1, 3.1 and 3.4.

viscous forces normal to streamlines in order to avoid an instability which occurs near the body surface. This modification does not remove the $(\mu\, v_n)_n$ term, but does alter its special role described above. Kao also reports an instability near the body surface, and he consequently uses a modified set of equations near the surface. Ho and Probstein use a knowledge of the general properties of the variables near the wall to eliminate any numerical difficulty with the singularity. It seems likely that such difficulties are related to the attempted use of a characteristic surface as a boundary surface.

In addition, Shih and Krupp have computed an alternate solution to an example solved by Ho and Probstein, verifying the non-uniqueness which may occur from such a formulation of the problem.

F. Boundary Conditions at the Body Surface

Hayea and Probstein [18] state that the effects of slip and temperature jump on heat transfer and wall shear are negligible provided that the wall temperature is low, even if the shock layer cannot be considered a continuum. All the investigations cited in the preceding section have used no-slip boundary conditions for this reason. In this present work, however, the wall boundary conditions will take the slip and temperature-jump effects into consideration since they are $O(\epsilon)$ in the boundary layer and therefore should be included to be consistent with the retention of terms of $O(\epsilon)$ in the partial differential equations. Thus the examples to be calculated will not be restricted to very low wall temperatures. Davis and Flügge-Lotz, in their study of the second-order boundary-layer, have found that the effect on the stagnation-point

heat transfer is not negligible for moderately cold walls.

The wall boundary conditions are

$$u(s,0) = \epsilon \frac{\mu[T(s,0)]}{p(s,0)} \; a_1 \sqrt{\frac{\gamma-1}{\gamma} T(s,0)} \left.\frac{\partial u}{\partial n}\right|_{n=0} \tag{2.10}$$

$$T(s,0) = T_b(s) + \epsilon \frac{\mu[T(s,0)]}{p(s,0)} \; c_1 \sqrt{\frac{\gamma-1}{\gamma} T(s,0)} \left.\frac{\partial u}{\partial n}\right|_{n=0} \tag{2.11}$$

$$v(s,0) = 0 \tag{2.12}$$

a_1 and c_1 are dimensionless constants which are $0(1)$. These conditions are seen to be those given by Van Dyke [32], except that a term proportional to $\frac{\partial T}{\partial s}$ has been omitted from equation (2.10) since it is $0(\epsilon^2)$ in the boundary layer. For comparison with the results of the second-order boundary-layer investigation of Davis and Flügge-Lotz, the values of a_1 and c_1 are taken to be $(\frac{\pi}{2})^{1/2}$ and $\frac{15}{8}(\frac{\pi}{2})^{1/2}$ respectively. Equation (2.11) may be replaced with a suitable condition on the heat transfer. In Chapter III, several examples will be considered in which an adiabatic wall is specified. In this case equation (2.11) is replaced with

$$T_n(s,0) + \sigma \, u(s,0) \, u_n(s,0) = 0 \tag{2.11a}$$

G. Shock Conditions

As stated earlier, the shock is assumed to be vanishingly thin, and therefore the Rankine-Hugoniot conditions may be applied. These conditions may be written in a form in which the values of the variables

immediately behind the shock are given explicitly:

$$u(s,\bar{\Delta}) = \cos(\theta-\phi)\,\sin\phi + \frac{1}{\rho(s,\bar{\Delta})}\sin(\theta-\phi)\,\cos\phi \tag{2.13}$$

$$\epsilon v(s,\bar{\Delta}) = \sin\phi\,\sin(\theta-\phi) - \frac{1}{\rho(s,\bar{\Delta})}\cos\phi\,\cos(\theta-\phi) \tag{2.14}$$

$$p(s,\bar{\Delta}) = \frac{2}{\gamma+1}\left[\cos^2\phi - \frac{\gamma-1}{2\,\gamma\,M_\infty^2}\right] \tag{2.15}$$

$$\frac{1}{\rho(s,\bar{\Delta})} = \frac{\gamma-1}{\gamma+1} + \frac{2}{(\gamma+1)\,M_\infty^2\cos^2\phi} \tag{2.16}$$

$$T(s,\bar{\Delta}) = \left[\frac{\gamma-1}{\gamma+1} + \frac{2}{(\gamma+1)\,M_\infty^2\cos^2\phi}\right]\frac{2}{\gamma+1}\left[\frac{\gamma\cos^2\phi}{\gamma-1} - \frac{1}{2\,M_\infty^2}\right] \tag{2.17}$$

Equations (2.15)-(2.17) are not independent, of course, but are related through the state equation (2.6). The factors of $\cos(\theta-\phi)$ and $\sin(\theta-\phi)$ in equations (2.13) and (2.14) represent a rotation of axes to change from velocity components tangential and normal to the shock to components tangential and normal to the body surface.

The assumption of a thin shock is consistent with the rest of the mathematical model proposed here as the shock thickness is $0(\epsilon^2)$ [18 , 32] and thus need not be considered here.

It is advantageous at times to replace one of the Rankine-Hugoniot conditions with an equation that expresses the overall balance of mass flow:

$$(r + \epsilon\bar{\Delta}\sin\theta)^{j+1} = 2^j\,\epsilon\int_0^{\bar{\Delta}} \rho\,u\,(r + \epsilon n\sin\theta)^j\,dn \tag{2.18}$$

H. Additional Relations

There are several geometric relationships which are useful in the solution of the problem. The most essential equation expresses the relation between the shock position and its slope:

$$\epsilon \frac{d\bar{\Delta}}{ds} = (1 + \epsilon \kappa \bar{\Delta}) \tan (\theta - \phi) \tag{2.19}$$

In addition, the body geometry gives

$$\kappa = \frac{d\theta}{ds} \tag{2.20}$$

and

$$\frac{dr}{ds} = \cos \theta \tag{2.21}$$

The shear stress and heat transfer at the body surface are useful for evaluating solutions of the equations. The non-dimensional shear stress and heat transfer are given by

$$\tau(s,0) = \epsilon \left[\mu \frac{\partial u}{\partial n} \right]_{n = 0} \tag{2.22}$$

and

$$q(s,0) = \frac{\epsilon}{\sigma} \left[\mu \left(\frac{\partial T}{\partial n} + \sigma u \frac{\partial u}{\partial n} \right) \right]_{n = 0} \tag{2.23}$$

I. Summary

Equations (2.2)-(2.7), (2.10)-(2.17) comprise the system for which we seek a solution. These equations are uniformly valid to $0(\epsilon)$

throughout the entire shock layer and therefore may be used to describe the flow when the fluid is slightly rarified. The equations should be well suited for an initial-value problem and thus should avoid the numerical instabilities attendant to solving the Euler equations in the subsonic portion of the flow. Having one set of equations for the entire shock layer eliminates the need of solving a series of inter-related problems as is done in boundary-layer theory; but, of course, the ability to determine the individual second-order effects of longitudinal and transverse curvature, vorticity interaction, etc. is lost.

Chapter III

METHOD OF SERIES TRUNCATION

In the previous chapter it was noted that the set of equations describing the flow in the shock layer were of such a nature that they should be solvable as an initial-value problem. A necessary step in such a solution is to obtain an accurate set of initial values. The initial station for this problem is the axis of symmetry of the flow. Since the values of the variables on the axis are not known a priori, it is necessary to obtain a solution to equations (2.2)-(2.7) that is valid in the neighborhood of the axis. In this chapter a method is described by which such a solution can be found. The results of the computation of several examples are presented in order to evaluate the accuracy of the method of solution and to evaluate the range of validity of the basic flow model. The concept of local similarity as a method of analysis of blunt-body flows is reviewed.

A. Description of Series Truncations

The most apparent method of obtaining a solution at the axis is to expand each of the variables about the axis into a series in the s - coordinate. The coefficients of these series are functions of the normal coordinate, n. When these series are substituted into equations (2.2)-(2.7), the problem is reduced to solving a set of ordinary differential equations for the coefficients of the series. Determining the first coefficient of each of the series gives the desired solution et

the axis. Determination of higher-order coefficients extends the solution to points away from the axis. In theory, this may be continued to give results as accurate as are desired within the interval of convergence of the basic series.

Such a method of analysis has been widely employed for solving nonlinear partial differential equations in two independent variables. The Blasius-series solution of the boundary-layer equations is a well-known example of such a procedure. In the Blasius series, the coefficient of the first term of the series may be calculated independently of the other coefficients. The coefficient of any term of the series beyond the first depends only on the lower-ordered terms. Thus the coefficients may be calculated successively, starting with the first, until the desired degree of accuracy is attained throughout the region of interest.

In the present problem, however, the ordinsry differential equations for the coefficients of the series may not be solved so simply. Due to the nature of the problem, the first coefficients of the series are not independent of the higher-order coefficients. As a consequence, any finite number of the ordinary differential equations contain more unknown variables than there are equations. Thus, in order to solve the equations, it is necessary to introduce some additional approximations for the higher coefficients. The procedure used to handle this situation is known as the method of series truncation and is described below.

The variables are expanded into the following series:

$$u(s,n) = u_1(n) \sin\theta + u_3(n) \sin^3\theta + \ldots \qquad (3.1a)$$

$$v(s,n) = -\cos\theta \left[v_o(n) + v_2(n) \sin^2\theta + \ldots \right] \qquad (3.1b)$$

$$p(s,n) = p_0(n) + p_2(n) \sin^2\theta + p_4(n) \sin^4\theta + \ldots \qquad (3.1c)$$

$$T(s,n) = T_0(n) + T_2(n) \sin^2\theta + \ldots \qquad (3.1d)$$

$$\rho(s,n) = \rho_0(n) + \rho_2(n) \sin^2\theta + \ldots \qquad (3.1e)$$

where the relation between θ and s depends on the body shape. The particular form of the expansions is, in general, quite important for the ultimate success of the method of series truncation. Expansions quite similar to those of equations (3.1) have been used in previous investigations, and they are reported to have yielded favorable results for flow around spherical bodies [21]. For other body shapes, if one expects accurate results over a significant distance in the s-direction, the expansion should probably be chosen to take advantage of the individual characteristics of that particular problem. For example, various types of flows around a paraboloid of revolution have been analysed with excellent results by transforming to parabolic coordinates and expanding into a suitable series in these new coordinates [10,31,36,4]. Although no answer can be given to the question of what form of expansions provides the best results for an arbitrary body shape, the expansions (3.1) should yield reasonable results at the axis of symmetry for any body.

The use of θ rather than s in equations (3.1) is recommended since the expansion of the governing equations is expected to be somewhat simpler with the use of θ. The arc length s does not appear explicitly in the equations (except in $\frac{\partial(\ )}{\partial s}$, which can be written as $\kappa \frac{\partial(\ )}{\partial \theta}$). On the other hand, θ appears in both the partial differential equations and the shock boundary conditions. Thus an expansion

in powers of sin(s) would require that θ be expanded in powers of sin(s). The resulting equations would then be correspondingly more complex (the shock conditions become particularly difficult to handle). In addition, the geometric description of the body is frequently simpler in terms of θ, which again simplifies the expansion of the equations. (As an example, consider the parabola. In terms of θ, we have $r = \tan\theta$ and $\kappa = \cos^3\theta$. In terms of the arc length s, we have only implicit relations such as $s = \frac{1}{2}\left[r\sqrt{r^2+1} + \log(r+\sqrt{r^2+1})\right]$.) This distinction disappears for a spherical body since $\theta = s$ for the sphere.

The sphere has been extensively treated in the literature despite certain unpleasant aspects of the flow around such bodies (flow separation, trailing wake, etc.). Since this choice of body shape provides numerous opportunities for comparison with the results of other investigations, the rest of the work in this chapter will be directed toward the analysis of the flow around spherical bodies.[1] This choice is not essential to the method of analysis, however, since the expansions which follow could have been made for some other choice of body shape.

For a spherical body, we have

$$r(\theta) = \sin\theta, \tag{3.2a}$$

$$\kappa(\theta) = 1, \tag{3.2b}$$

$$s(\theta) = \theta \tag{3.2c}$$

[1] This also includes bodies such as spherically blunted cones hemisphere-cylinder bodies, etc. The actual requirement here is that the curvature, κ, be equal to unity to the order of the solution obtained. The results of the second-truncation problem obtained later in this chapter are applicable to any body for which $\kappa_2 = 0$ where $\kappa(s) = 1 + \kappa_2 \sin^2\theta + \kappa_4 \sin^4\theta + \ldots$

and, of course, $j = 1$ for axisymmetric flow.

Since there is no distinction between θ and s for the sphere, the work which follows will be given in terms of the coordinate s. The shock location, $\bar{\Delta}$, and the shock angle, ϕ, must be expanded in order to be applied in the shock boundary conditions. Thus

$$\bar{\Delta}(s) = \Delta_0 + \Delta_2 \sin^2 s + \ldots \tag{3.3a}$$

$$\phi(s) = \theta - (\phi_1 \sin s + \phi_3 \sin^3 s + \ldots) \tag{3.3b}$$

If $\phi_1 = \phi_3 = \ldots = 0$, the shock will be a sphere, concentric to the body. Thus ϕ_1, ϕ_3, ... measure the deviation of the shock shape from a concentric sphere.

Equations (3.1) and (3.2) are substituted into the governing partial differential equations, (2.2)-(2.7). The equations are expanded into powers of sin(s), and like powers of sin(s) are equated. The lowest-ordered terms from the expanded equations yield

$$v_o \rho_{o_n} + \rho_o v_{o_n} = \frac{2\rho_o}{1+\epsilon n} (u_1 - \epsilon v_o) \tag{3.4a}$$

$$\rho_o \left(\frac{u_1^2}{1+\epsilon n} - v_o u_{1_n} - \frac{\epsilon v_o u_1}{1+\epsilon n} \right) + \frac{2 p_2}{1+\epsilon n} =$$

$$\mu(T_o) \left[u_{1_{nn}} + 2 \epsilon u_{1_n} \right] + \mu'(T_o) T_{o_n} \left[u_{1_n} - \epsilon u_1 \right] \tag{3.4b}$$

$$p_{o_n} + \epsilon^2 \rho_o v_o v_{o_n} = 0 \tag{3.4c}$$

$$v_o p_{o_n} - \rho_o v_o T_{o_n} = \frac{\mu(T_o)}{\sigma}\left[T_{o_{nn}} + 2\epsilon T_{o_n}\right] + \frac{\mu'(T_o)}{\sigma} T_{o_n}^2 \qquad (3.4d)$$

$$p_o = \frac{\gamma-1}{\gamma} \rho_o T_o \qquad (3.4e)$$

Examining these equations, we find that they involve six unknowns, u_1, v_o, p_o, p_2, T_o, and ρ_o, while there are only five equations svailsble. A second set of equations can be obtained by equating the next higher-ordered terms of each expanded equstion. This results in

$$v_o \rho_{2_n} + \rho_2 v_{o_n} + v_2 \rho_{o_n} + \rho_o v_{2_n} =$$

$$\frac{2}{1+\epsilon n}\left[\rho_o(2u_3 - \epsilon v_2) + \rho_2(2u_1 - \epsilon v_o)\right] \qquad (3.5s)$$

$$(\rho_2 - \tfrac{1}{2}\rho_o)\left(\frac{u_1^2}{1+\epsilon n} - v_o u_{1_n} - \frac{\epsilon u_1 v_o}{1+\epsilon n}\right) +$$

$$\rho_o\left[\frac{4u_1u_3}{1+\epsilon n} - v_o u_{3_n} - v_2 u_{1_n} - \frac{\epsilon}{1+\epsilon n}(v_o u_3 + u_1 v_2)\right] +$$

$$\frac{4p_4 - p_2}{1+\epsilon n} = \mu(T_o)\left[u_{3_{nn}} + 2\epsilon u_{3_n}\right] + \mu'(T_o)\left[(u_{1_{nn}} +\right.$$

$$\left.2\epsilon u_{1_n}) T_2 + (u_{3_n} - \epsilon u_3) T_{o_n} + (u_{1_n} - \epsilon u_1) T_{2_n}\right] +$$

$$\mu''(T_o) T_2 T_{o_n}\left[u_{1_n} - \epsilon u_1\right] \qquad (3.5b)$$

$$p_{2_n} + \epsilon^2 \rho_2 v_o v_{o_n} + \epsilon \rho_o \left[\frac{\epsilon u_1}{1+\epsilon n} (v_o - 2v_2) + \right.$$

$$\left. \epsilon(v_o v_{2_n} + v_2 v_{o_n} - v_o v_{o_n}) - \frac{u_1^2}{1+\epsilon n} \right] = 0 \qquad (3.5c)$$

$$v_o p_{2_n} + v_2 p_{o_n} - \frac{1}{2} v_o p_{o_n} - \frac{2p_2 u_1}{1+\epsilon n} +$$

$$\rho_o \left[\frac{2u_1 T_2}{1+\epsilon n} - v_2 T_{o_n} - v_o T_{2_n} + \frac{1}{2} v_o T_{o_n} \right] - \rho_2 v_o T_{o_n} =$$

$$\mu(T_o) \left[\frac{1}{\sigma} \left(T_{2_{nn}} + 2\epsilon T_{2_n} \right) + u_{1_n} \left(u_{1_n} - 2\epsilon u_1 \right) \right] +$$

$$\frac{\mu'(T_o)}{\sigma} \left[\left(T_{o_{nn}} + 2\epsilon T_{o_n} \right) T_2 + 2 T_{o_n} T_{2_n} \right] + \frac{\mu''(T_o)}{\sigma} T_2 T_{o_n}^2 \qquad (3.5d)$$

$$p_2 = \frac{\gamma-1}{\gamma} (\rho_o T_2 + \rho_2 T_o) \qquad (3.5e)$$

There are now a total of ten equations, but the number of unknowns has become eleven as u_3, v_2, T_2, ρ_2, and p_4 have been added. This pattern continues as the higher-order equations are considered; there is always at least one more unknown than there are equations. Thus we have an infinite set of coupled differential equations. In the case of the Blasius-series solution cited earlier, the coupling between the equations goes in only one direction; i.e., the lower-order terms do not depend on the higher-order terms, and thus the equations can be solved a few at s time until as many terms as are desired have been computed. In

the present case, however, the coupling of the equations is complete, and it would appear to be necessary to solve all of the equations simultaneously, clearly an intractable situation.

By introducing approximations for the excess unknowns, the equations can be solved to give approximate values for the coefficients. The accuracy of these solutions will depend on the nature of the approximations introduced and on the nature of the problem itself. However, the accuracy of these approximations can be systematically evaluated and improved.

Consider equations (3.4) again. Only one of the second-order coefficients, p_2, appears and it occurs in only one term. A crude approximation would be to set $p_2 = 0$. This would permit the solution of the equations and yield a first approximation for u_1, v_o, p_o, and T_o. A simultaneous solution of equations (3.4) and (3.5) could also be obtained if p_4 were set equal to zero. This second approximation would yield not only an approximate solution to the second-order coefficients (u_3, v_2, p_2, and T_2) but would also yield values for the first-order coefficients which should be more accurate than those previously obtained. The improved accuracy should result from the fact that the set of equations (3.4) would be solved in their entirety with more accurate values of p_2 than were used in the first approximation. This would then afford an estimate of the accuracy of the first approximation ($p_2 = 0$). This process could, in theory, be continued. At each step, as the degree of approximation is improved an estimate of the accuracy of the previous approximation is obtained.

The process of setting the excess unknowns equal to zero is equivalent to assuming that the variables can be described with simple algebraic expressions rather than with the infinite series of equations (3.1). In the first approximation above, a one-term expression is used, and, in the second case, a two-term polynomial. The use of simple algebraic expressions to evaluate the flow around a blunt body has been widely employed and is known as the method of local similarity [19, 17, 24, 28]. The series-truncation method may be considered to be a generalization of the method of local similarity, allowing a systematic improvement of the degree of approximation. As such the series truncations can be used to test the validity of the concept of local similarity.

A truncation procedure very similar to the scheme outlined above has been used previously [31]. The results of reference 31 indicate that the first approximation ($p_2 = 0$) of this scheme would yield very poor results. In order to improve the results, it would then be necessary to retain more terms of the series than are desirable for this problem. Setting $p_2 = 0$ in equation (3.4) is equivalent to requiring a zero streamwise pressure gradient, clearly a poor approximation for the flow around a blunt body. A reasonable value for the pressure terms is needed, and this can be sccomplished in several ways. The "indented truncation" method introduced by H. C. Kao [21] is used here. This method makes use of equation (3.5c) to approximate the value of p_2.

The addition of equation (3.5c) to equations (3.4) results in eight unknowns appearing in six equations. The "excess" unknowns which are truncated to permit a solution are ρ_2 and v_2. The solution obtained

in this manner provides a reasonable value for p_2. Therefore this first approximation is far more accurate than the one described earlier. Equations (3.4) and equation (3.5c) (with $\rho_2 = v_2 = 0$) constitute the first-truncation problem. The values of the variables which are obtained from the first truncation are denoted by $u_1^{(1)}$, $v_o^{(1)}$, $p_o^{(1)}$, $T_o^{(1)}$ and $p_2^{(1)}$. The boundary conditions for the first truncation are obtained from the expansion of equations (2.10)-(2.17) by use of equations (3.1)-(3.3). The boundary conditions which apply to the variables of the first truncation are given below. At the body surface the velocity- and temperature-jump conditions yield

$$u_1(0) = \frac{\epsilon a_1 \mu(T_o(0))}{p_o(0)} \sqrt{\frac{\gamma-1}{\gamma} T_o(0)}\, u_{1_n}(0) \tag{3.6a}$$

$$T_o(0) = T_{b_o} + \frac{\epsilon c_1 \mu(T_o(0))}{p_o(0)} \sqrt{\frac{\gamma-1}{\gamma} T_o(0)}\, T_{o_n}(0) \tag{3.6b}$$

$$v_o(0) = 0 \tag{3.6c}$$

where the specified body temperature has been expanded into

$$T_b(s) = T_{b_o} + T_{b_2} \sin^2 s + \ldots \tag{3.7}$$

Immediately behind the shock, the following conditions must be applied.

$$u_1(\Delta_o) = 1 - \frac{2}{\gamma+1}\left[1 - \frac{1}{M_\infty^2}\right]\phi_1 \tag{3.8a}$$

$$\epsilon\, v_o(\Delta_o) = \frac{\gamma-1}{\gamma+1} + \frac{2}{(\gamma+1)M_\infty^2} \tag{3.8b}$$

$$p_o(\Delta_o) = \frac{2}{\gamma+1}\left[1 - \frac{\gamma-1}{2\gamma\, M_\infty^2}\right] \tag{3.8c}$$

$$p_2(\Delta_o) + \Delta_2\, p_{o_n}(\Delta_o) = -\frac{2}{\gamma+1}(1 - \phi_1)^2 \tag{3.8d}$$

$$T_o(\Delta_o) = \frac{1}{(\gamma+1)^2}\left[\gamma - 1 + \frac{2}{M_\infty^2}\right]\left[\frac{2\gamma}{\gamma-1} - \frac{1}{M_\infty^2}\right] \tag{3.8e}$$

The following geometric relation between ϕ_1 and Δ_2 is obtained by substituting equations (3.3) into equation (2.19).

$$\phi_1 = \frac{2\,\epsilon\,\Delta_2}{1+\epsilon\,\Delta_o} \tag{3.9}$$

The solution to this first truncation problem is discussed in section C where it will be found that it is also necessary to approximate the value of ϕ_1 in equations (3.8a) and (3.8d).

To assess the accuracy of the first truncation (and to simultaneously improve it), equations (3.4) and (3.5) are solved simultaneously by making a suitable assumption for the value of p_4. As was the case in the first truncation, the necessary value is obtained from the normal

momentum equation. The third-order terms of the expanded normal momentum equation, when equated, yield

$$p_4 + \epsilon^2 \rho_4 v_o v_{o_n} + \epsilon \rho_2 \left[\frac{\epsilon u_1}{1+\epsilon n} (v_o - 2v_2) + \right.$$

$$\left. \epsilon \left(v_o v_{2_n} + v_2 v_{o_n} - v_o v_{o_n} \right) - \frac{u_1^2}{1+\epsilon n} \right] +$$

$$\epsilon \rho_o \left\{ \frac{\epsilon}{1+\epsilon n} \left[u_1 (3v_2 - 4v_4) + u_3 (v_o - 2v_2) \right] + \right.$$

$$\left. \epsilon \left(v_o v_{4_n} + v_2 v_{2_n} + v_4 v_{o_n} - v_o v_{2_n} - v_2 v_{o_n} \right) - \frac{2u_1 u_3}{1+\epsilon n} \right\} = 0 \tag{3.10}$$

As before, it is necessary to truncate two excess unknowns. Therefore we equate ρ_4 and v_4 to zero. Equations (3.4), (3.5) and (3.10) (with $\rho_4 = v_4 = 0$) constitute the second-truncation problem, and the values obtained from its solution are denoted by $u_1^{(2)}$, $v_o^{(2)}$, ..., $u_3^{(2)}$, $v_2^{(2)}$, $T_2^{(2)}$, $p_4^{(2)}$. In theory, this procedure could be continued with more equations being solved at each step. As the order of the truncation is increased in this manner, the problem more closely approximates the infinite set of coupled differential equations which govern the flow variables. It is assumed that the solutions to the truncated equations approach the solution of the full equations. That is, the basic premise of the method of series truncation is that the sequence of solutions for each variable, e.g. $u_1^{(1)}$, $u_1^{(2)}$, ... $u_1^{(n)}$, ... converges to the desired solution of the infinite set of ordinary

differential equations. A brief examination of the increasing complexity of equations (3.4), (3.5) and (3.10) shows that if the method is to be practical the convergence of the sequence of solutions must be rather rapid. To proceed beyond the second truncation becomes rather difficult for this problem. However, there is reason to believe that the convergence is rapid for this particular problem. In fact, the method of local similarity assumes that the flow is adequately described by expressions equivalent to those used in the first truncation.

To complete the formulation of the second truncation problem, additional boundary conditions are obtained in the same manner that equations (3.6), (3.8) and (3.9) were obtained. At the wall, we have

$$u_3(0) = \frac{\epsilon\, a_1\, \mu(T_o(0))}{p_o(0)} \sqrt{\frac{\gamma-1}{\gamma} T_o(0)} \left\{ u_{3_n}(0) + u_{1_n}(0) \left[\frac{1}{2} \frac{T_2(0)}{T_o(0)} + \frac{\mu'(T_o(0))}{\mu(T_o(0))} T_2(0) - \frac{p_2(0)}{p_o(0)} \right] \right\} \qquad (3.11a)$$

$$T_2(0) = T_{b_2} + \frac{\epsilon\, c_1\, \mu(T_o(0))}{p_o(0)} \sqrt{\frac{\gamma-1}{\gamma} T_o(0)} \left\{ T_{2_n}(0) + T_{o_n}(0) \left[\frac{1}{2} \frac{T_2(0)}{T_o(0)} + \frac{\mu'(T_o(0))}{\mu(T_o(0))} - \frac{p_2(0)}{p_o(0)} \right] \right\} \qquad (3.11b)$$

$$v_2(0) = 0 \qquad (3.11c)$$

After considerable algebraic manipulation the following boundary conditions at the shock are obtained.

$$u_3(\Delta_o) + \Delta_2\, u_{1_n}(\Delta_o) = -\frac{2}{\gamma+1}\left(1 - \frac{1}{M_\infty^2}\right)\left(\phi_3 - \frac{1}{6}\phi_1^3\right) -$$

$$\frac{1}{2}(1 - \phi_1)\left[1 + \phi_1^2 + \left(\gamma - 1 - \frac{2}{M_\infty^2}\right)\left(\frac{1 + \phi_1}{\gamma + 1}\right)\right] \qquad (3.12a)$$

$$\epsilon\left[v_2(\Delta_o) + \Delta_2\, v_{o_n}(\Delta_o)\right] = -\frac{2(1 - \phi_1)}{\gamma + 1}\left(\phi_1 - \frac{1}{M_\infty^2}\right) \qquad (3.12b)$$

$$p_4(\Delta_o) + \Delta_2\left[\frac{\Delta_2}{2}\, p_{o_{nn}}(\Delta_o) + p_{2_n}(\Delta_o)\right] + \Delta_4\, p_{o_n}(\Delta_o) =$$

$$\frac{4(1 - \phi_1)}{\gamma + 1}\left[\phi_3 - \frac{1}{6}\phi_1(\phi_1^2 - 3\phi_1 + 3)\right] \qquad (3.12c)$$

$$T_2(\Delta_o) + \Delta_2\, T_{o_n}(\Delta_o) = -2\left(\gamma + \frac{1}{M_\infty^2}\right)\left(\frac{1 - \phi_1}{\gamma + 1}\right)^2 \qquad (3.12d)$$

$$\phi_3 = -\frac{1}{3}\phi_1^3 + \frac{\epsilon}{1+\epsilon\Delta_o}\left[4\Delta_4 - \Delta_2 - \frac{2\epsilon\Delta_2^2}{1+\epsilon\Delta_o}\right] \qquad (3.13)$$

These boundary conditions are used together with those previously given in equations (3.6)-(3.9) to complete the formulation of the second truncation problem.

To evaluate the shear stress and heat transfer at the body surface from these series solutions, it is necessary to expand the expressions for shear stress, τ, and heat transfer rate, q, by substituting equations (3.1) into equations (2.22). The shear stress is then given by

$$\tau(s,0) = \epsilon(\tau_1 \sin s + \tau_3 \sin^3 s + \ldots) \tag{3.14}$$

where

$$\tau_1 = \mu[T_o(0)]\, u_{1_n}(0) \tag{3.14a}$$

and

$$\tau_3 = \mu[T_o(0)]\, u_{3_n}(0) + \mu'[T_o(0)]\, T_2(0)\, u_{1_n}(0) \tag{3.14b}$$

The heat transfer rate becomes

$$q(s,0) = \frac{\epsilon}{\sigma}(q_o + q_2 \sin^2 s + \ldots) \tag{3.15}$$

where

$$q_o = \mu[T_o(0)]\, T_{o_n}(0) \tag{3.15a}$$

and

$$q_2 = \mu[T_o(0)]\left(T_{2_n}(0) + \sigma\, u_1(0)\, u_{1_n}(0)\right) + \mu'[T_o(0)]\, T_2(0)\, T_{o_n}(0) \tag{3.15b}$$

It can be seen that the solution to the first truncation problem yields values for τ_1 and q_o. From the second truncation problem, values for τ_1, τ_3, q_o and q_2 can be computed.

The solution of the first and second truncations will be obtained for several blunt-body flows in section D. These solutions provide a measure of the range of validity of the flow model adopted in Chapter II and provide a test of the validity of the concept of local similarity as well as fulfilling their original purpose of providing initial data at the axis of symmetry. Before the equations are actually solved, however, some of the previous investigations based on series truncations will be discussed in section B.

B. Previous Applications of Series Truncations

There is no mathematical proof of the convergence of the method described in the previous section and thus no assurance of its validity. Further, the necessity of obtaining a rapid convergence means that an evaluation of the effectiveness of the method must come from an analysis of the application of the method to specific examples. Most of the previous applications of series truncations have been to the blunt-body problem [31, 6, 7, 21, 36, 4]. However, other examples of its use include incompressible boundary-layer flow over paraboloids [10]; viscous flow over a semi-infinite plate [8]; and incompressible, viscous flow around a circular cylinder [34]. These investigations, except for ref. 10 , have been reviewed by M. Van Dyke in reference 35. The work that is discussed in this reference clearly illustrates certain important aspects of the series-truncation method. In particular it should be noted that the accuracy of the method may be quite dependent upon the form of the expansion and that the method may be expected to work best for problems in which the flow field is thin (one dimension much smaller than the other). This later aspect is anticipated in the use of the method of

local similarity for such problems.

The coupling of the lowest-ordered terms to the higher-ordered terms is a consequence of the upstream influence which occurs in the flow. That is, it represents the fact that the flow at the axis depends upon the flow in the region away from the axis. Clearly the method will be most successful when this dependence is weak. This will be the case when the equations are "nearly parabolic" (or hyperbolic) and/or the region of interest is thin. For thin regions the solution should depend most strongly on the locally imposed boundary conditions. In fact, in the limit as the width of the region goes to zero, e.g., in boundary-layer theory and in thin-shock-layer theory, the governing differential equations become parabolic. There is then no upstream influence at all, and no truncations are necessary.

It can be seen that the investigations cited above pose tests of varying degrees of difficulty. The boundary-layer flow over a paraboloid considered by R. T. Davis in reference 10 is exactly the type of flow for which the method is expected to work. Since the equations are parsbolic, an expansion about the axis of symmetry would need no truncation snd would lead to the Blasius-series solution. However, Davis has used a variation of the method which is referred to as the method of local truncations. The varisbles are expanded about sn arbitrary downstream station. The resulting problem is then solved st various downstream positions, and the results of each solution sre used only locally. A more accurste representstion of the downstream flow can be obtained in this manner than could be obtained from s ressonable number of terms of an expsnsion at the sxis. However, this method has two disadvantsges:

the flow symmetry is lost, thereby requiring more terms in the expansion; and the coupling between different-ordered terms must now describe the influence of the flow in regions both upstream and downstream of the point of expansion. In the flow considered by Davis, there is no upstream influence, but a coupling does occur since the solution at the expansion station depends on the flow near the axis. However, for the boundary-layer equations, it is known that this dependence is weak since the influence of the initial data dies out rapidly away from the initial station. Even though this flow problem is a weak test of the method, it is a significant test since exact numerical solutions are available from finite-difference methods. Davis shows that the second truncation produces highly accurate results over the entire paraboloid.

The investigation of reference 8 uses local truncations to solve the Navier-Stokes equations for flow over a semi-infinite plate. Since the equations are elliptic, this problem poses a more difficult test of the method. Although no exact solution exists for comparison, the results obtained for this problem are remarkable and substantiate the value of the method.

Van Dyke has posed a particularly severe test of the method of series truncation in reference 34 . He has used both the linearized Oseen equations and the full Navier-Stokes equations to describe the flow around a circular cylinder. The method is not expected to be highly accurate for such elliptic equations in a thick (infinite) region and, indeed, the second-truncation solution of the Oseen equations shows only qualitative agreement with the exact Oseen solution. However, Van Dyke has shown that a knowledge of this error when combined with the

first-truncation solution to the Navier-Stokes equations yields very useful results even for this particularly severe problem.

The analyses of the blunt-body problem based on series truncations are also encouraging. Swigart [31] solved the inviscid flow of a perfect gas over spheres and paraboloids at small angles-of-attack. Three and four truncations produced accurate results at the axis. However, at the sonic line the results appeared to be considerably less accurate. R. J. Conti [6,7], investigating the inviscid flow of a chemically reacting gas, and H. C. Kao [21], investigating the viscous shock layer, improved the convergence of the method so that reasonable results were obtained near the axis with only two truncations. This is particularly important for the viscous shock layer since it is difficult to proceed beyond the second truncation due to the increasing complexity of the equations. Van Dyke [36] re-examined Swigart's solution for a paraboloidal shock wave and showed that a modified expansion procedure would produce a solution of remarkable accuracy over the entire body. P. Cheng and W. Vincenti [4] have used this knowledge to investigate the flow of a radiating, inviscid gas over a paraboloid. Each of the above analyses was based on the inverse method in which the shock shape is given and the body which produced that shock shape is calculated. This simplifies the computational procedures but leaves some ambiguity as to what problem has been solved, especially for the flow of a viscous, heat conducting fluid. The investigation by Kao is of particular interest for the work that follows in this chapter.

The success of the method of series truncation in the analysis of the difficult problems described above indicates that it is a valuable

analytical method and justifies its use for the computation of the flow variables at the axis of symmetry of a blunt body.

C. Solution of the Equations

The set of equations, (3.4) and (3.5c), which constitutes the first-truncation problem, is a seventh-order system of nonlinear ordinary differential equations for the six unknown functions, u_1, v_o, p_o, p_2, T_o and ρ_o. Equation (3.4e) may be used to eliminate ρ_o immediately. Together with the boundary conditions (equations (3.6), (3.8) and (3.9)), this system of equations comprises a two-point boundary-value problem. Due to the complexity of these equations, solutions must be obtained by numerical methods. The equations are solved numerically by reducing the two-point boundary-value problem to an equivalent initial-value problem. This is accomplished by guessing the values of the unknown variables at one of the boundaries. The equations may then be integrated to the other boundary by using any of the standard integration procedures designed for use with automatic digital computers. The computations of this chapter were made on the Burroughs B5500 computer using the Kutta-Merson method. The guessed initial values must then be altered until the boundary conditions at the second boundary are satisfied. This iteration on the guessed initial values is accomplished by using the Newton-Raphson method[1] to calculate the necessary corrections to the initial values. If the original guessed values are not sufficiently close to the correct

[1] A description of this method may be obtained from any standard text on numerical methods, e.g., Introduction to Numerical Analysis, F. B. Hildebrand, McGraw-Hill Book Company, Inc., 1956.

values, the iterations based on the Newton-Raphson method may not converge or may converge rather slowly. However, in such cases, it has been found that convergence can be obtained by using only a fraction of the corrections predicted by the Newton-Raphson method. The exact value of this fraction is selected so that the errors in the boundary conditions are minimized at the second boundary. The remainder of this section is a description of the details of these computations. The reader is referred to section D for the results of these computations. In Chapter II it was noted that difficulties with this computational method may be expected when the body surface is a characteristic surface for the governing partial differential equations. These difficulties are also illustrated in the remainder of this section.

The application of any of the numerical techniques for integration requires the reduction of the set of equations to a system of first-order differential equations having the form

$$\frac{dy}{dn} = f(n,y) \tag{3.16}$$

where y and f are vector quantities. This reduction is easily accomplished by considering u_{1_n} and T_{o_n} to be separate unknowns and introducing two additional equations, $\frac{d(u_1)}{dn} = u_{1_n}$ and $\frac{d(T_o)}{dn} = T_{o_n}$. The vector unknown, y, has seven components for this first-truncation problem: $y = (u_1, u_{1_n}, v_o, p_o, p_2, T_o, T_{o_n})$. In order to obtain the

first derivatives $\frac{dp_o}{dn}$ and $\frac{dv_o}{dn}$ explicitly, as required in (3.16), it is necessary to algebraically combine the continuity (3.4a), normal momentum (3.4c) and state (3.4e) equations. The remaining first derivtives are obtained immediately from the appropriate equations. The seven components of equation (3.16) for the first-truncation problem are[1]

$$\frac{du_1}{dn} = f_1(n,y) = u_{1_n} \tag{3.17a}$$

$$\frac{du_{1_n}}{dn} = f_2(n,y) = \frac{1}{\mu(T_o)}\left[\rho_o\left(\frac{u_1^2}{1+\epsilon n} - v_o u_{1_n} - \frac{\epsilon u_1 v_o}{1+\epsilon n}\right) + \frac{2p_2}{1+\epsilon n}\right] - 2\epsilon u_{1_n} - \frac{\mu'(T_o)}{\mu(T_o)}\,(u_{1_n} - \epsilon u_1)\,T_{o_n} \tag{3.17b}$$

$$\frac{dv_o}{dn} = f_3(n,y) = \frac{\frac{2}{1+\epsilon n}(u_1 - \epsilon v_o) + \frac{v_o T_{o_n}}{T_o}}{1 - \epsilon^2 \frac{\gamma}{\gamma-1}\frac{v_o^2}{T_o}} \tag{3.17c}$$

$$\frac{dp_o}{dn} = f_4(n,y) = -\epsilon^2 \rho_o v_o\, f_3(n,y) \tag{3.17d}$$

$$\frac{dp_2}{dn} = f_5(n,y) = -\epsilon\rho_o\left[\frac{\epsilon u_1 v_o}{1+\epsilon n} - \epsilon\, v_o\, f_3(n,y) - \frac{u_1^2}{1+\epsilon n}\right] \tag{3.17e}$$

[1] The superscript (1), denoting the values obtained from the first truncation, has been dropped for simplicity.

$$\frac{dT_o}{dn} = f_6(n,y) = T_{o_n} \tag{3.17f}$$

$$\frac{dT_{o_n}}{dn} = f_7(n,y) = \frac{\sigma}{\mu(T_o)} \; v_o \left[f_4(n,y) - \rho_o \, T_{o_n} \right] -$$

$$T_{o_n} \left[2\epsilon + \frac{\mu'(T_o)}{\mu(T_o)} \; T_{o_n} \right] \tag{3.17g}$$

where $$\rho_o = \frac{\gamma}{\gamma - 1} \frac{p_o}{T_o}$$

There are nine boundary conditions available in equations (3.6), (3.8) and (3.9). However, there are three additional unknown quantities, Δ_o , Δ_2 and ϕ_1 , which appear in these boundary conditions. Thus there is actually one less boundary condition available than is needed to define a solution to equations (3.17). The problem is made determinate by truncating the series that describes the shock position or shock angle, equation (3.3). Setting $\phi_1 = 0$ (and therefore $\Delta_2 = 0$) is equivalent to assuming that the shock and body are concentric. Thus, with this approximation, the first truncation problem becomes consistent with the analyses based on local similarity and the thin-shock-layer model.

Equations (3.6 a,b,c) provide three relations for the seven dependent variables at the body surface. Thus, to begin the integration of equations (3.17) at the wall, it is necessary to guess the values of four of the variables. The recommended procedure is to choose values of

$p_o(0)$, $p_2(0)$, $u_{1_n}(0)$ and $T_{o_n}(0)$. Equation (3.6c) gives $v_o(0) = 0$, and equations (3.6a) and (3.6b) must be solved to obtain the values of $u_1(0)$ and $T_o(0)$ that are consistent with the guessed values for $p_o(0)$, $u_{1_n}(0)$ and $T_{o_n}(0)$. The solution of equation (3.6b) for $T_o(0)$ is not immediate since T_o appears in an implicit manner. Using a power law for the viscosity,

$$\mu = T^{\omega} ,$$

we may rewrite equation (3.6b) in the form

$$T_o(0) = \frac{T_{b_o}}{1 - \epsilon c_1 \sqrt{\frac{\gamma-1}{\gamma}} \frac{T_{o_n}(0)}{p_o(0)} \left[T_o(0)\right]^{\omega - \frac{1}{2}}} \qquad (3.18)$$

This relation may be solved by successive substitution. That is, substituting an approximate value of $T_o(0)$, say $T_o(0) \approx T_{b_o}$, into the right-hand side yields an improved value for $T_o(0)$. This value is in turn substituted into the right-hand side. This process is continued until convergence is obtained. Note that for the special csse, $\omega = 1/2$, the solution is obtained immediately since $T_o(0)$ is removed from the right-hand side of the equation. With $T_o(0)$ available, equation (3.6a) can be solved for $u_1(0)$. The functions $f(n,y)$, defined by equations (3.17), may now be evaluated at $n = 0$, and the numerical integration of equations (3.17) can be performed in a step-wise manner until the

shock is located. The shock condition on v_o has been found to work well for the determination of Δ_o. The numerical integration is continued for increasing n until the value of v_o satisfies equation (3.8b). This defines the value of Δ_o. There remain four shock conditions which are satisfied by iterating on the four initial values $u_{1_n}(0)$, $T_{o_n}(0)$, $p_o(0)$ and $p_2(0)$. Due to the nonlinearity of the equations, several such iterations using the Newton-Raphson method are generally required to obtain the correct values of the variables at the wall. Each iteration proceeds in the following manner.

1) Each of the guessed initial values is varied by a small increment. The equations are integrated, and the effect of the change in the initial value on the unsatisfied shock conditions is evaluated. This step requires the numerical integration of equations (3.17) four additional times.

2) With the assumption that the shock conditions depend on changes in the initial data in a linear manner, a correction to the initial data is computed.

3) The equations are then integrated with the corrected initial values, and the shock conditions are evaluated again.

This process continues until the shock conditions are satisfied to the desired degree of accuracy.

The application of the temperature-jump condition, equation (3.6b) or (3.18), is simpler if an alternative procedure of guessing $T_o(0)$ and computing the consistent value of $T_{o_n}(0)$ is adopted. This

procedure works quite well for low values of the Reynolds number. However, numerical difficulties frequently occur when ϵ is very small (large Reynolds number). The computed value of $T_{o_n}(0)$ (and therefore the solution to equations (3.17)) is, in this case, quite sensitive to the guessed value of $T_o(0)$. Hence, in the iteration procedure described above, the increments added to $T_o(0)$ must be kept very small. It occasionally becomes difficult to keep the errors that result from the numerical integration smaller than this increment in $T_o(0)$. If this is not accomplished, the predicted corrections to the initial conditions are meaningless, and the iterations do not converge. For this reason it was recommended that the value of $T_{o_n}(0)$ be guessed.

Probstein and Kemp [28] considered several approximate methods based on local similarity and showed that some of the schemes could lead to an overdetermined system of differential equations. However, one generally encounters a system which appears to be underdetermined. In the case of the first-truncation problem described above, this was resolved by requiring the body and shock to be concentric. In the thin-shock-layer investigations based on local similarity, e.g. ref. 19 , the systems of ordinary differential equations usually appear to be underdetermined even though such investigations assume that the body and shock are concentric. This is a result of the fact that the $(\mu v_n)_n$ term has been retained in the equations. The order of the system is then one greater than the system defined by equations (3.17). Hence, one additional boundary condition or constraint is required to determine the value of $v_n(0)$. It was also noted in Chapter II that keeping

$(\mu v_n)_n$ in the normal momentum equation could lead to difficulties in the formulation of the problem. Thus it is of interest to examine the form that equations (3.17) would take if the $(\mu v_n)_n$ term were included.

In this case, the vector unknown, y, would have eight components since v_n would have to be considered as a separate variable. Several of the equations in (3.17) would change since the normal momentum equation is of the form

$$p_{o_n} + \epsilon^2 \rho_o v_o v_{o_n} = -\mu(T_o)\, v_{o_{nn}}$$ [1]

In particular, the expressions for $\frac{dv_o}{dn}$ and $\frac{dp_o}{dn}$ given in (3.17c) and (3.17d) would be replaced with

$$\frac{dv_o}{dn} = f_3(n,y) = v_{o_n}$$

and

$$\frac{dp_o}{dn} = f_4(n,y) = \frac{p_o T_{o_n}}{T_o} + \frac{p_o}{v_o}\left[\frac{2(u_1 - \epsilon v_o)}{1+\epsilon n} - v_{o_n}\right]$$

The eighth equation would be

$$\frac{dv_{o_n}}{dn} = f_8(n,y) = -\frac{1}{\mu(t_o)}\left[f_4(n,y) + \epsilon^2 \rho_o v_o v_{o_n}\right]$$

[1] The right-hand side of this equation is not complete, but in this form the equation has the same essential features as the more complete equation.

When there is no mass transfer at the wall ($v_o(0) = 0$), the value of $\frac{dp_o}{dn}$ (and therefore $\frac{dv_{o_n}}{dn}$) is infinite at $n = 0$ unless

$$\left(\frac{2(u_1 - \epsilon v_o)}{1 + \epsilon n} - v_{o_n} \right)_{n=0} = 0 .$$

This is consistent with the analysis in Chapter II based on the characteristic surfaces of the governing partial differential equations (page 22). There it was noted that the inclusion of the $(\mu v_n)_n$ term meant that streamlines were characteristics. Thus, for no mass transfer, the body surface is characteristic, and one cannot determine the highest-ordered derivatives normal to the body unless the specified initial data satisfy a compatability equation. It is now seen that the compatibility equation requires

$$2u_1(0) - v_{o_n}(0) = 0 .$$

In the case of no slip at the boundary, this simplifies to a requirement that $v_{o_n}(0) = 0$. This compatability condition is the additional constraint or boundary condition which is used in numerous investigations [19, 21, 24, 28] to make the system of equations determinate. However, it was noted in Chapter II that all difficulties are not removed by this step as there is no guarantee that the solution is unique when the initial data satisfy this compatability relation. Shih and Krupp [30] have computed an alternative solution to one of the

examples considered by Ho and Probstein [19], thus verifying the non-uniqueness of such a formulation of the problem.

In an investigation similar to that of Ho and Probstein, L. Goldberg [17] has considered examples in which there is mass transfer at the wall. In such a case there is no compatability relation at the wall, and the system of differential equations again appeara to be underdetermined. Goldberg uses the integral form of the mass-conservation equation (c.f. equation (2.18)) as the necessary additional constraint. However, in general, this is not an independent condition. If the continuity equation is satisfied throughout the shock layer and all the boundary conditions are properly enforced, the overall mass conservation is assured. An examination of Goldberg's equations shows that in the continuity equation a factor of the form $1+\epsilon n$ has been approximated by unity. This is consistent with the thin-shock-layer model, but a similar approximation in the integral equation has not been made. Thus the relation is independent due to the approximate nature of the continuity equation that is used. The problem is then determinate, and the shock stand-off distance can be computed (a concentric shock interface and body surface had already been assumed).

As noted in Chapter II, Shih and Krupp modify their governing equations in such a way that the special role of the $(\mu v_n)_n$ term is altered. In this manner the difficulties associated with obtaining $v_{o_n}(0)$ are apparently avoided (although this point is not clear). However, they have not assumed a concentric shock and body, thus raising by one the number of boundary conditions needed. This additional relation

is again taken to be the integral form of mass conservation. It is not clear why this equation should give an independent constraint for their analysis, and this point is not discussed by the authors. However, it is probably related to the fact that the shock conditions are applied only at a specified number of stations downstream of the axis of symmetry.

It is quite obvious that in any analysis of the type considered in this chapter the question of the determinacy of the system of differential equations may be rather complicated. For the present analysis it appears to be necessary to make some assumption about the shock slope. Hence ϕ_1 was taken to be zero in the first-truncation problem described above. The use of the integral form of mass conservation gains nothing. If equation (2.18) is expanded, it becomes, for the first-truncation problem for flow around a sphere,

$$(1+\epsilon\Delta_o)^2 = 2\int_o^{\Delta_o} \rho_o u_1 (1+\epsilon n)\, dn \,. \qquad (3.19)$$

If the continuity equation (3.4a) is rewritten in the form

$$\left((1+\epsilon n)^2 \rho_o v_o\right)_n = \rho_o u_1 (1+\epsilon n)$$

and substituted into equation (3.19), equation (3.19) immediately reduces to $\rho_o(\Delta_o)v_o(\Delta_o) = 1$. This result, however, has already been assured by the application of the Rankine-Hugoniot shock conditions.

The computation of the second-truncation problem proceeds in the same manner as did the first-truncation problem. The vector unknown,

y , of equation (3.16) now has thirteen components: $y = (u_1, u_{1_n}, v_o, p_o, p_2, T_o, T_{o_n}, u_3, u_{3_n}, v_2, p_4, T_2, T_{2_n})$. Equations (3.4), (3.5) and (3.10) are reduced to a system of thirteen first-order differential equations. Of the first seven of these equations, all except $\frac{dp_2}{dn} = f_5(n,y)$ are identical to the corresponding equations of the first truncation problem. $\frac{dp_2}{dn}$ must now be obtained from an algebraic combination of equations (3.5a), (3.5c) and (3.5e). Thus the explicit formulation of the second-truncation problem consists of equations (3.17a)-(3.17d), (3.17f), (3.17g) plus the following equations.[1]

$$\frac{dp_2}{dn} = f_5(n,y) = 1 + \left(\frac{\epsilon^2 \rho_o v_o^2}{p_o - \epsilon^2 \rho_o v_o^2}\right) \beta_1(n) - \epsilon^2 v_o \beta_2(n) \qquad (3.20)$$

where

$$\beta_1(n) = \frac{\epsilon \rho_o u_1}{1+\epsilon n}\left[u_1 + \epsilon(2v_2 - v_o)\right] - \epsilon^2\left[\rho_o(v_2 - v_o) + \rho_2 v_o\right] f_3(n,y)$$

and

$$\beta_2(n) = -\frac{\gamma}{\gamma-1}\frac{v_o}{T_o^2}\left(p_2 T_{o_n} - T_2 f_4(n,y) - p_o T_{2_n}\right) +$$

$$\rho_2\left(\frac{2v_o T_{o_n}}{T_o} - f_3(n,y)\right) - \rho_o v_2\left(\frac{f_4(n,y)}{p_o} - \frac{T_{o_n}}{T_o}\right) +$$

$$\frac{2}{1+\epsilon n}\left[\rho_o(2u_3 - \epsilon v_2) + \rho_2(2u_1 - \epsilon v_o)\right]$$

---

[1] The superscript (2), denoting the values obtained from the second truncation, have been dropped for simplicity. It should be remembered, however, that these variables are a second approximation to the correct values of the flow variables. In particular it should be noted that the function $f_5(n,y)$ which appears in equations (3.21c) and (3.21f) is the function $f_5^{(2)}$ defined in equation (3.20) and <u>not</u> the function $f_5^{(1)}$ defined previously in equation (3.17e).

$$\frac{du_3}{dn} = f_8(n,y) = u_{3_n} \tag{3.21a}$$

$$\frac{du_3}{dn} = f_9(n,y) = \frac{1}{\mu(T_o)} \left\{ \left(\rho_2 \cdot \frac{1}{2} \rho_o \right) \left[\frac{u_1}{1+\epsilon n} (u_1 - \epsilon v_o) - v_o u_{1_n} \right] + \right.$$

$$\rho_o \left[\frac{1}{1+\epsilon n} \left(u_1 (4u_3 - \epsilon v_2) - \epsilon v_o u_3 \right) - v_o u_{3_n} - v_2 u_{1_n} \right] +$$

$$\left. \frac{4p_4 - p_2}{1+\epsilon n} \right\} - 2\epsilon u_{3_n} - \frac{\mu'(T_o)}{\mu(T_o)} \left[T_2 \left(f_2(n,y) + 2\epsilon u_{1_n} \right) + \right.$$

$$\left. \left(u_{3_n} - \epsilon u_3 \right) T_{o_n} + \left(u_{1_n} - \epsilon u_1 \right) T_{2_n} \right] - \frac{\mu''(T_o)}{\mu(T_o)} T_2 \left(u_{1_n} - \epsilon u_1 \right) T_{o_n}$$

(3.21b)

$$\frac{dv_2}{dn} = f_{10}(n,y) = \frac{\beta_2(n)}{\rho_o} - \frac{v_o}{p_o} f_5(n,y) \tag{3.21c}$$

$$\frac{dp_4}{dn} = f_{11}(n,y) = \frac{\epsilon \rho_o}{1+\epsilon n} \left\{ u_3 \left[2u_1 + \epsilon (2v_2 - v_o) \right] - 3\epsilon u_1 v_2 \right\} +$$

$$\frac{\epsilon \rho_2 u_1}{1+\epsilon n} \left[u_1 + \epsilon (2v_2 - v_o) \right] - \epsilon^2 (v_2 - v_o) \left[\rho_o f_{10}(n,y) + \right.$$

$$\left. \rho_2 f_3(n,y) \right] - \epsilon^2 \left[\rho_2 v_o f_{10}(n,y) - \rho_o v_2 f_3(n,y) \right] \tag{3.21d}$$

$$\frac{dT_2}{dn} = f_{12}(n,y) = T_{2_n} \tag{3.21e}$$

$$\frac{dT_2}{dn} = f_{13}(n,y) = \frac{c}{\mu(T_o)}\left[v_o f_5(n,y) + \left(v_2 - \frac{1}{2}v_o\right) f_4(n,y) + \right.$$

$$\frac{2u_1}{1+\epsilon n}\left(\rho_o T_o - p_2\right) - \rho_o\left(v_2 - \frac{1}{2}v_o\right)T_{o_n} - v_o\left(\rho_o T_{2_n} + \rho_2 T_{o_n}\right)\Big] -$$

$$\left[2\epsilon T_{2_n} + \sigma u_{1_n}\left(u_{1_n} - 2\epsilon u_1\right)\right] - \frac{\mu'(T_o)}{\mu(T_o)}\left[T_2 f_7(n,y) + \right.$$

$$\left. 2\left(\epsilon + T_{2_n}\right)T_{o_n}\right] - \frac{\mu''(T_o)}{\mu(T_o)} T_2 T_{o_n}^2 \qquad (3.21f)$$

where $\rho_o = \frac{\gamma}{\gamma-1}\frac{p_o}{T_o}$ and $\rho_2 = \frac{\gamma}{\gamma-1}\left[\frac{p_2 T_o - p_o T_2}{T_o^2}\right]$

Despite the complexity of these expressions, they are in a form which is easily evaluated numerically on a computer, given a value of n and the corresponding values of the dependent variables. There are seventeen boundary conditions available from equations (3.6), (3.8), (3.9), (3.11)-(3.13). The conditions at the shock contain an additional five unknowns, Δ_o, Δ_2, Δ_4, ϕ_1 and ϕ_3, which describe the shock shape. Thus the problem is again underdetermined, and some suitable assumption regsrding the shock shape must be made. Unlike the first-truncation problem, setting $\Delta_4 = 0$ does not imply that $\phi_3 = 0$. Hence we can truncate either the shock-position series or the shock-angle series with equation (3.13) supplying the coefficient of the

other series. Since there is no clear choice here, it also seems reasonable to truncate both series, in which case the geometric relation given by equation (3.13) is not satisfied. These various possibilities are considered in the next section. It should be noted that ϕ_1 and Δ_2 are computed in this second-truncation problem. Therefore a check is provided on the accuracy of the assumption that $\phi_1 = \Delta_2 = 0$ in the first-truncation problem.

Now it is necessary to guess seven unknown values at the body surface: $u_{1_n}(0)$, $p_0(0)$, $p_2(0)$, $T_{o_n}(0)$, $u_3(0)$, $p_4(0)$ and $T_{2_n}(0)$. The boundary conditions (3.6a-c) and (3.11a-c) provide the remaining six values. The equations are then integrated numerically until the value of v_o satisfies equation (3.8b). This defines the value of Δ_o. The value of ϕ_1 can be obtained by solving equation (3.12b). Since this equation is quadratic in ϕ_1, two values are obtained. However, it has been found in all of the examples considered thus far that the larger value of ϕ_1 corresponds to a shock of negative curvature ($\frac{d\phi}{ds} < 0$) and thus is unacceptable. The requirement for a positive shock curvature is found by differentiating equation (3.3b). At the axis, a positive curvature requires that $\phi_1 < 1$. After Δ_o and ϕ_1 are determined, there are seven boundary conditions--equations (3.8a), (3.8c)-(3.8e), (3.12a), (3.12c), (3.12d)--which can be used to determine the correct values of the seven guessed initial conditions. The iteration procedure by the Newton-Raphson method now requires the solution of the second-truncation equations an additional seven times for each iteration. Clearly, if many iterations are required to obtain the

correct solution, this procedure will be quite time consuming and hence expensive. Thus it is important to have an accurate guess for the seven initial values in order to reduce the number of iterations that are necessary. The solution to the first-truncation problem provides reasonable values for u_1, v_o, p_o, p_2 and T_o. In order to obtain a first approximation to $u_{3_n}(0)$, $p_4(0)$ and $T_{2_n}(0)$, it is advantageous to solve equations (3.21) using the first-truncation solution to provide values for u_1, v_o, p_o, p_2, and T_o. Except for several terms in the equation for $\frac{dp_4}{dn}$, these equations are linear in u_3, p_4, and T_2. If these nonlinear terms are omitted and if the shock parameters Δ_o, Δ_2, ϕ_1 are kept at the first-truncation values, one iteration on equations (3.21) converges due to the linearity of the problem. This preliminary solution provides an approximation for $u_{3_n}(0)$, $p_4(0)$ and $T_2(0)$ whose accuracy depends on the accuracy of the first truncation. If the first-truncation solution is accurate, this preliminary step described above can result in a considerable reduction in computation time. It will be seen in the next section that the accuracy of the first truncation solution for a common class of problems can be greatly improved by using a more realistic approximation for ϕ_1 than $\phi_1 = 0$.

The time required to solve these equations numerically depends very strongly on the individual problem. Problems for large values of the Reynolds number require more time than those for moderate values of Re. The accuracy of the initial guess for the unknown boundary conditions is also quite important. Typical computation times for the first-truncation solution range from 15 seconds per iteration at $Re_s = 10^2$ to

50 seconds per iteration at $Re_s = 10^4$. For the second-truncation problem these times are 30 seconds per iteration at $Re_s = 10^2$ and 200 seconds per iteration at $Re_s = 10^4$. The number of iterations that are necessary is usually small (two or three) unless the guessed values for the initial data are very poor. The large computation times at large values of Re_s are a consequence of having to maintain a small step size in the integration procedure while integrating across the "inviscid" region of the shock layer, despite the fact that the unknowns do not vary rapidly in that region. This feature appears to be a consequence of solving for the second derivatives u_{nn} and T_{nn} as principle terms. In the outer, "inviscid" region, u_{nn} and T_{nn} must be considerably smaller than the other terms (in boundary-layer theory, they go to zero exponentially as the edge of the boundary layer is approached). If a large number of computations are to be made at large values of Re_s, it may he worthwhile to devise a scheme that will reduce the equations (3.4) and (3.5) to first order in the outer flow.

A possible reduction in computation time may be achieved by originating the integration of the differential equations at the shock instead of at the body surface. For the first-truncation problem it would then be necessary to guess only three initial conditions: Δ_o, $u_{1_n}(\Delta_o)$ and $T_{o_n}(\Delta_o)$. Thus an iteration based on this alternate procedure requires one less solution of the differential equations than does the procedure described earlier. A similar reduction would occur in the second-truncation problem since it would be necessary to guess only six values at the shock in order to initiate the integration.

D. Results

Several examples are considered in this section in order to evaluate the accuracy of the method of solution and the accuracy of the basic flow model. In addition, a comparison of the first- and second-truncation results provides a test of the validity of local similarity.

1. A Comparison to Second-Order Boundary-Layer Theory.

The flow around a sphere at $M_\infty = 10$, $\gamma = 1.4$, $\sigma = 0.7$ and $\mu = T^{1/2}$ is used to test the accuracy of the series-truncation method. For this example, the body temperature is constant at 0.6 of the inviscid stagnation temperature; i.e.,

$$b_o = 0.6 \quad \text{and} \quad b_2 = 0$$

$$\text{where} \quad b = \frac{T_b}{T_{stag.}} = b_o + b_2 \sin^2 s + \cdots \tag{3.22}$$

The results of a boundary-layer analysis by Davis and Flügge-Lotz [12] are used as a standard of comparison for the series-truncation results. These boundary-layer computations were made for both the first- and second-order boundary-layer equations by use of an implicit finite-difference scheme. A numerical scheme of this nature has been shown to provide accurate solutions to the boundary-layer equations. The inviscid pressure distribution on which the boundary-layer computations were based was provided by H. Lomax of the Ames Research Center of NASA. The method of solution for the inviscid flow is described in reference 20 and has been shown to be quite accurate [25]. Thus the solution of the first- and second-order boundary-layer equations

computed by Davis and Flügge-Lotz may be considered to be exact and to provide a standard against which the series-truncation method may be measured.

The results for the shear stress, τ/ϵ (see equations (2.22) and (3.14)), are compared in figure 3.1. In order to have a significant difference between the first- and second-order boundary-layer results, the rather low value of 100 was chosen for the shock Reynolds number, $Re_s = \frac{\rho^*_\infty U^*_\infty a^*}{\mu^*_{sh}}$. Note that the second-order boundary-layer effects decrease the wall shear slightly for this example. Since the truncation results are in the form of a power series centered at the axis, $s = 0$, the results can be expected to agree only near $s = 0$. However, from figure 3.1 it can be seen that the first truncation gives a poor result even at the axis: the curve that represents the first-truncation result has an incorrect slope at $s = 0$. The second-truncation result appears to have the correct slope at $s = 0$, but the agreement does not extend over any significant distance. The second truncation does, however, give a far more accurate solution than does the first truncation.

The shear-stress results can be more precisely evaluated if they are compared to a series solution of the boundary-layer equations rather than to the finite-difference solution shown in figure 3.1. The expression

$$\tau(s,0)/\epsilon = 1.2 \sin s - 0.6 \sin^3 s \qquad (3.23)$$

agrees to $O(s^3)$ with the two-term series solution of the first-order boundary-layer equations presented by Davis and Flügge-Lotz. The

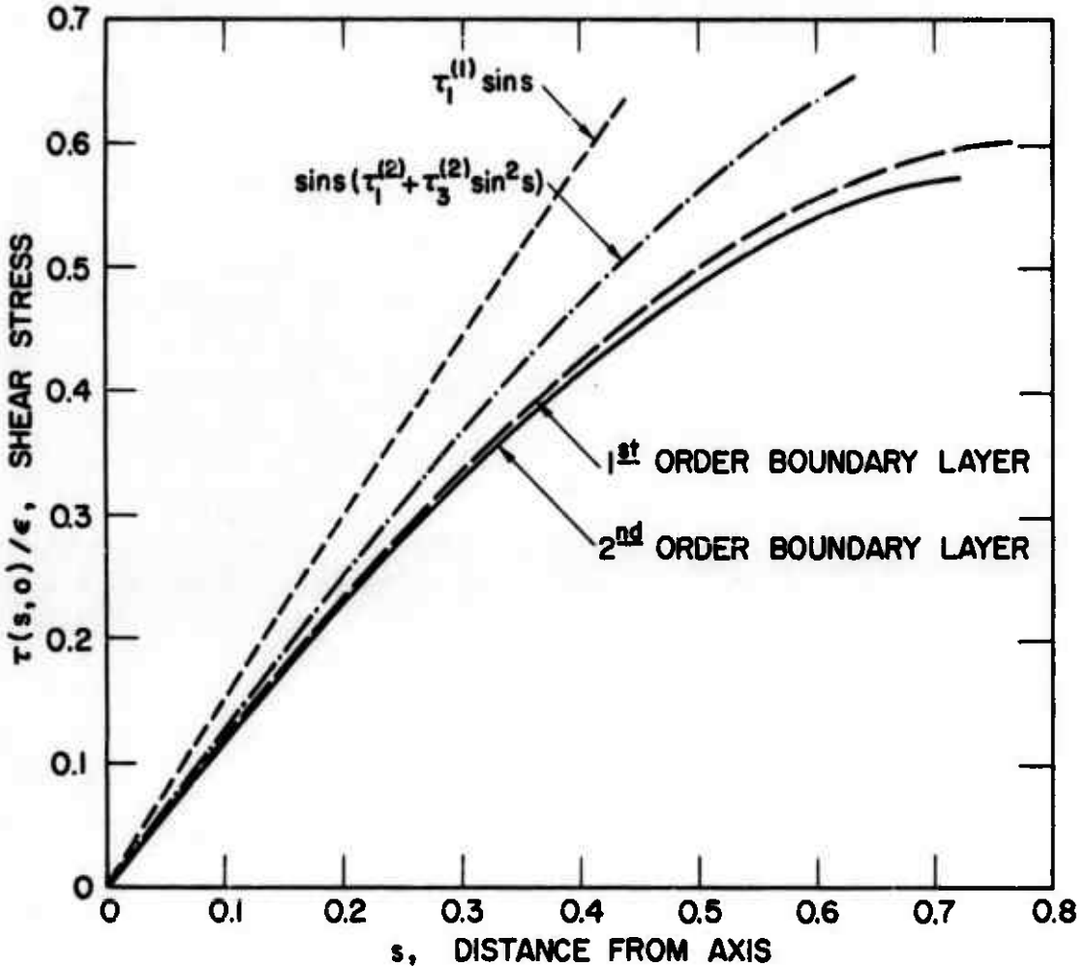

Figure 3.1

Shear stress on a sphere at $\gamma = 1.4$, $M_\infty = 10$, $Re_s^{\sim} = 100$, $b = 0.6$, $\sigma = 0.7$, and $\omega = 1/2$ ($\epsilon = 0.118$); comparison of truncation results with the boundary-layer results of Davis and Flügge-Lotz [12].

second-order boundary-layer effects would decrease the coefficients of this expression slightly. However, in figure 3.1 these effects appear to be smaller than the computational errors associated with the truncation method and are ignored for the moment. The present investigation yields

$$\tau^{(1)}/\epsilon = 1.50 \sin s \tag{3.24a}$$

and

$$\tau^{(2)}/\epsilon = 1.29 \sin s - 0.51 \sin^3 s \tag{3.24b}$$

for the first and second truncations respectively. Thus despite the pronounced improvement of the results shown by the second truncation, there is still an inaccuracy in the value of τ_1. However, it should be noted that these errors are somewhat less than is indicated in figure 3.1: the curve representing the series solution to the boundary-layer equations (equation 3.23) lies above the finite-difference curve shown in figure 3.1 just as the series truncations do.

In contrast to the wall-shear results, the results shown in figure 3.2, for the heat-transfer rate, q/ϵ (see equations (2.23) and (3.15)), agree with the boundary-layer values remarkably well. The first-truncation value is about five percent too high at $s = 0$.[1]

---

[1] The fact that the first-truncation result for q is a constant is a consequence of having expanded the temperature into $T(s,n) = T_o(n) + T_2(n)\sin^2 s + \dots$. If an expansion such as $T(s,n) = T_o(n)\cos^2 s + T_2(n)\sin^2 s + \dots$ had been used, the first-truncation problem would remain the same but would yield $q^{(1)} = \frac{\epsilon}{\sigma} q_o^{(1)} \cos^2 s$. This function would then agree reasonsbly well with the boundary-layer values over a more significant range of values of s.

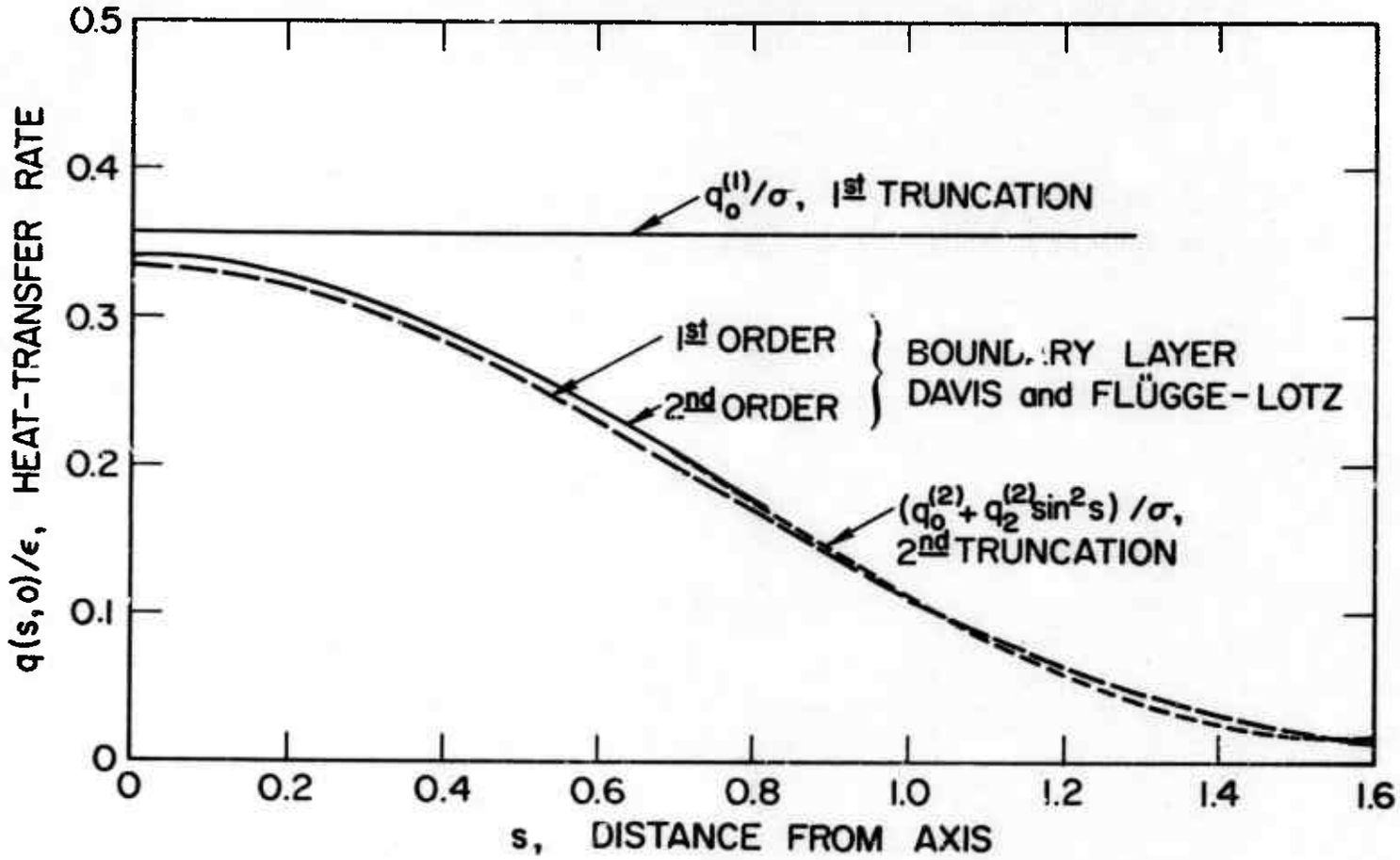

Figure 3.2

Heat-transfer rate on a sphere at $\gamma = 1.4$, $M_\infty = 10$, $Re_s = 100$, $b = 0.6$, $\sigma = 0.7$, and $\omega = 1/2$ ($\epsilon = 0.118$); comparison of truncation results with the boundary-layer results of Davis and Flügge-Lotz [12].

This small inaccuracy in q_o is corrected by the second-truncation computation. In addition, the second-truncation heat-transfer rate, $q_o^{(2)} + q_2^{(2)} \sin^2 s$, agrees extremely well with the second-order boundary-layer result over the entire s-interval for which the boundary-layer result is available.

The relative inaccuracy of the shear-stress values seems to be strongly related to the description of the shock shape. An examination of equations (3.8) shows that a change in the shock angle, ϕ_1, affects the value of u_1 at the shock, i.e., $u_1(\Delta_o)$, but not the values of $T_o(\Delta_o)$ and $p_o(\Delta_o)$. The first-truncation solution of this problem is based on an assumed value of zero for ϕ_1, and it leads to a computed value of 1.085 for the shock standoff distance Δ_o. The second-truncation solution yields calculated values for both ϕ_1 and Δ_o:

$$\Delta_o = 1.232 \quad \text{and} \quad \phi_1 = 0.1236$$

The effect of these changes in the shock shape can be evaluated from figure 3.3 where the first- and second-truncation values of the flow variables u_1, p_o, and T_o are shown. It can be seen that the changes in ϕ_1 and Δ_o influence the value of u_1 across the entire shock layer, but near the body surface the temperature and pressure profiles are affected only slightly by the change in value of Δ_o. For a very cold wall, it may be expected to have a slightly larger effect on the temperature than is shown in figure 3.3. However, from this example, it is evident that the major errors of the first truncation should be expected to occur in the tangential-velocity profile and hence in the

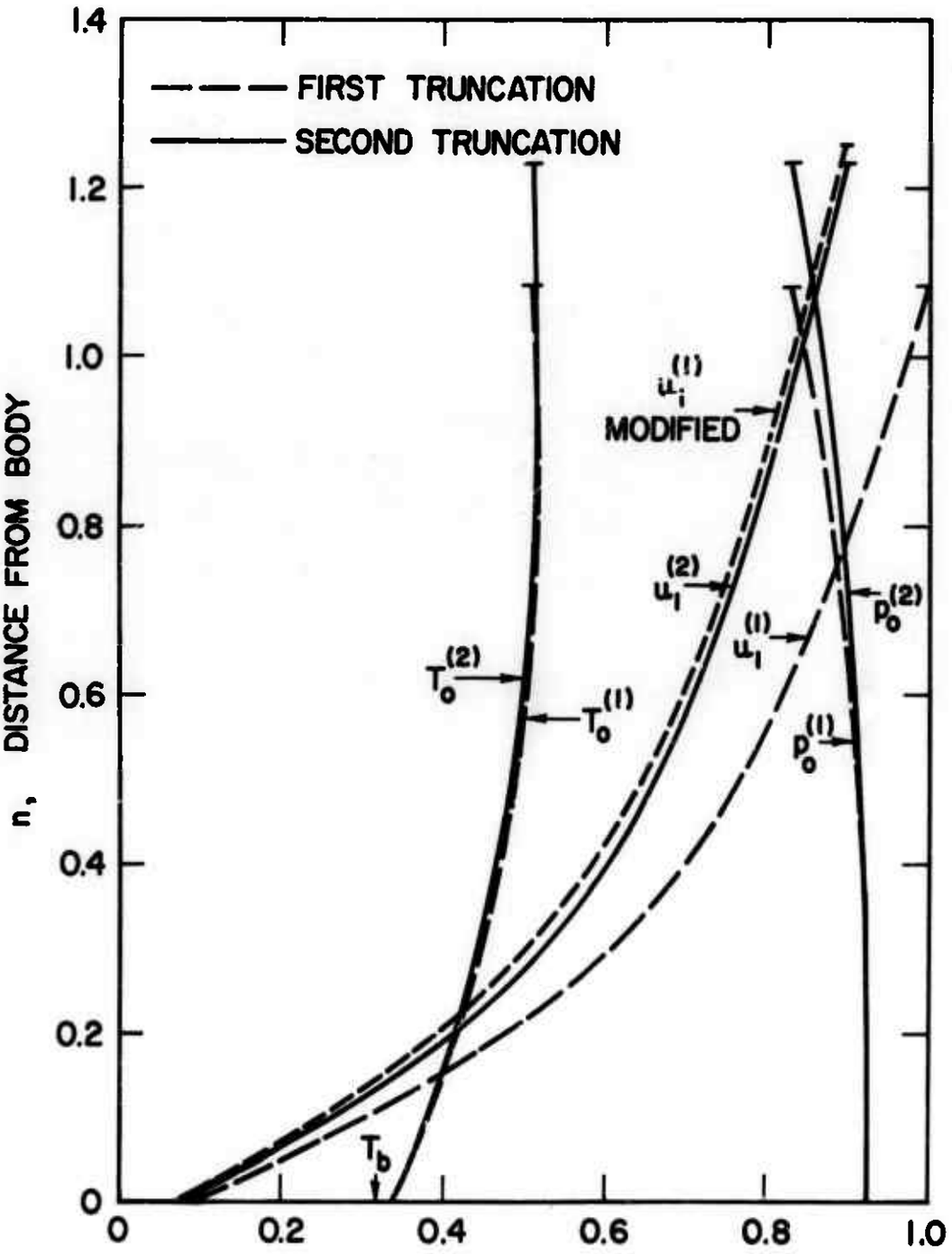

Figure 3.3

Flow variables near the stagnation streamline of a sphere at $\gamma = 1.4$, $M_\infty = 10$, $Re_s = 100$, $b = 0.6$, $\sigma = 0.7$, and $\omega = 1/2$.

wall shear. Further, these errors appear to be primarily a result of truncating the series that describes the shock angle ϕ.

This last assertion requires further verification, however, since the truncation of the "excess" variables from the normal momentum equation is also a source of error. As a check, the first-truncation equations have been re-solved for this example. However, instead of setting $\phi_1 = 0$, the value found from the second-truncation solution is used; i.e., a value of $\phi_1 = 0.1236$ is specified. The resulting tangential-velocity profile is shown in figure 3.3 for comparison. This profile corresponds to a value of 1.22 for $\tau_1^{(1)}$. The temperature profile and the heat-transfer rate do not differ appreciably from the values previously given. It can be concluded that the major error in the first truncation originates from the approximation for ϕ_1; the influence of the truncation of ρ_2 and v_2 from the normal momentum equation, (3.5c), though not negligible, is considerably smaller.

The influence of the shock shape on the second-truncation problem is somewhat more complex. As noted in section C, the second-truncation problem can be made determinate in several ways. The second-truncation results that were presented in figures 3.1-3.3 and in equation (3.24b) were based on an assumption that $\phi_3 = \Delta_4 = 0$. In figure 3.4 the effect of assuming only the value of Δ_4 and computing the consistent value of ϕ_3 from equation (3.13) is shown. Values of ϕ_3, $\tau_1^{(2)}$, and $\tau_3^{(2)}$ are plotted as functions of Δ_4. For comparison, the value of $\tau_1^{(2)}$ and $\tau_3^{(2)}$ given in equation (3.24b) for $\Delta_4 = \phi_3 = 0$ are also shown. As expected, the value of τ_3 is strongly influenced by the choice of Δ_4 since $u_3(\Delta_0)$ is a function of ϕ_3 and thus a

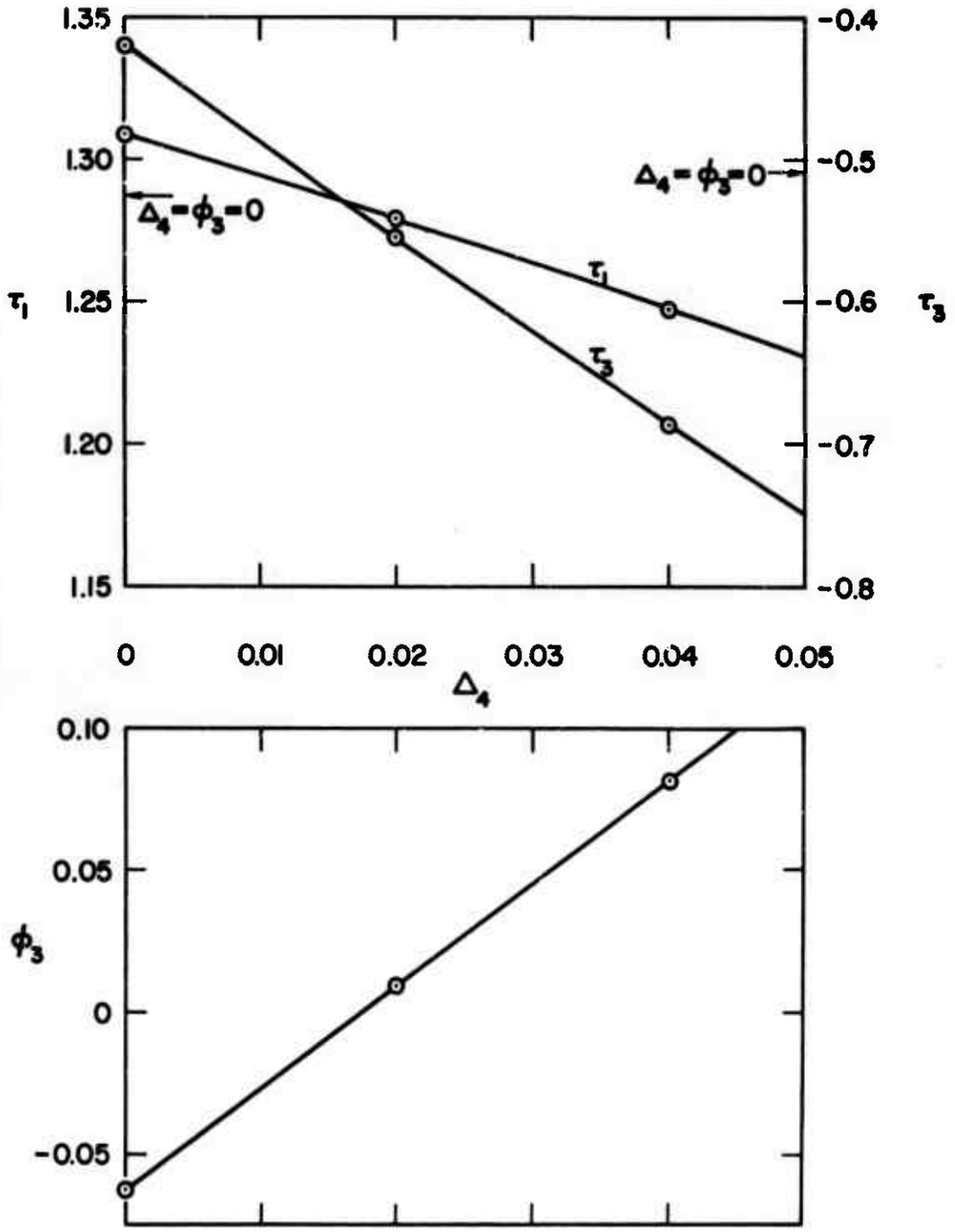

Figure 3.4

Influence of the shock shape on the second-truncation problem; $\gamma = 1.4$, $M_\infty = 10$, $Re_s = 100$, $b = 0.6$, $\sigma = 0.7$, and $\omega = 1/2$.

function of Δ_4 (see equation (3.11a)). More surprising is the noticable influence of Δ_4 on τ_1. However, values of Δ_4 greater than 0.04 begin to have a noticable effect on the heat-transfer results. Hence if the outstanding heat-transfer results were not simply fortuitous, the shock errors alone do not account for all the difference between the boundary-layer results and the second-truncation solution.

It should be noted that at low Reynolds numbers the present formulation of the problem cannot be expected to yield results that are identical to those of the second-order boundary-layer theory. Although the equations of Chapter II are uniformly valid to $O(\epsilon)$ throughout the shock layer and thus contain all second-order boundary-layer effects, the current formulation does not isolate these effects and analyze each one separately as is done in boundary-layer theory. Consequently, the present formulation contains some higher-order effects that are not contained in the second-order boundary-layer results. These differences in the two formulations of the problem are $O(\epsilon^2)$ and can be expected to diminish as the Reynolds number is increased.

The variation with Reynolds number of the ratio of the wall shear to the first-order boundary-layer wall shear is shown in figure 3.5. It can be seen that the second-truncation results do indeed approach the boundary-layer results as the Reynolds number is increased, but somewhat slowly. At a Reynolds number of 10^3, $\epsilon = 0.037$ and the difference between the two formulations should be $O(10^{-3})$. At $Re_s = 10^2$, the difference should be $O(10^{-2})$. Yet, in both cases, the actual differences in the shear-stress values are about an order of magnitude larger than

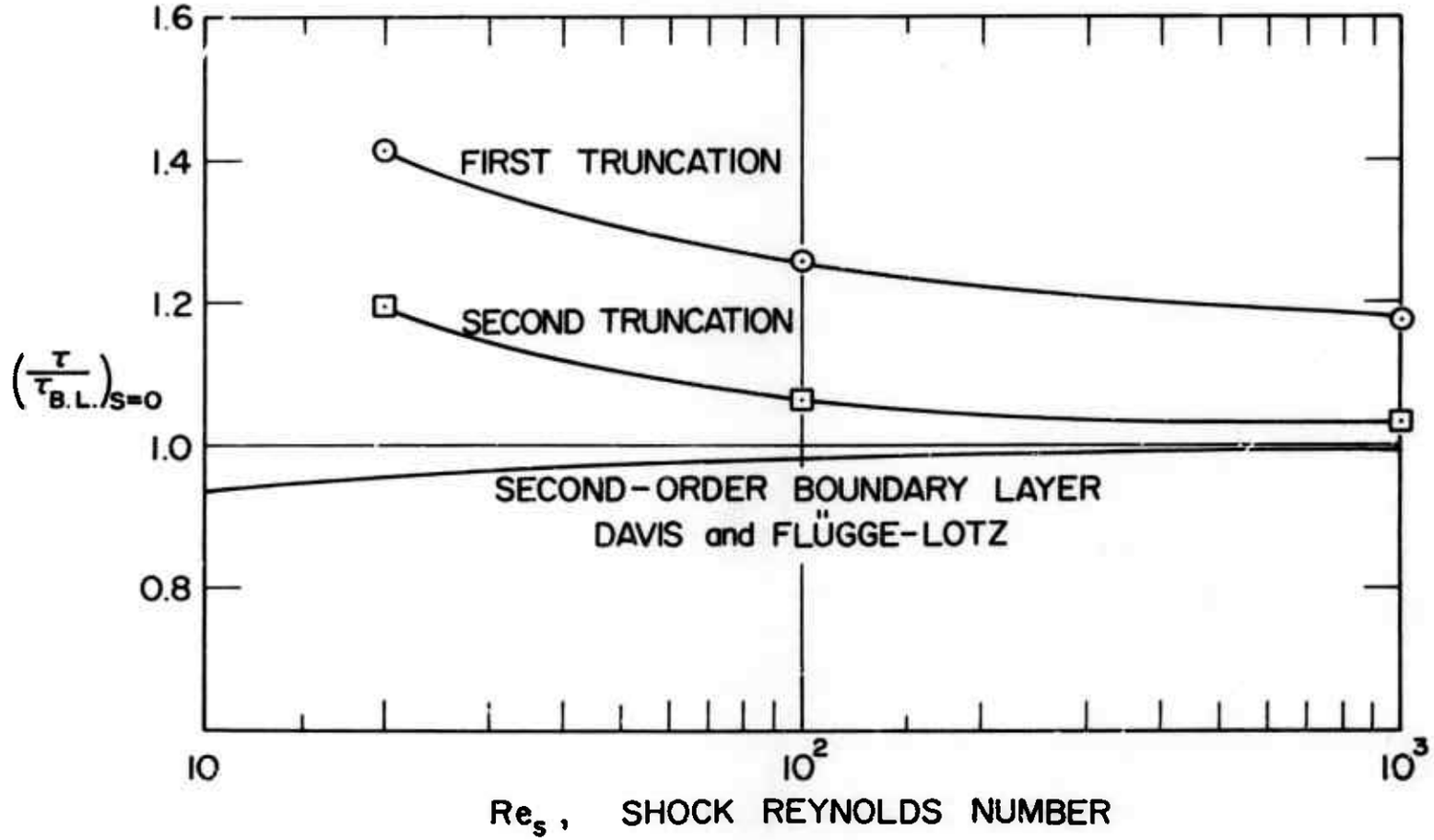

Figure 3.5

Variation of the stagnation-point shear stress with the shock Reynolds number; $\gamma = 1.4$, $M_\infty = 10$, $b = 0.6$, $\sigma = 0.7$, and $\omega = 1/2$.

expected. Note, however, that the difference is only a few percent at the larger values of Re_s and is within the variation due to the uncertainty about the shock shape.

Accepting the accuracy of the results of Davis and Flügge-Lotz, we arrive at the following conclusions.

a. The first truncation results are considerably less accurate than those of the second truncation, even at the axis of symmetry.

b. The heat-transfer rate is determined quite accurately, but significant errors occur in the values of shear stress.

c. The error in the shear-stress values is primarily due to the sensitivity of the tangential velocity to approximations for the shock shape.

d. The errors due to the truncations increase as the Reynolds number is decreased.

2. Local Similarity

The results of the first example, particularly those shown in figure 3.5, are of interest for an evaluation of the results of local-similarity analyses, e.g. Ho and Probstein [19], Probstein snd Kemp [28], and Goldberg [17]. In each of these investigations, comparisons to boundary-layer results much like those in figure 3.5 are presented. In each case the low-Reynolds-number results are qualitatively very similar to those presented above; that is, the shear-stress values are found to be considerably larger than predicted by first-order boundary-

layer theory. Further, the method of analysis that is used in these investigations is very similar to the first-truncation analysis. The variables have been assumed to be "locally similar" in the region of the axis and hence are assumed to be adequately described by expressions such as $u = s\, u_1(n)$, $v = (1 - \frac{1}{2} s^2)\, v_o(n)$, $p = (1-s^2)\, p_o(n) - \frac{1}{2} s^2\, p_2(n)$, etc. The similarity to the expressions used in the first truncation is evident. In addition, these investigations have assumed that the body and shock are concentric ($\epsilon_1 = 0$), a fact that has been shown to be of considerable importance. The results of the first example of this section imply that a portion of the divergence from boundary-layer theory found in these investigations is a consequence of the method of analysis and not a property of the low-Reynolds-number flow. That is, the use of the method of local similarity leads to errors which exaggerate the differences with the results of boundary-layer theory.

A verification of the above conclusions by a direct comparison of the results of a series-truncation analysis to those of the local-similarity analyses is somewhat difficult. The series-truncation analysis has been applied to the problem defined by Ho and Probstein, i.e., $\gamma = \frac{11}{9}$, $M_\infty = \infty$, $\sigma = 0.71$, $b_o = 0.05$, $b_2 = 0.0$, $\mu = T^{1/2}$, and no-slip boundary conditions at the body surface. However, Goldberg gives only a range of values of flight velocities, altitudes, and body temperatures at which his computations were made. Thus there is some uncertainty about what values of Mach number, Prandtl number, and body temperature should be used in the series-truncation analysis for comparison with his results. However, Goldberg does present a result

for $\frac{\rho_\infty}{\rho_{sh}} = 0.10$, which corresponds to the choice of $\gamma = \frac{11}{9}$ above, and he specifies no-slip boundary conditions. Further, for large values of the Mach number, the precise value of M_∞ should have only a minor effect; and the normalization of the results with respect to first-order boundary-layer values, as was done by Goldberg, should minimize the influence of the unknown parameters. Hence a comparison of the shear-stress results of Goldberg, Ho and Probstein, and the series-truncation method is given in figure 3.6. The results of Ho and Probstein and of the series truncation have been normalized by $\tau_{B.L.} = 1.11\sqrt{Re_s}\sin s + \cdots$. This function was obtained from reference 19 and is based on an inviscid pressure gradient that was obtained from a thin-shock-layer analysis. Interpretation of these results is complicated by the general lack of agreement among the several results.

Goldberg's results illustratc two effects not contained in the other results. First, as the shock density ratio, $\frac{\rho_\infty}{\rho_{sh}}$, becomes smaller (requiring $\gamma \to 1$), there is a greater deviation from the first-order boundary-layer values (note that the choice of $(\frac{\rho_\infty}{\rho_{sh}})^3 Re_s$ as the abscissa in figure 3.6 reduces the appearance of this effect). This is to be expected since the shock layer becomes thinner and the second-order displacement-thickness effect becomes more pronounced than it was in the first example of this section. Second, Goldberg's results show a decrease in the shear stress at very low Reynolds numbers. This decrease is a consequence of having used a modified set of shock conditions which account for the thickening of the shock. The truncation results and those of Ho and Probstein are based on the Rankine-Hugoniot

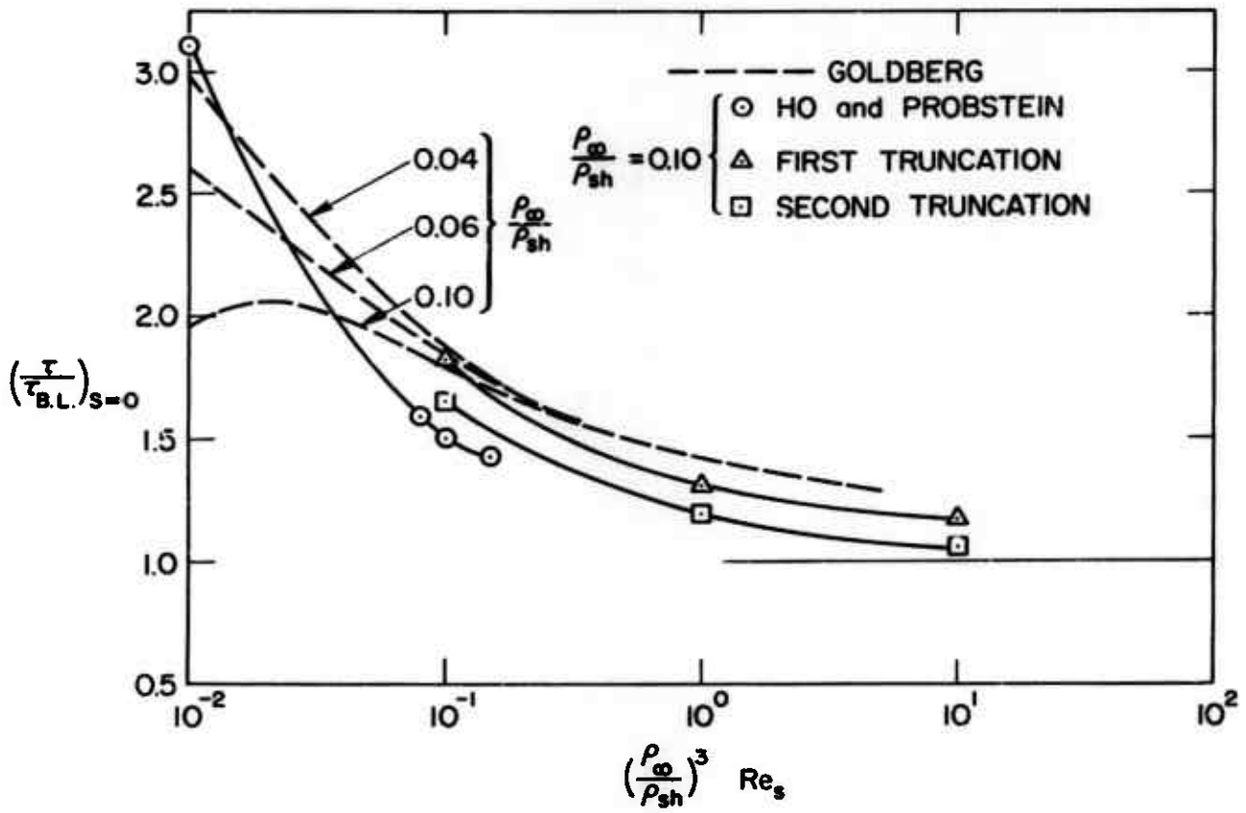

Figure 3.6

Stagnation-point shear stress from the series-truncation method and Ho and Probstein [19] -- $\gamma = 11/9$, $M_\infty = \infty$, $b = 0.05$, $\sigma = 0.71$, $\omega = 1/2$, and no-slip boundary conditions $\frac{\rho_\infty}{\rho_{sh}} = 0.10$ -- and from Goldberg [17] -- $\frac{\rho_\infty}{\rho_{sh}} = 0.10$, 0.06, 0.04; Sutherland viscosity law; and no-slip boundary conditions.

shock relations and thus do not exhibit this effect.

The agreement between the first truncation and Goldberg's result for $\frac{\rho_\infty}{\rho_{sh}} = 0.10$ is actually fairly good considering the uncertainty about some of the flow conditions. At $Re_s = 10^4$, Goldberg's results (when slightly extapolated) predict a shear stress which is about 25 percent higher than the boundary-layer value, and the first-truncation solution is about 17 percent higher. In addition, computations have shown that approximating factors of $1+\epsilon$ by unity, as done by Goldberg, reduces the difference between these two results by about one fourth.

The second-truncation results are qualitatively the same as they were in the first example. The decrease in wall shear below the first-truncation values is somewhat less than it was before, but is still substantial. In fact, at $Re_s = 10^4$, the second-truncation result is only six percent higher than the boundary-layer value (compared to 25 and 17 percent cited above). Since the displacement-thickness effect is larger for this example than it was for the first example of this section, the total second-order boundary-layer effect can be expected to be positive, unlike the result shown in figure 3.5. As anticipated, the second-truncation results provide a much better agreement with the boundary-layer values than the results of a local-similarity analysis do.

A comparison to the results of Ho and Probstein, however, is not conclusive since the results of the first truncation and those of Ho and Probstein are not in agreement. The reasons for this difference are not fully understood. Approximately one third of the difference (at $Re_s = 100$) is the result of the omission of the viscous terms

$\epsilon\kappa\mu' u\, T_n$ and $\epsilon\mu(\kappa + j\,\frac{\sin\theta}{r})u_n$ from the tangential momentum equation (see equation (2.3)) by Ho and Probstein.[1] On the other hand, they retain several viscous terms in the normal momentum and energy equations which are not included in equations (2.4) or (2.5). The influence of all these terms except those that are proportional to $(\mu v_n)_n$ has been investigated and has been found to change the results by less than one percent. The effect of $(\mu v_n)_n$ was not checked since the computational difficulties described earlier in this chapter would require extensive modification of the computational procedures. Thus the major part of the difference is unexplained.

However, it should be noted that the pressure distribution across the shock layer computed by Ho and Probstein differs radically from the truncation result for pressure. In all the examples that have been computed, the inviscid pressure mechanisms which are included in equation (2.4) yield pressure distributions like that shown in figure (3.3); i.e., the pressure increases monotonically from the shock to the body surface. In contrast, the computations of Ho and Probstein yield a pressure distribution that has a rather steep drop immediately behind the shock before increasing to the surface value (for an example, see figure 3.7). As pointed out by Shih and Krupp [30], this decrease in pressure, which is apparently a result of viscous effects, is suspect because one does not expect the viscous forces to be larger immediately behind the shock than near the body surface. The investigation by Kao [21] has yielded

---

[1] The term $\frac{\epsilon\mu}{\sigma}(\kappa + j \sin\theta/r)T_n$ is also omitted from the energy equation. This term has a significant influence only on the heat transfer, however.

a similar pressure distribution, but Levinsky and Yoshihara [24] and Goldberg have obtained pressure distributions that do not show this effect despite their use of equations that are quite similar to those used by Ho and Probstein.

It may be possible, of course, that the method of local similarity yields a more accurate solution to the equations of reference 19 than it does to those of Chapter II. However, it seems more likely that a series-truncation analysis of the equations used by Ho and Probstein would yield results like those exhibited in the two examples considered in this section; i.e., the local similarity, or first truncation, results would be significantly improved at the axis by the more complete analysis of the second truncation. This conclusion is further substantiated by the following discussion of the analysis by Kao: Kao's results are similar to those of Ho and Probstein, and it will be shown that, in general, his analysis should yield substantial differences between the first- and second-truncation results.

3. Influence of the Body Temperature

The results that have been described above appear to be in contradiction to the results of an investigation by H.C. Kao [21]. He solved the Navier-Stokes equations by use of the method of series truncation and found very little difference between the results of the first and second truncations. Hence he concluded that the method of local similarity was valid (in the sense that it yields correct values for the first term of a more complete series solution). The contradiction, however,

is more apparent than real and can be resolved by a comparison of the computational procedure of Kao to that used in this chapter.

The truncation procedure used in this chapter has been adapted from Kao's analysis, and hence the two formulations of the problem are quite similar. However, since Kao solved the inverse blunt-body problem, the location of the body surface appears as an unknown quantity instead of the shock location. In the integration of the equations inward from the shock, the location of the body can be determined from one of the wall boundary conditions. However, Kao adopted an alternative procedure of specifying the body location in which case the surface temperature cannot be imposed as a boundary condition but must be considered to be a result, much like the shear stress and heat transfer. More specifically, if both T_{b_2} (see equation (3.7)) and the body location away from the axis of symmetry are specified in the second-truncation problem, the equations are over-determined. Hence, Kao specifies that the body and shock be concentric and obtains, as part of his solution, the temperature distribution of the body surface. Thus Kao's conclusion about local similarity is valid only if the temperature of the body is such that the body and the shock are concentric.

The temperature distribution which produces this spherical symmetry is one in which the body is strongly cooled downstream of the axis of symmetry. Kao solved the problem defined by $\gamma = \frac{11}{9}$, $M_\infty = 10$, $Re_s = 10$, $\sigma = 0.7$, $b_o = 0.048$, and no-slip boundary conditions. The resulting temperature distribution is given by $b_2 = -0.516$. When the present series-truncation analysis is applied to this problem (with b_2

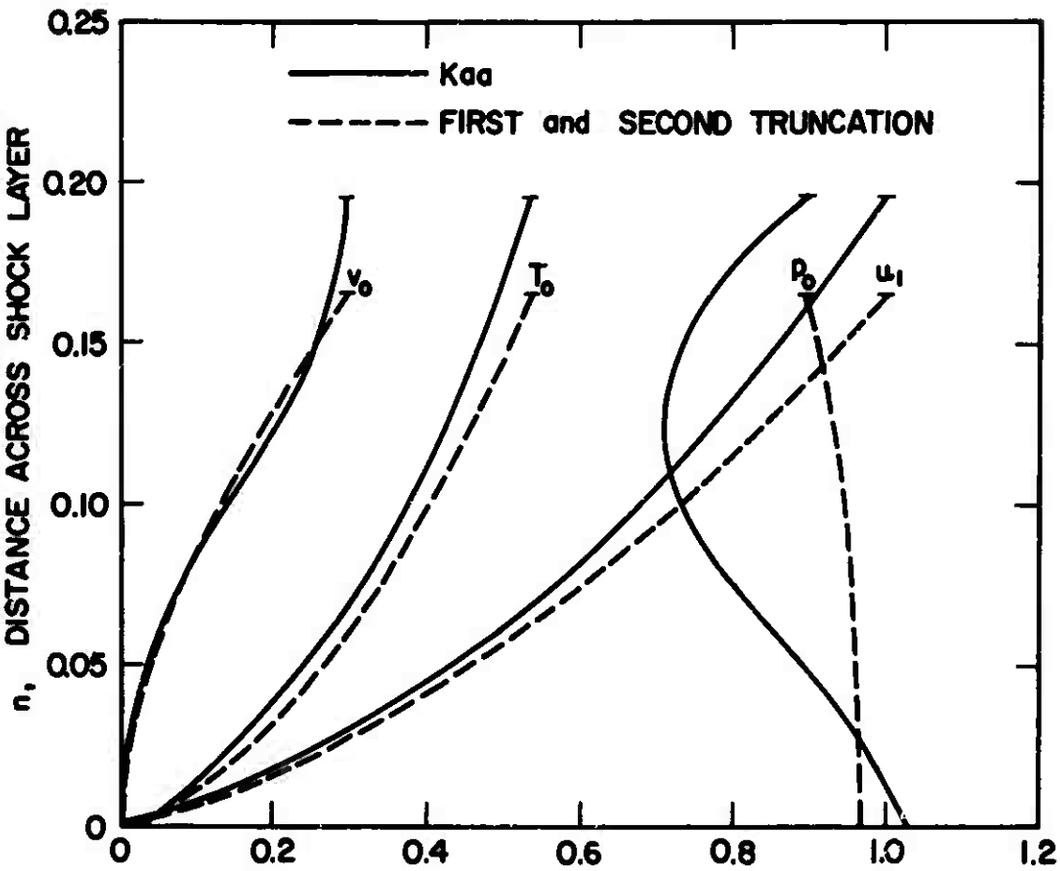

Figure 3.7

Comparison with the flow variables computed by Kao [21];
$\gamma = 11/9$, $M_\infty = 10$, $Re_s = 10$, $b_0 = 0.048$, $b_2 = -0.516$,
$\sigma = 0.7$, $\omega = 1/2$, and no-slip boundary conditions ($\epsilon = 0.369$).

specified as -0.516), it is found that the equations of Chapter II yield a nearly spherically symmetric problem for this temperature distribution (more specifically, we obtain $\frac{\Delta_o^{(2)}}{\Delta_o^{(1)}} = 1.003$ and $\phi_1^{(2)} = 0.0036$). Despite this agreement with the results of Kao, the flow variables obtained from these two solutions do not agree well, as seen in figure 3.7. The choice of $Re_s = 10$ is undoubtedly outside the range of validity of the basic flow model of this investigation (note that the viscous effects extend across the entire shock layer). Further, the radically different pressure distributions that were discussed with regard to the previous example are also encountered here and preclude the possibility of making more than a brief comparison.

The influence of the downstream temperature distribution has also been investigated for the flow problem defined in the first example; i.e., $\gamma = 1.4$, $M_\infty = 10$, $Re_s = 100$, $\sigma = 0.7$, and $b_o = 0.6$. In figure 3.8a, the variation of τ_3 and q_2 with b_2 is shown. As is to be expected, the values of τ_3 and q_2 are strongly dependent upon the value of b_2. In addition, however, the results of these computations clearly show the presence of an upstream influence in the flow since τ_1, q_o, and Δ_o are significantly influenced by the downstream wall temperature. These quantities are shown in figure 3.8b where they have been normalized by their respective values computed in the first truncation. Also shown is the value of ϕ_1. In the first-truncation computation, the value of b_2 is of no concern. If no coupling occurred between different-ordered coefficients of the series expansions (equations (3.1)), the first-truncation results would be valid for all

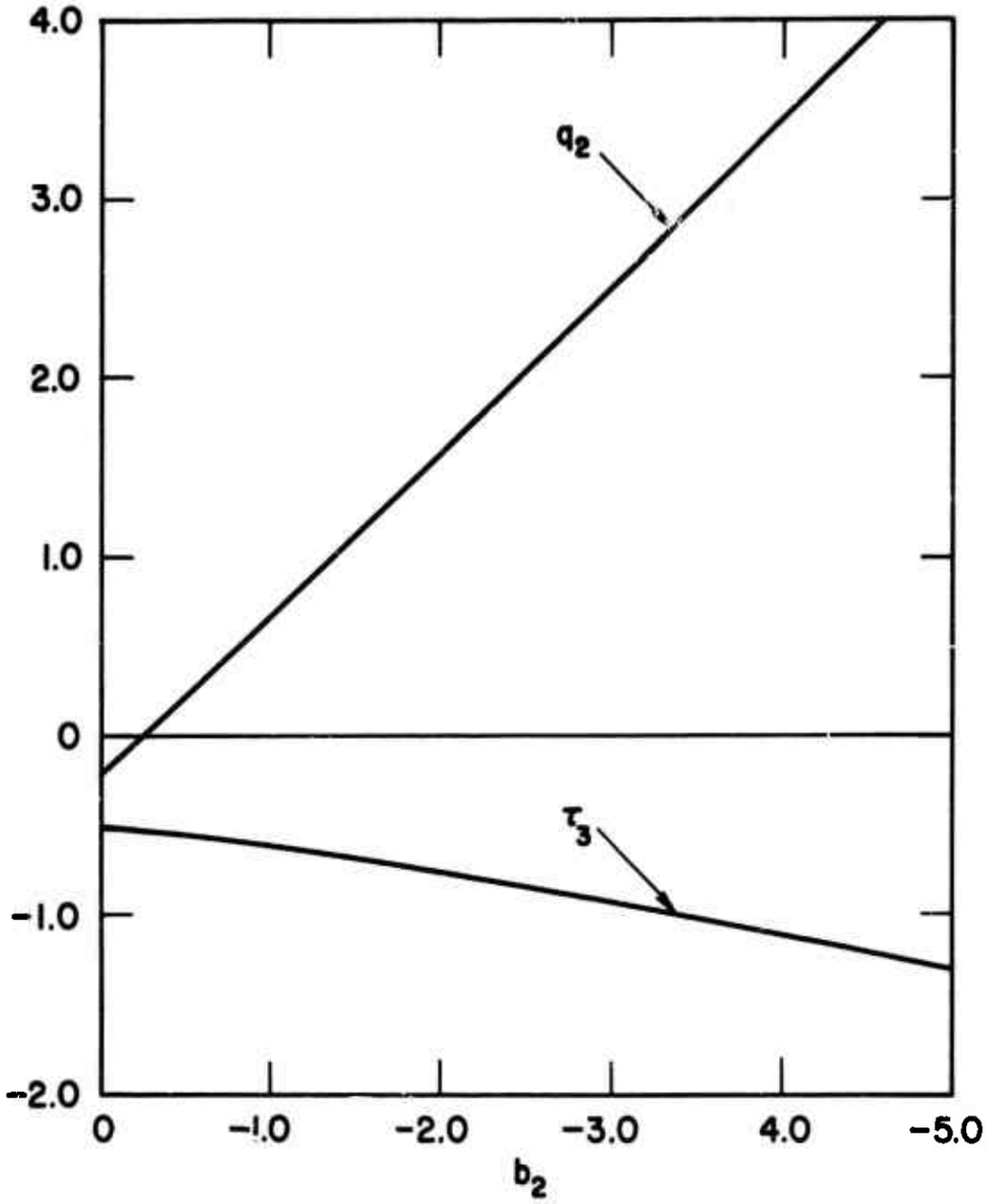

Figure 3.8a

Influence of the downstream body temperature (at $\gamma = 1.4$, $M_\infty = 10$, $Re_s = 100$, $\sigma = 0.7$, and $\omega = 1/2$) on the second coefficients of the expansions for the shear stress and heat-transfer rate.

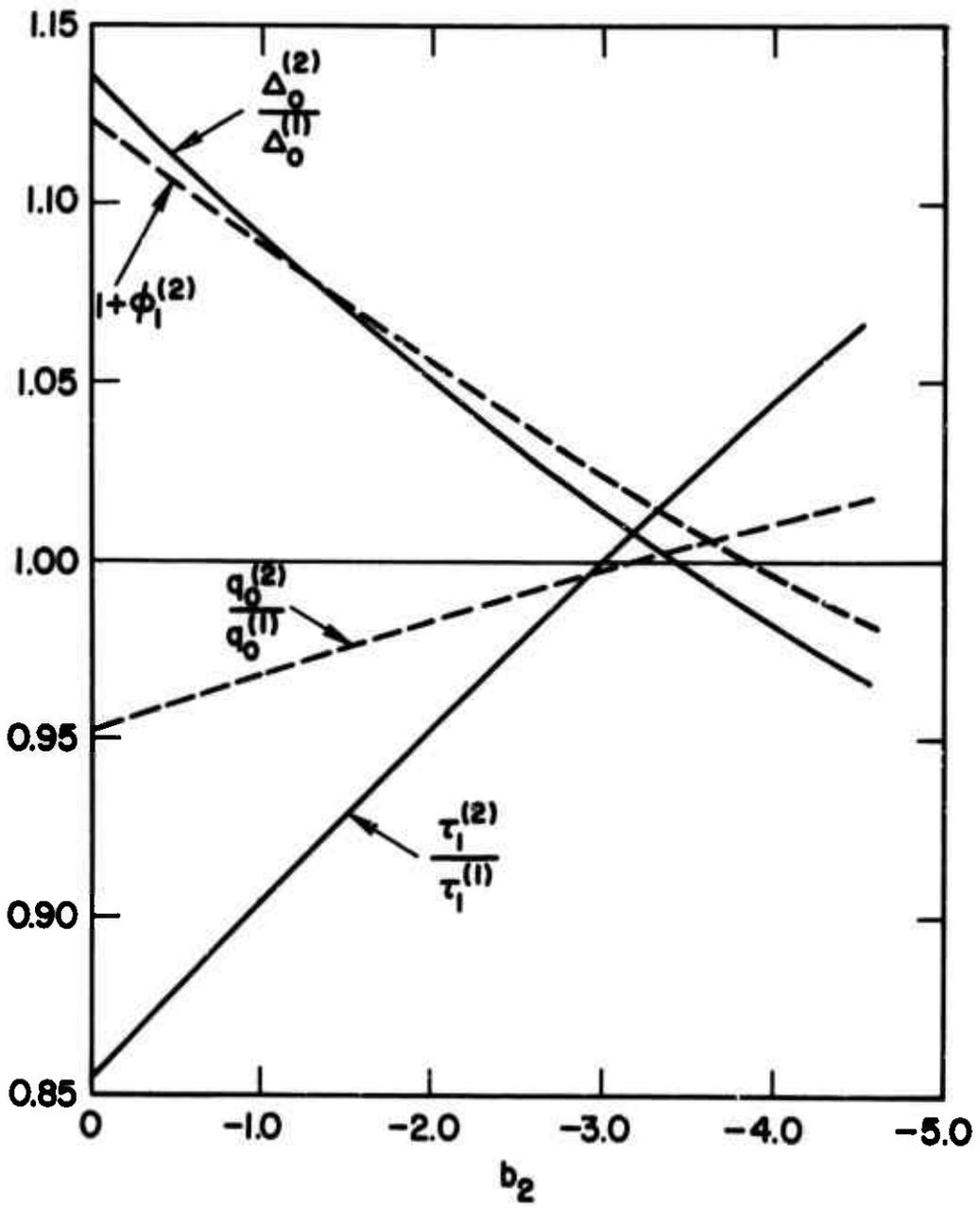

Figure 3.8b

Influence of the downstream body temperature (at $\gamma = 1.4$, $M_\infty = 10$, $Re_s = 100$, $\sigma = 0.7$, and $\omega = 1/2$) on the shock shape, and the first coefficients of the expansions for the shear stress and heat-transfer rate.

values of b_2. Hence the deviation of these normalized quantities from a value of 1 represents an error in the first truncation due to an upstream influence in the flow. It can be seen that the magnitude of this error depends on the value of the downstream temperature, i.e., on b_2. For the case of $b_2 \sim -3.8$, the body and shock are essentially concentric since $\phi_1 \sim 0$. For this case, our computation is equivalent to the computational method used by Kao. It can be seen that the changes in shear stress, heat transfer, and shock standoff distance are considerably smaller than they are for the constant wall-temperature case. The smallest changes occur at slightly larger values for b_2 and ϕ_1, but it is obvious that the overall agreement between the first- and second-truncation results is considerably improved by requiring the shock and body to be concentric. Hence, as before, we find that there is a temperature distribution that yields a spherically symmetric flow, and for this case, the local-similarity analysis is fairly accurate. However, the required temperature distribution differs quite markedly from the constant wall temperature which is commonly used as a boundary condition.

It has also been found that the specification of an adiabatic wall condition leads to results much like those obtained from a constant wall temperature. Specifying adiabatic conditions with the flow parameters of the above example leads to a temperature distribution of $b = 0.989 - 0.100 \sin^2 s$. The magnitude of the changes between the first and second truncations are described by $\frac{\Delta_o^{(2)}}{\Delta_o^{(1)}} = 1.138$, $\phi_1 = 0.128$, and $\frac{\tau_1^{(2)}}{\tau_1^{(1)}} = 0.851$.

In summary, we conclude that the results of the method of local similarity are accurate if the geometry of the flow boundaries has a spherical symmetry. However, the most commonly used boundary conditions on the temperature, an adiabatic wall and a constant wall temperature, do not correspond to flows having such symmetry.

4. Influence of the Shock Thickness

The simplification of the Navier-Stokes equations made in Chapter II and the use of the Rankine-Hugoniot shock relations restrict the accuracy of the flow model at very low Reynolds numbers. A comparison to the results of Levinsky and Yoshihara [24] provides some insight into the range of validity of the flow model used in this investigation. The equations that are used in reference 24 are also a simplified form of the Navier-Stokes equations, similar to those used in references 19 and 28. Since these equations omit several terms of $O(\epsilon)$ (see page 80), they cannot be expected to test the validity of the omission of terms of $O(\epsilon^2)$ from equations (2.2)-(2.7). However, more important is the fact that no discontinuous shock is used in the formulation of the flow model by Levinsky and Yoshihara. Instead, the differential equations are applied from the body to the free stream, and the effect of a thickening shock at low Reynolds numbers is obtained. Although we have noted that the method of solution which is used -- the method of local similarity -- may not be particularly accurate, we have seen that it is equivalent to the first-truncation analysis, and therefore meaningful comparisons can be made. In addition, an inability to

adequately describe the shock shape has been shown to be responsible for much of the inaccuracy of the first truncation. Hence, it is of interest to investigate whether similar inaccuracies occur when the flow model does not contain a discontinuous shock.

The problem considered by Levinsky and Yoshihara is defined by $\gamma = \frac{5}{3}$, $M_\infty = 10$, $\sigma = 0.75$, $\mu = T^{1/2}$, and no-slip boundary conditions. Both cold walls and adiabatic walls were considered. Three values of the free-stream Reynolds numbers were used: 13,652; 1,382; and 152. These values correspond to a shock Reynolds number of 2409, 244, and 26.8, respectively. The first-truncation analysis of this chapter has been applied to the adiabatic wall case, and the results are shown in figures 3.9 a-c. The functions shown in these figures were defined by Levinsky and Yoshihara and are given in terms of the truncation variables by

$$\bar{u} = u_1 \ , \ \bar{v} = \epsilon v_o \ , \ \bar{p} = \frac{p_o}{\rho_{AW}} \ , \ \bar{p}_2 = \frac{p_o + p_2}{\rho_{AW}}$$

where ρ_{AW} is the stagnation-point density for adiabatic wall conditions. The last relation above is a consequence of the pressure being represented by an expression of the form $p(s,n) = \rho_{AW}[\bar{p}(n)\cos^2 s + \bar{p}_2(n)\sin^2 s]$ in reference 24 (compare to equation (3.1c)).

At the largest value of Reynolds number considered, $Re_s = 2409$, the results of Levinsky and Yoshihara exhibit a very thin shock-transition region and a distinct separation of a narrow, viscous boundary layer from the main region of inviscid flow (figure 3.9a). The first-truncation results agree reasonably well except for the location of

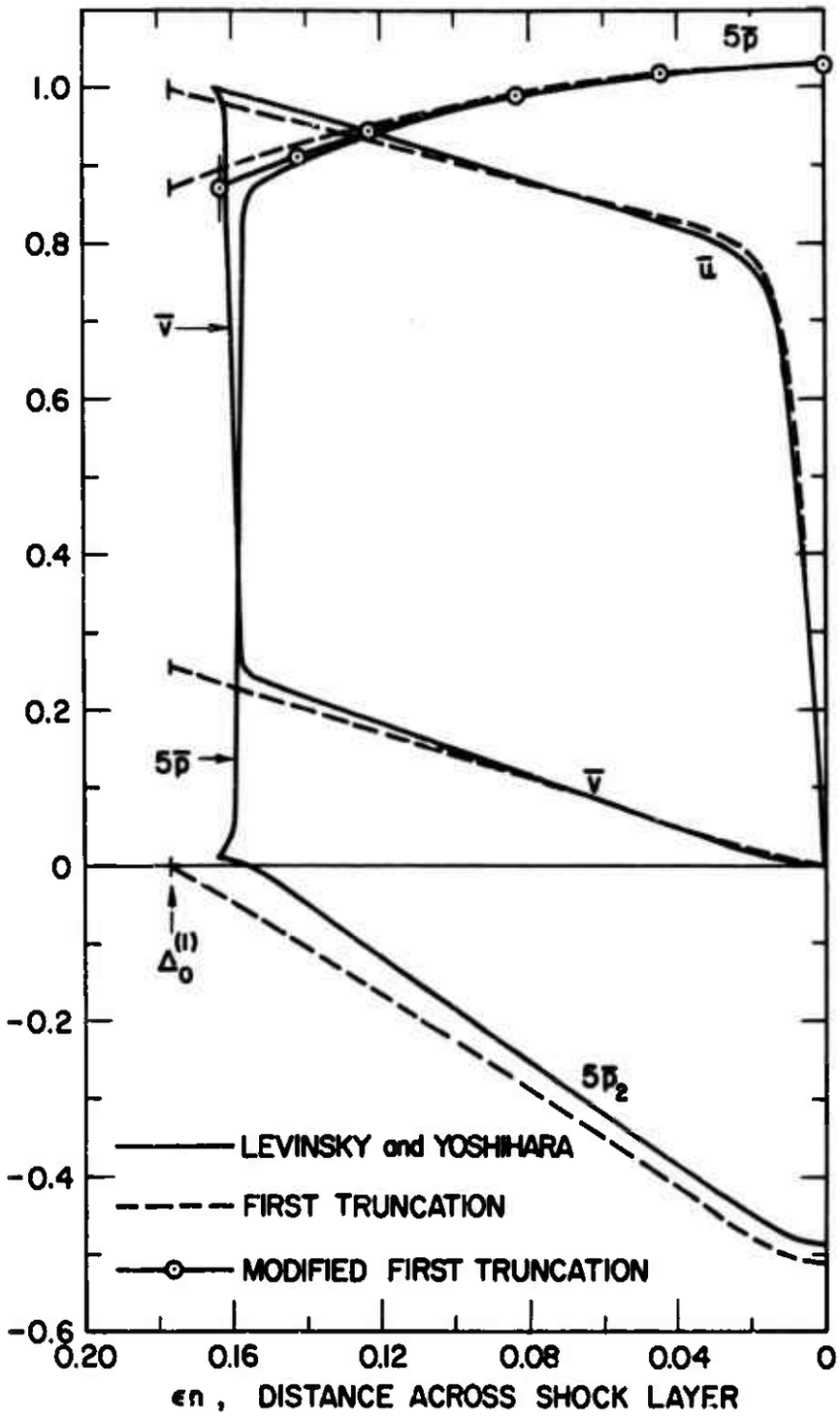

Figure 3.9a

Comparison with the results of Levinsky and Yoshihara [24] at $\gamma = 5/3$, $M_\infty = 10$, $\sigma = 0.75$, $\omega = 1/2$, adiabatic wall, no-slip boundary conditions, and $Re_s = 2409$ ($\epsilon = 0.024$).

the shock. This discrepancy has been found to be a result of an approximation, $1 + \epsilon n \sim 1$, which was used in the equations of reference 24. When this approximation is made in the first-truncation problem, the shock position corresponds to the outer edge of the shock-transition region obtained by Levinsky and Yoshihara. This has been illustrated in figure 3.9a by the results for the pressure. Hence, as is to be expected, the agreement is quite good at large Reynolds numbers since the shock thickness is quite small. Unless otherwise noted, the series-truncation computations that follow do not use the approximation $1 + \epsilon n \sim 1$.

At $Re_s = 244$, the shock has thickened considerably, and the "boundary-layer" is a substantial portion of the shock layer, as shown in figure 3.9b. The variables still match rather well, however, except for the details of the shock-transition region; the effects of the thickening of the shock do not appreciably alter the flow in the viscous layer. The results cited earlier in this section have shown that the assumption of $\phi_1 = 0$ in the first truncation is quite influential. The good agreement shown in figure 3.9b indicates that an analogous assumption must be inherent to the analysis by Levinsky and Yoshihara despite the fact that there is no discontinuous shock in their flow model. The second-truncation solution is again significantly different from the first-truncation solution, as is shown in figure 3.9b by the result for the tangential velocity.

At $Re_s = 26.8$, the shock-transition region and the "boundary layer" have merged, as shown in figure 3.9c; and, of course, the model defined

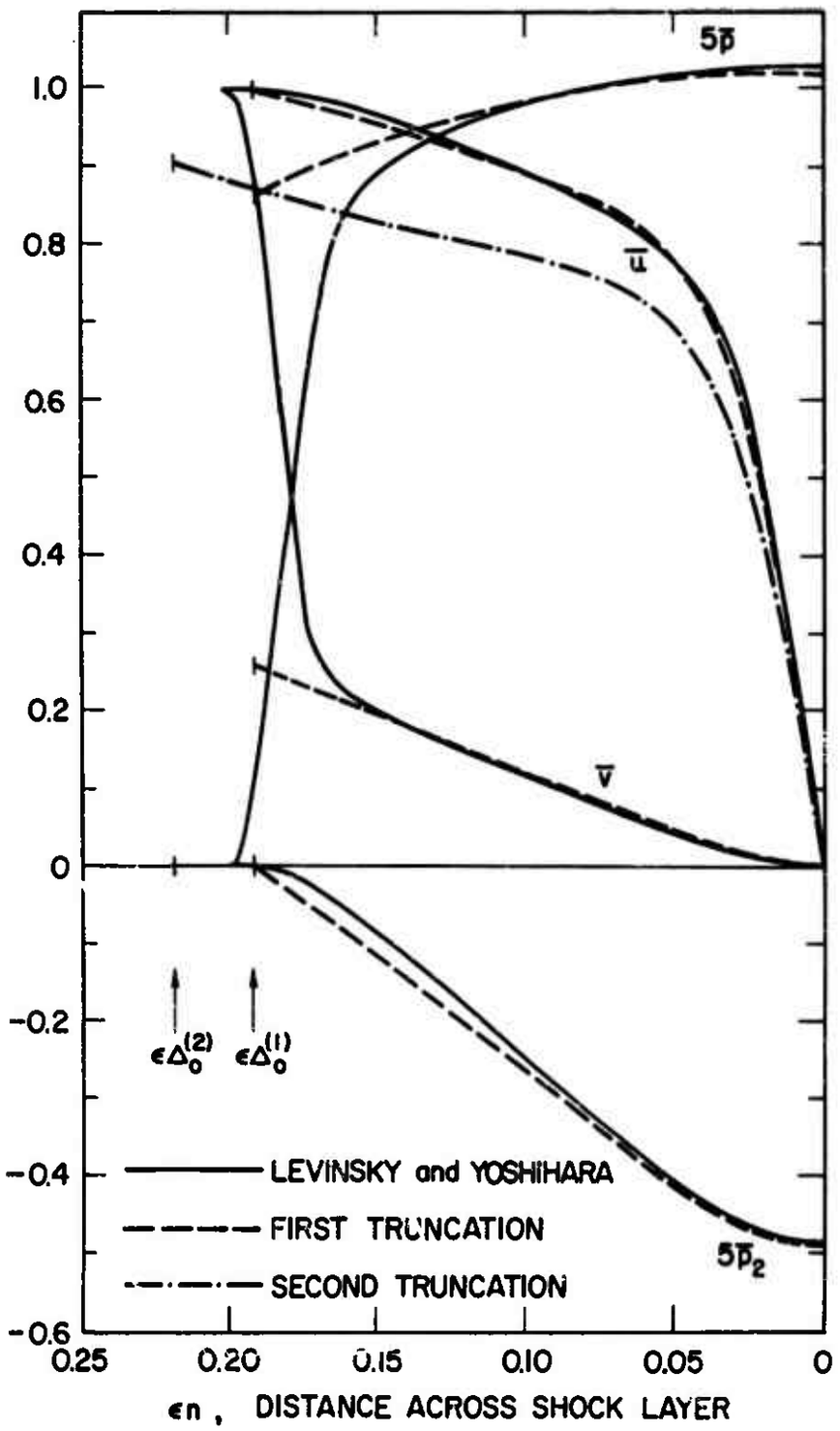

Figure 3.9b

Comparison with the results of Levinsky and Yoshihara [24] at $\gamma = 5/3$, $M_\infty = 10$, $\sigma = 0.75$, $\omega = 1/2$, adiabatic wall, no-slip boundary conditions, and $Re_s = 244$ ($\epsilon = 0.077$).

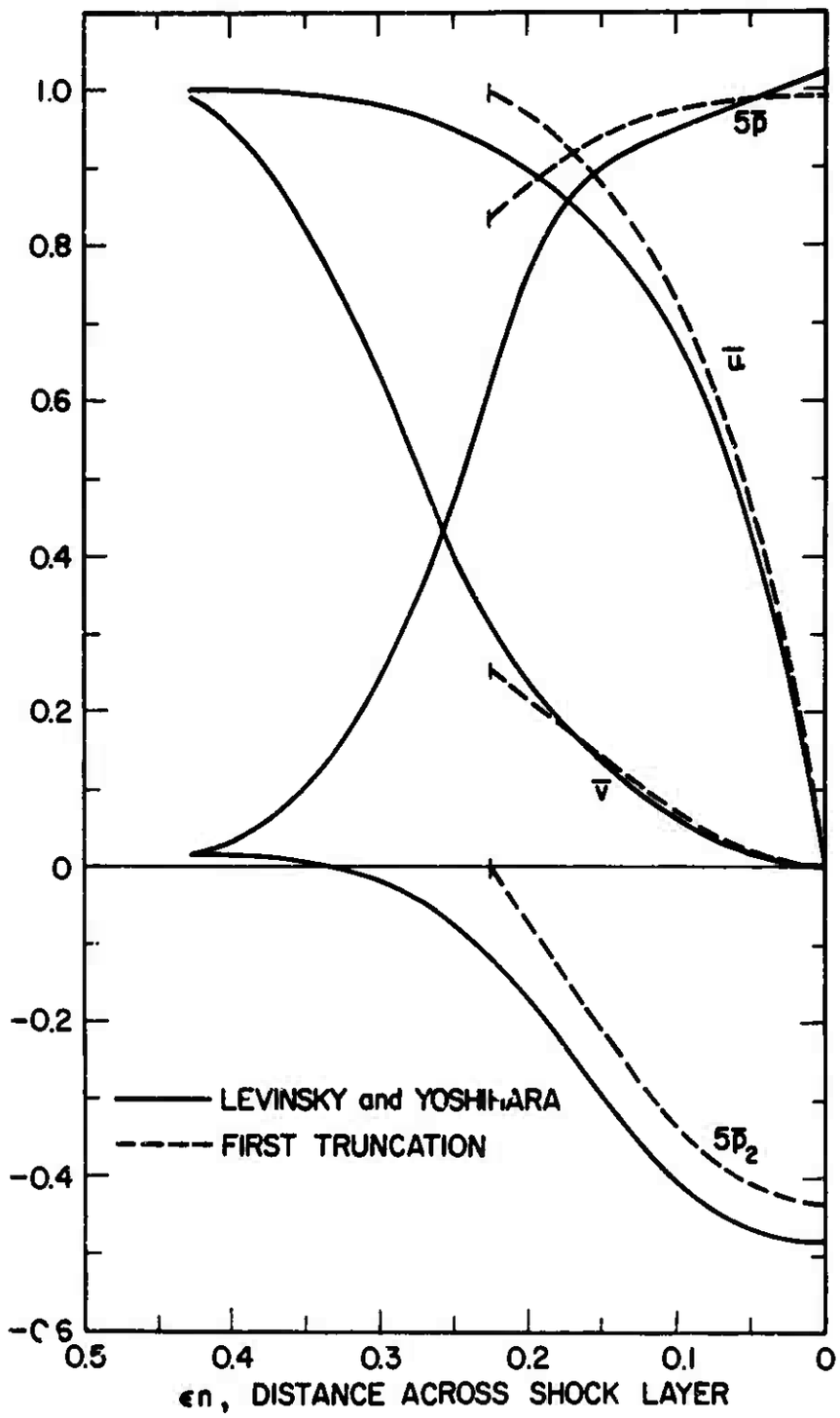

Figure 3.9c

Comparison with the results of Levinsky and Yoshihara [24] at $\gamma = 5/3$, $M_\infty = 10$, $\sigma = 0.75$, $\omega = 1/2$, adiabatic wall, no-slip boundary conditions, and $Re_\varepsilon = 26.8$ ($\epsilon = 0.232$).

in Chapter II cannot describe this. The agreement with the truncation results now deteriorates, and the influence of the thickened "shock" causes a considerable reduction in the shear stress at the wall. (This effect was previously noted in a comparison with the results of Goldberg [17].) Hence at such low values of Re_s, it is necessary to either modify the shock conditions (e.g., references 29, 2, and 17) or integrate the differential equations through the shock-transition region. In addition, it can be seen that the omission of terms of $O(\epsilon^2)$ from equations (2.3)-(2.5) leads to a noticable error for such a low Reynolds number. With no viscous terms in the normal momentum equation, (2.5), the pressure gradient $\frac{dp_o}{dn}$ is zero at the wall, as in boundary-layer theory. With the addition of the terms

$$\epsilon^2 \left\{ \left[\frac{4\mu}{3} v_n \right)_n - \left[\frac{2\mu}{3} \left(\frac{u_s + \cot s\, u}{1+\epsilon n} \right) \right]_n + \frac{(\mu u_n)_s + \mu(\cot s) u_n}{1+\epsilon n} \right\} [1]$$

to the normal momentum equation (as in references 17, 19, 21, 24), the normal pressure gradient at the wall becomes

$$\left. \frac{dp_o}{dn} \right|_{n=o} = -2\epsilon^2 \mu(T_o(0)) u_{1_n}(0) \; . \; [2]$$

It can be seen from figure 3.9c that this pressure gradient becomes quite important at this low Reynolds number. Hence, it appears that for values of the shock Reynolds number of the order of 100 or lower

---

[1] These terms are based on an assumption of zero bulk viscosity.

[2] This equation is valid only for no-slip boundary conditions at the wall.

the formulation of the problem as done in Chapter II can lead to significant errors. For these cases, the problem should be formulated to be valid to $O(\epsilon^2)$, including the effect of a shock of finite thickness.

In passing, it should be noted that the results of Levinsky and Yoshihara do not exhibit the type of pressure distribution across the shock layer that was obtained in references 19 and 21 (and that was illustrated in figure 3.7) although the equations which are solved are nearly identical to those of reference 19.

E. Summary

In this chapter, the method of series truncation has been used to obtain solutions to the equations of Chapter II for flow around shperical bodies. Due to the complexity of the equations, it was not possible to compute a large number of terms and to thus extend the validity of the solutions beyond the immediate neighborhood of the axis. However, the purpose of this investigation has been to provide accurate data at the axis to serve as initial data for a separate computational scheme (which is discussed in the next chapter). In addition, the solutions have yielded considerable information about the validity of the basic flow model that was adopted in Chapter II and about the accuracy of the method of local similarity -- a method that has been used in numerous investigations of the blunt-body problem. The main results are summarized below.

1. The basic flow model that was adopted in Chapter II appears to be accurate for values of the shock Reynolds number down to the order

of 100. Below that point, terms of $O(\epsilon^2)$ that have been omitted from the differential equations and the effect of a thickening shock become increasingly important.

2. The first-truncation results are not, in general, accurate even near the axis of symmetry. The first truncation consistently yields values of the wall shear stress that are substantially too large and values of the shock standoff distance that are substantially too small. The heat-transfer rate is overestimated, but the error in this quantity is moderate.

The second-truncation results are considerably more accurate but still contain noticeable errors at the axis. These errors, however, are generally small for Reynolds numbers within the range of validity of the basic flow model. The main error occurs in the shear stress while the heat-transfer results are quite accurate. The sensitivity of the tangential velocity component to changes in the shock slope and an inability to adequately determine the shock shape are the primary sources of this error.

3. The large errors of the first truncation indicate that the method of local similarity may also result in quite large errors since the method of local similarity is equivalent to the first approximation of the series-truncation analysis.

4. The magnitude of the errors of the first truncation are dependent on the wall-temperature distribution. For a body that is highly cooled downstream of the axis, the body and shock are concentric, and the first truncation is very accurate. However, the most commonly used

boundary conditions -- a constant wall temperature and an adiabatic wall -- do not correspond to a flow that has this spherical symmetry.

Chapter IV

FINITE DIFFERENCE METHODS

The investigation of the preceding chapter has provided solutions of reasonable accuracy to the equations of Chapter II but only in the vicinity of the axis of symmetry. To obtain solutions that are valid over a larger region of the shock layer, it is necessary to turn to other methods. In Chapter II it was noted that the characteristic surfaces of the governing partial differential equations are real, and hence, since the equations do not have an elliptic character, they may be suitable for solution as an initial-value problem. The solutions of Chapter III would appear to contradict this since they have shown an upstream influence in the flow, and such an influence is generally associated with an elliptic character in the flow equations. However, for the present, it is assumed that a solution can be obtained by using the axis of symmetry as the initial line and the solutions of Chapter III as the initial data. A method that is ideally suited to the purpose of finding such a solution is one that is based on the use of an implicit finite-difference scheme. Implicit finite-difference schemes have been used to provide accurate solutions to parabolic partial differential equations (such as the boundary-layer equations). In addition, investigations have shown that the method works quite well on simple hyperbolic equations. Hence, it appears feasible to apply such a method to the equations of Chapter II.

A. Background

Two previous applications of implicit finite-difference methods to the viscous blunt-body problem have been made (other than boundary-layer analyses). The first of these was by H.K. Cheng [2] to obtain solutions to the thin-shock-layer equations. The second application was by R. T. Davis and W. J. Chyu [11] to the equations of Chapter II but for the case of constant density throughout the shock layer.

The equations that were used by Cheng were parabolic in character, and thus were ideally suited for solution by the finite-difference scheme. However, several terms of $O(\epsilon)$ have been omitted from the equations of that investigation. Hence, the equations of Chapter II should provide a more accurate representation of the flow at moderately low Reynolds numbers than is provided by the equations of reference 2. The addition of these terms to the equations (and the addition of slip and temperature jump conditions at the wall) does not change the parabolic nature of the equations and thus should not appreciably add to the difficulty of obtaining solutions. However, two additional terms that do not appear in the thin-shock-layer equations have been retained in equation (2.4), the normal momentum equation, and these terms do have an effect on the basic nature of the problem. These terms, $\rho v v_n$ and $\frac{\rho u v_s}{1+\kappa\epsilon n}$, are of order unity in the inviscid region of the flow field and thus are essential to an adequate description of the inviscid flow field (of course, this conclusion is reached without regard to the fact that the shock layer is thin). A discussion of the significance of these terms for the description of the flow in the shock layer was contained in Chapter II.

The addition of these two terms to the equations results in the appearance of two "non-parabolic" characteristic surfaces that are described by equation (2.9). Hence the equations are no longer of a purely parabolic type, and the implications of this fact with regard to the use of a finite-difference scheme are unknown.

In addition, the thin-shock-layer concept simplifies the description of the shock shape and the determination of the shock position. The location of the shock can be determined by a balance of the mass flow in the shock layer with the mass flow that enters the shock layer from the free stream. Equation (2.18) is a formal representation of this balance. The mass flow that crosses the shock from the free stream into the shock layer is proportional to $(r + \epsilon\bar{\Delta} \sin \theta)^{j+1}$. In general, since this expression is a function of $\bar{\Delta}$, the value of the expression depends upon the solution of the flow variables in the shock layer. However, to the first approximation of the thin-shock-layer theory, the body and shock coincide, i.e. $\bar{\Delta} \to 0$, and the mass flow in the shock layer is proportional to r^{j+1}. Thus, in the thin-shock-layer approach, the locations of the flow boundaries are known prior to solving for the flow in the shock layer. In addition, the shock angle is the same as the local body angle $(\phi = \theta)$, and the values of u, v, T, and p at the shock are also known independently of the solution within the shock layer. Thus, in the more general case considered in this chapter, the computation of the boundary position and shape represents a complication which was not encountered by Cheng: it will be necessary to compute the location of the shock position and slope at each step since the

amount of mass flow along the shock layer is not known a priori as it is under the thin-shock-layer assumption. It has already been seen in Chapter II that such a computation can lead to difficulties.

Both of these complications were encountered by Davis and Chyu when they solved the constant-density case using equations that were equivalent to those in Chapter II. It was found that valid results could be obtained but that two additional approximations were needed to successfully use the method. First, it was found that the computation of the shock position and slope led to instabilities in the solution, and hence an approximation was introduced for the shock slope. Second, the inclusion of the terms ρuv_s and ρvv_n led to instabilities in the computation near the axis of symmetry. These terms entered into the computation of the pressure, and the pressure influenced the other variables through the $\frac{\partial p}{\partial s}$ term of the tangential momentum equation. To remove the instability, Davis and Chyu omitted the contributions of ρuv_s and ρvv_n to the tangential pressure gradient, $\frac{\partial p}{\partial s}$. That is, $\frac{\partial p}{\partial s}$ was approximated by a function $\frac{\partial p_T}{\partial s}$ where p_T is obtained from a simplified form of the normal momentum equation:

$$\frac{\partial p_T}{\partial n} - \frac{\epsilon \rho \kappa u^2}{1 + \epsilon \kappa n} = 0 \qquad (4.1)$$

The function p_T is identical to the pressure which is computed in the thin-shock-layer theory. Hence, with these two approximations--on the shock angle and on the pressure gradient--the problem becomes similar to the thin-shock-layer problem.

The specific procedure used by Davis and Chyu is outlined below.

1) The tangential momentum equation is programmed into the implicit finite-difference scheme, and under suitable assumptions about the shock slope and pressure gradient, the tangential velocity, u, is computed from the scheme.

2) The continuity equation is integrated term by term, and the normal velocity, v, is then determined by a simple numerical evaluation of an integral.

3) The pressure, p, is obtained by a similar integration of the normal momentum equation.

The first two steps of this procedure are identical to the procedure which has been successfully used for solving the boundary-layer equations [14, 12, 13] (for a variable density, the temperature, T, is computed along with u in the first step). In boundary-layer theory, of course, the pressure is a known function. Hence the addition of the third step is the most obvious means of extending the method to the shock-layer computations. The further extension of this method of solution to flows of variable density is considered in section C and is referred to as method I.

It was noted in Chapter II that Weinbaum and Garvine, in an investigation of the flow in a laminar wake, have solved a set of equations that are identical to equations (2.2)-(2.7). The method of solution that was proposed in reference 40 and considered further in reference 39 is discussed with regard to its application to blunt-body flows in section D (method II). This method makes use of the characteristic surfaces of the equations to evaluate the pressure and normal velocity.

One additional variation of the basic method of implicit finite-differences is considered in section E. In this method, all four variables, u, v, T, and p (or ρ), are programmed into the implicit finite-difference scheme (method III).

In the forms that are considered in the following sections, none of these methods has been found to be entirely satisfactory. The use of the first and third methods led to instabilities in the computations, while the second can be seen to be somewhat inconvenient for the blunt-body problem. It should be emphasized, however, that only the first of these methods has been explored in detail, and the lack of success in applying these methods cannot be interpreted as conclusive evidence that such methods are not feasible. Hence the methods are described below in order to indicate the type of problems that are encountered and, wherever possible, to indicate the causes and possible corrections for instabilities and errors. Several suggestions have been made for the incorporation of certain features of the first two methods into the method which is described in section E.

B. Basic Equations of the Implicit Finite-Difference Method

Since the basis of each of the methods outlined above is an implicit finite-difference scheme, we first describe the basic principles of such a scheme. All necessary equations have been given, but some details of the method have not been included. For a more detailed discussion of the method and for discussions of the merits of various numerical schemes, the reader is referred to the investigations of Flügge-Lotz and

Blottner [14], Davis and Flügge-Lotz [12], and Fannelöp and Flügge-Lotz [13].

The region between the shock and the body is replaced with a grid, which is depicted in figure 4.1. The values of the flow variables are to be evaluated only at the mesh points, which are denoted by the subscripts m and N. If the grid spacing is constant (this is not essential but is assumed in this chapter), the coordinates are given by $s = m\Delta s$ and $n = N\Delta n$. It is further assumed that the values of the flow variables are known at all mesh points for $s \leq m\Delta s$ and that we wish to solve for the values at all mesh points on the line $s = (m+1)\Delta s$.

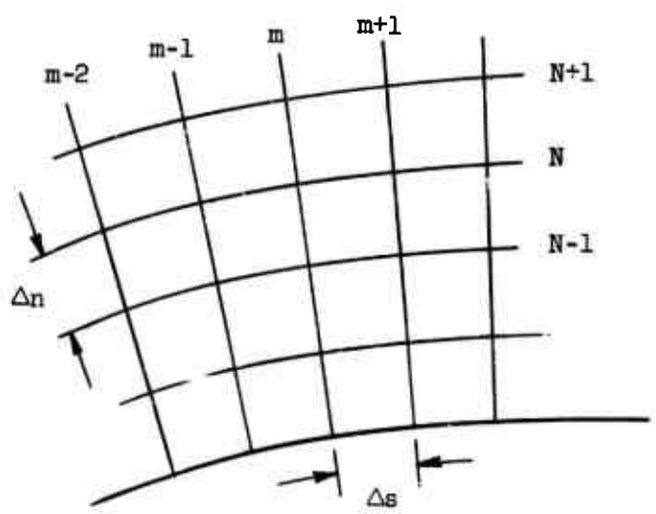

Figure 4.1. Finite-difference grid.

If the partial derivatives of equations (2.2)-(2.5) are replaced with difference quotients, the nonlinear partial differential equations, (2.2)-(2.5), for the functions $u(s,n)$, $v(s,n)$, etc. are replaced with algebraic difference equations for the values of the functions evaluated at the mesh points. The unknown quantities in this case are denoted by $u_{m+1,N}$, $v_{m+1,N}$, etc. for $N = 0,1,\ldots,N_s$. N_s denotes the grid point immediately inside the shock and therefore is the greatest integer which is less than or equal to $\frac{\overline{\Delta}}{\Delta n}$.

The difference quotients that are used for this reduction are given by

$$\frac{\partial F}{\partial s} = \frac{3F_{m+1,N} - 4F_{m,N} + F_{m-1,N}}{2\Delta s} + O(\Delta s^2) \qquad (4.2a)$$

$$\frac{\partial F}{\partial n} = \frac{F_{m+1,N+1} - F_{m+1,N-1}}{2\Delta n} + O(\Delta n^2) \qquad (4.2b)$$

$$\frac{\partial^2 F}{\partial n^2} = \frac{F_{m+1,N+1} - 2F_{m+1,N} + F_{m+1,N-1}}{\Delta n^2} + O(\Delta n^2) \qquad (4.2c)$$

and

$$\left(\frac{\partial F}{\partial n}\right)\left(\frac{\partial G}{\partial n}\right) = \frac{1}{4\Delta n^2}\left[\left(G_{m,N+1} - G_{m,N-1}\right)\left(F_{m+1,N+1} - F_{m+1,N-1}\right)\right.$$
$$+ \left(F_{m,N+1} - F_{m,N-1}\right)\left(G_{m+1,N+1} - G_{m+1,N-1}\right)$$
$$\left. - \left(F_{m,N+1} - F_{m,N-1}\right)\left(G_{m,N+1} - G_{m,N-1}\right)\right]$$
$$+ O(\Delta s^2) + O(\Delta n^2) \qquad (4.2d)$$

where each of the derivatives has been evaluated at the point $(m+1,N)$. Thus, the s-derivative is replaced with a "backward" difference quotient, and the n-derivatives are replaced with "central" difference quotients. The order of magnitude of the errors associated with the use of such difference quotients has been shown in the equations. The form of equation (4.2d) was chosen so that the unknown variables at $m+1$ appear in a linear manner.

The partial differential equations are evaluated at the grid points $(m+1,N)$, $N = 1,2,\ldots,N_s$, by use of the difference quotients (4.2). This leads to a system of simultaneous algebraic equations for the unknown variables. This coupling of the equations is a result of having used a "backward" difference formula in equation (4.2a) and is the feature which gives the method its "implicit" character. Due to the presence of such terms as $u \frac{\partial u}{\partial s}$, the algebraic equations will be nonlinear. To facilitate the solution of the equations, they are generally linearized by the use of extrapolation formulas such as

$$F_{m+1,N} = 2F_{m,N} - F_{m-1,N} + O(\Delta s^2) \qquad (4.2e)$$

The solution that is obtained from the linear difference equations may itself be used to linearize the equations for a computation of an improved solution if the errors from the original linearization prove to be excessive. Such an iteration procedure can be continued until the difference between successive solutions is as small as desired. Hence, the solution may be considered to be an iterative solution of nonlinear algebraic equations even though the emphasis in

this chapter is on linear equations. It is generally desirable to avoid such iterations since they can lead to excessive computation times. In previous applications of the method [14, 12, 13], it has been found that such iterations are not necessary. However, E. Krause [22] has considered several examples where iteration was either necessary or was more convenient than alternatives.

The nonlinear partial differential equations may now be considered to have been reduced to a system of coupled, linear algebraic equations. For the method considered in section C, the tangential momentum equation and the energy equation are reduced in this manner and lead to difference equations of the form

$$A1_N\, u_{m+1,N+1} + B1_N\, u_{m+1,N} + C1_N\, u_{m+1,N-1} + D1_N\, T_{m+1,N+1} + E1_N\, T_{m+1,N} + F1_N\, T_{m+1,N-1} = G1_N \qquad (4.3a)$$

and

$$A2_N\, u_{m+1,N+1} + B2_N\, u_{m+1,N} + C2_N\, u_{m+1,N-1} + D2_N\, T_{m+1,N+1} + E2_N\, T_{m+1,N} + F2_N\, T_{m+1,N-1} = G2_N \qquad (4.3b)$$

where $N = 1,2,\ldots,N_s$. The coefficients A1, B1, ..., G2 are functions only of the known values of the flow variables at $s = m\Delta s$ and $(m-1)\Delta s$ and of the extrapolated values (or values obtained from the preceding iteration) at $s = (m+1)\Delta s$. Hence, they can be assigned numerical values. This system of $2N_s$ simultaneous equations has a special "tridiagonal" form [14] and consequently can be solved without recourse

to the usual matrix-inversion procedures (which would be inefficient for the fairly large values of N_s that are used).

For this case of two variables, u and T, the solution can be written out in terms of the coefficients A1, B1,...,G2 fairly easily. However, for the case of four variables, which is considered in section E, the equations become unwieldy unless written in matrix notation. Hence, a matrix notation is adopted at this point in order to handle both cases at once. The function $w(N)$ is defined as a column vector of the dependent variables. In sections C and D, it has two components,

$$w(N) = \begin{bmatrix} u_{m+1,N} \\ \\ T_{m+1,N} \end{bmatrix},$$

and in section E, it has four components,

$$w(N) = \begin{bmatrix} u_{m+1,N} \\ T_{m+1,N} \\ v_{m+1,N} \\ \rho_{m+1,N} \end{bmatrix}.$$

Let the number of components be denoted by i. A complete solution of the difference equations has been obtained when $w(N)$ has been evaluated at $N = 0,1,\ldots,N_s+1$.

The linear algebraic equations that replace the partial differential equations now have the form

$$A(N)\, w(N-1) + B(\,)\, w(N) + C(N)\, w(N+1) = D(N) \qquad (4.4)$$

for $N = 1,2,\ldots,N_s$. For each value of N, the coefficients $A(N)$, $B(N)$, and $C(N)$ are $i \times i$ matrices, and the coefficient $D(N)$ is a column vector with i elements. It is emphasized again that they are functions that can be evaluated from known data, from extrapolated data, or from data obtained in the preceding iteration. For future reference, it is noted that, in the case of $i = 2$, one component of $D(N)$ is a function of the tangential pressure gradient, $\frac{\partial p}{\partial s}$, evaluated at $(s,n) = ((m+1)\Delta s, N\Delta n)$. Equation (4.4) is a linear, second-order difference equation and represents N_s equations for the N_s+2 unknowns, $w(0),\ldots,w(N_s+1)$. Two additional equations are obtained from boundary conditions. These boundary conditions may take the form of first-order difference equations without altering the tridiagonal form of the equations. Hence,

$$B(C)\, w(0) + C(0)\, w(1) = D(0) \tag{4.5a}$$

and

$$A(N_s+1)\, w(N_s) + B(N_s+1)\, w(N_s+1) = D(N_s+1) \tag{4.5b}$$

are the acceptable forms of the boundary conditions. In practice, the requirement that the boundary conditions take this form does not pose a restriction. As an example, consider a boundary condition of the form $\left.\frac{\partial T}{\partial n}\right|_{n=o} = 0$. The derivative must be replaced with a difference quotient. If a two-point form is used,[1] $T(1) - T(0) = 0$, the boundary

[1] The notation that was adopted to describe the vector w is also frequently used for the other variables. In this notation, the subscript $m+1$ is dropped, and it is understood that the function is evaluated at $s = (m+1)\Delta s$. In addition, the variable is considered to be a function of the index, N, and this functional dependence is written explicitly.

condition has the form of equation (4.5a). Unfortunately, the two-point form generally does not result in a sufficiently accurate description of this boundary condition. Use of a three-point difference quotient, $\left.\frac{\partial T}{\partial n}\right|_{n=o} \approx - \frac{3T(0) - 4T(1) + T(2)}{2\Delta n} = 0,$ is more accurate but results in a boundary condition of the form

$$B(0)\ w(0) + C(0)\ w(1) + w(2) = D(0)\ ,$$

which does not conform to the desired tridiagonal form. However, we know from the theory of linear algebra that we can add to any equation a linear combination of the other equations without altering the solution. Hence, we combine the "non-conforming" boundary condition with equation (4.4) evaluated at $N = 1$ in such a way that $w(2)$ is eliminated. Thus

$$[A(1) + C(1)\ B(0)]\ w(0) + [B(1) + C(1)\ C(0)]\ w(1)$$

$$= D(1) + C(1)\ D(0)$$

would contain the desired information that $3T(0) - 4T(1) + T(2) = 0$ and would still conform to the necessary tridiagonal form.

The solution to the second-order difference equations, (4.4) and (4.5), is given by a first-order difference equation

$$w(N) = H(N) + K(N)\ w(N+1)\ ,\quad N = 0,1,\ldots,N_s \qquad (4.6)$$

(for proof of this statement, see reference 14). The coefficients, H (a column vector) and K (an $i \times i$ matrix), are evaluated from

recursion formulas, which are obtained as follows. Replace N with N-1 in equation (4.6) to obtain

$$w(N-1) = H(N-1) + K(N-1)\, w(N) , \quad N = 1,2,\ldots,N_s+1$$

This equation can be used to eliminate $w(N-1)$ from (4.4):

$$[B(N) + A(N)\, K(N-1)]\, w(N) + C(N)\, w(N+1) = D(N) - A(N)\, H(N-1)$$

Solving this equation for $w(N)$ and comparing the result to equation (4.6), we obtain

$$H(N) = [B(N) + A(N)\, K(N-1)]^{-1}\, [D(N) - A(N)\, H(N-1)] \qquad (4.7a)$$

and

$$K(N) = -[B(N) + A(N)\, K(N-1)]^{-1}\, C(N) \qquad (4.7b)$$

The values of H and K at the surface of the body can be obtained by inspection when the equation $w(0) = H(0) + K(0)\, w(1)$ is compared to the boundary condition (4.5a), i.e.,

$$H(0) = B(0)^{-1}\, D(0)$$

and (4.8)

$$K(0) = -B(0)^{-1}\, C(0)$$

Recursive application of equations (4.7) for $N = 1,2,\ldots,N_s$ yields the values of H and K at all grid points across the shock layer. Algebraic combination of the equation $w(N_s) = H(N_s) + K(N_s)\, w(N_s+1)$ with the boundary condition (4.5b) yields the value of $w(N_s+1)$. Then a recursive application of equation (4.6) for $N = N_s, N_s-1,\ldots,1,0$ yields the desired solution to the system of equations. It should be

noted that a straightforward solution to equations (4.4) and (4.5) by standard matrix inversion techniques would require, at each s-step, the inversion of a square matrix of dimensions $(N_s+1)i \times (N_s+1)i$. This would require prohibitive computation times if N_s is large. The solution given by equations (4.6) and (4.7), on the other hand, requires, at each s-step, N_s inversions of an $i \times i$ matrix. Since i is never greater than four for the shock layer equations, these operations can be efficiently carried out for large values of N_s.

The use of matrix notation has resulted in a rather concise description of the solution in equations (4.6) and (4.7). The matrix formulas can be used intact in a computer program if one makes use of arrays (or subscripted variables) in the machine. However, this generally results in inefficient operation of the program due to an increase in access time to the stored data. It should be noted that it is necessary to store the values of $w(N)$, $H(N)$, and $K(N)$ at each grid point across the shock layer ($A(N)$, $B(N)$, $C(N)$, and $D(N)$ are needed only once and hence need not be stored). This would result in the function $K(N)$ being a three-dimensional array in the machine--with N_s+1 elements in one dimension and i elements in the other two. The access time to data that is stored in such higher-dimensional arrays is usually significantly larger than that for one-dimensional arrays. For the case when only u and T are programmed into the implicit finite-difference scheme, $i = 2$, and the solutions given by equations (4.6) and (4.7) can easily be written out explicitly in terms of the coefficients of equation (4.2) and the individual elements of H and K.

These expressions, though less concise than those given above, are more efficient for the actual computation of the solution. The reader is referred to reference 14, 12, or 13 for these expressions. To a certain extent, this can be done for the case when $i = 4$, but the expressions are lengthy, and unless the computation time is a critical factor, the extra effort needed to obtain the expressions may not be considered worthwhile.

Using these basic expressions for the solution of the implicit finite-difference equations, we can now consider specific methods.

C. Method I

The computation procedure that has been most thoroughly examined is one that is similar to the method used by Davis and Chyu in their study of the constant-density shock layer. In this method, only the tangential momentum equation and the energy equation have been reduced to linear difference equations of the form (4.3). The specific expressions for A1,B1,...,G2 have been listed in Appendix A.

The boundary conditions which complete the set of equations are obtained from the slip and temperature-jump conditions at the wall, equations (2.10) and (2.11), and from the Rankine-Hugoniot conditions for u and T, equations (2.13) and (2.17). In both (2.10) and (2.11), we set $\left.\frac{\partial u}{\partial n}\right|_{n=o} = -\frac{3u(0) - 4u(1) + u(2)}{2\Delta n}$. It has already been explained how the resulting three-point boundary condition can be reduced to the necessary two-point form. The function $\frac{\mu(T(0))}{p(0)} \sqrt{\frac{\gamma-1}{\gamma} T(0)}$, which appears in both (2.10) and (2.11), must

be evaluated by extrapolation (equation (4.2e)) or from a previous iteration in order to have a linear boundary condition. The shock conditions are somewhat more difficult to impose since the shock location will not, in general, coincide with a grid point. Hence, it is necessary to use interpolation formulas in order to apply the Rankine-Hugoniot conditions. Remembering that N_s is the largest integer which is less than or equal to $\frac{\bar{\Delta}}{\Delta n}$, we define the shock location as

$$\bar{\Delta} = (N_s + \alpha_s)\Delta n \tag{4.9}$$

Hence, $0 \leq \alpha_s < 1$. The values of the dependent variables behind the shock, which we denote by $w_\Delta(\phi)$, are given as functions of ϕ by equations (2.13) and (2.17). Suitable interpolation formulas that can be used as boundary conditions in the difference scheme are

Two-point or linear interpolation

$$w(N_s)(1-\alpha_s) + w(N_s+1)\alpha_s = w_\Delta(\phi) \tag{4.10a}$$

and

Three-point or quadratic interpolation

$$w(N_s+1)\frac{\alpha_s}{2}(1+\alpha_s) + w(N_s)(1-\alpha_s^2)$$

$$- w(N_s-1)\frac{\alpha_s}{2}(1-\alpha_s) = w_\Delta(\phi) \tag{4.10b}$$

The latter formula requires a reduction to the proper two-point form. This can lead to some rather unpleasant algebra, and therefore, in one case to be considered later, the simpler equation (4.10a) was used.

For the application of these boundary conditions and thus for the computation of u and T from the difference equations, it is necessary to know the values of $\bar{\Delta}$ and ϕ. This can be handled in several ways. For the moment, we treat $\bar{\Delta}$ and ϕ in the same manner that the flow variables are handled. That is, we extrapolate their values from previous data, and using this extrapolated data, we can compute new values of $\bar{\Delta}$ and ϕ at a later point in the procedure. Actually, only one of the variables, $\bar{\Delta}$ or ϕ, needs to be extrapolated; the remaining quantity can be obtained from a difference representation of equation (2.19). It will later be shown that it is possible to compute $\bar{\Delta}$ simultaneously with the computation of u and T without using this extrapolation. However, for the moment, we consider u and T to be computed from equations that make use of approximate values of $\bar{\Delta}$ and ϕ.

The normal velocity, v, is obtained from the continuity equation after the computation of u and T has been accomplished. An integration of the terms of equation (2.2) yields

$$\rho(s,n)v(s,n) = \frac{1}{(r+\epsilon n \sin\theta)^j(1+\kappa\epsilon n)} \int_0^n [(r+\epsilon n \sin\theta)^j \rho u]_s \, dn \tag{4.11}$$

In order to evaluate v from this equation, it is necessary to use an extrapolated value for ρ. This is, however, consistent with the linearization of the difference equations for u and T. The boundary condition (2.12) has already been incorporated into (4.11). The

numerical evaluation of the integral in equation (4.11) is carried out by the use of a formula similar to Simpson's rule[1]:

$$\int_{(N-1)\Delta n}^{N\Delta n} F\, dn = \frac{\Delta n}{12}\left[5F(N-1) + 8F(N) - F(N+1)\right] \qquad (4.12)$$

This formula is derived by replacing $F(n)$ with a quadratic curve which passes through the three points, $F(N-1)$, $F(N)$, and $F(N+1)$. At this point in the computation, an improved value for the shock position, $\bar{\Delta}$, may be obtained simply by observing where the integrated value of v reaches the Rankine-Hugoniot value given by equation (2.14). One may, of course, now repeat the computation of u and T using the new value of $\bar{\Delta}$ (and hence ϕ) until the value of $\bar{\Delta}$ is as accurate as desired. Alternatively, one can proceed to the computation of the pressure and then iterate on all of the approximated variables simultaneously.

Once the values of u, T, and v have been obtained at each grid point, the pressure can be evaluated from an integration of the normal momentum equation. If the extrapolated value of ρ is used, the pressure can be evaluated from

$$p(s,n) = p(0) - \epsilon \int_0^n \rho\left[\frac{\epsilon u v_s}{1+\kappa\epsilon n} + \epsilon v v_n - \frac{\kappa u^2}{1+\kappa\epsilon n}\right]dn \qquad (4.13a)$$

Although this is consistent with the linearization of the finite-difference

---

[1] Simpson's rule is not used because it computes the integral from $(N-1)\Delta n$ to $(N+1)\Delta n$ and therefore would provide the value of the integral only at alternate grid points across the shock layer.

scheme, the approximate value of ρ need not be used since the state equation can be used to eliminate ρ from equation (2.7). This leads to

$$p(s,n) = p(0) \exp\left[-\int_0^n P(n)\, dn\right] \qquad (4.13b)$$

where

$$P(n) = \frac{\gamma}{\gamma-1}\,\frac{\epsilon}{T}\left[\frac{\epsilon u v_s}{1+\kappa\epsilon n} + \epsilon v v_n - \frac{\kappa u^2}{1+\kappa\epsilon n}\right] .$$

Since all the variables that appear in the expression for P have been computed, equation (4.13b) can be evaluated without use of the extrapolated data. In both (4.13a) and (4.13b), the value of $p(0)$ is chosen so that the pressure satisfies the Rankine-Hugoniot condition, equation (2.15).

Several possible variations in the details of the computation proccdure have already been noted. There are other variations that have been investigated but are not described here. In general, when both the shock shape and the tangential pressure gradient, $\frac{\partial p}{\partial s}$, were computed at each s-step, the computed values become meaningless within a few steps. In other cases, the procedure did not exhibit such strong instabilities but yielded incorrect results nevertheless. As noted above, such difficulties were not entirely unexpected and can be attributed to the determination of the shock shape and to the occurrence of uv_s and vv_n in the normal momentum equation. Qualitatively, the difficulty with the normal momentum equation is as follows. Equations such as (4.2a) or (4.2b) are used to numerically evaluate certain

derivatives. When an error exists in the value of the function F, the use of the difference quotients results in a magnification of the error in the derivative of F (due to the small value of Δs or Δn that is used in the denominator). In the basic implicit finite-difference scheme, this does not occur since equations (4.2) are only used formally but are not numerically evaluated. However, in the procedure described above, $\frac{\partial p}{\partial s}$ is evaluated from (4.2a) and is used in the determination of u and T. The resulting value of u is used in (4.2a) to evaluate $\frac{\partial u}{\partial s}$, which is in turn used in equation (4.11) to evaluate v. From v, we determine both $\frac{\partial v}{\partial s}$ and $\frac{\partial v}{\partial n}$, and these values are used in equation (4.13) to determine p. This value of p then goes back into the finite-difference scheme as $\frac{\partial p}{\partial s}$. At each step the evaluation of the derivatives results in a magnification of the errors, and these errors are eventually fed back into the scheme. In the application to boundary-layer flows, such a "feedback" does not occur since the pressure is a known, specified function. Even in the thin-shock-layer flow, where the pressure is computed, the feedback does not occur since uv_s and vv_n do not appear in the normal momentum equation.

We thus consider modifying the equations in the manner of Davis and Chyu [11]. This modification can be considered to be a first step to the more general analysis; the numerical scheme must be able to handle the simpler equations before they can be extended to the general case. Thus the shock angle, ϕ, is specified as a known function for the evaluation of the Rankine-Hugoniot conditions. During the course of the computation, the shock position, $\bar{\Delta}$, is calculated. The geometric relation between $\bar{\Delta}$ and ϕ, equation (2.19), cannot now

be applied but can only be used a posteriori to determine whether the results are consistent with the assumptions. In reference 11, for the constant-density flow, ϕ was specified as being equal to θ, and the resulting value of $\bar{\Delta}$ was found to be consistent with this assumption (i.e. $\bar{\Delta} \sim$ const). For a variable density, the modification of the normal momentum equation can be done in two ways. First, the terms proportional to uv_s and vv_n may be eliminated entirely from the problem, and the pressure p is approximated by the thin-shock-layer pressure p_T. The problem is then reduced to one that represents a slight extension of the investigation of H.K. Cheng. The additional terms of $O(\epsilon)$ that are included in equations (2.3)-(2.5) should not cause any major difficulty in the computation. Despite the fact that the shock angle is now assumed to be known (and therefore the boundary values at the shock are known), the treatment of the shock position is still somewhat more general than that used by Cheng since the mass flow in the shock layer is still not s specified quantity. The omission of the terms ρuv_s and ρvv_n results in a substantial reduction of the pressure, and therefore of the density, near the body surface. This reduction in the density alters the flow field considerably and, in an extreme case, can lead to the occurrence of the zero-pressure point which is common in thin-shock-layer theory. Hence, a second possibility that is analogous to the analysis made by Davis and Chyu is also considered. The complete pressure is used in the computation of the density, and the pressure gradient $\frac{\partial p}{\partial s}$ is approximated by $\frac{\partial p_T}{\partial s}$, where p_T is the thin-shock-layer pressure of equation (4.1).

This should result in a more realistic description of the density field, but the influence of $\rho u v_s$ and $\rho v v_n$, which is fed back into the finite-difference scheme through the density, may be large enough to cause instabilities.

The first of these possibilities is now considered. The computations proceed as follows. The solution of u, T, and v is based on extrapolated data as described earlier. The shock location is determined by a requirement that the integrated value of v be equal to the Rankine-Hugoniot value. Since ϕ has been taken to be a known value, this step is now particularly simple; and since equation (2.19) no longer acts as a constraint, the computed value of $\bar{\Delta}$ may undergo rather rapid changes in value. Using the newly computed values of u, v, T, and $\bar{\Delta}$, the pressure is obtained from equation (4.13b) (with the terms proportional to uv_s and vv_n omitted, of course). As many iterations as desired may be obtained at each step.

This procedure has been applied to the flow problem that was considered in Chapter III, section D.1, i.e., $\gamma = 1.4$, $M_\infty = 10$, $Re_s = 100$, $\sigma = 0.7$, $b = 0.6$, and $\mu = T^{1/2}$. These computations were started from initial data (at $s = 0.0$ and $s = 0.02$) that were obtained from the first truncation problem of Chapter III (the second truncation problem had not been solved when these computations were made). Thus the shock angle ϕ was set equal to the body angle θ. It has been found that the computed shock description is a sensitive indicator of the stability of the computations. Thus, the computed value of $\bar{\Delta}$ is shown in figure 4.2. The discontinuous jump in value that occurs

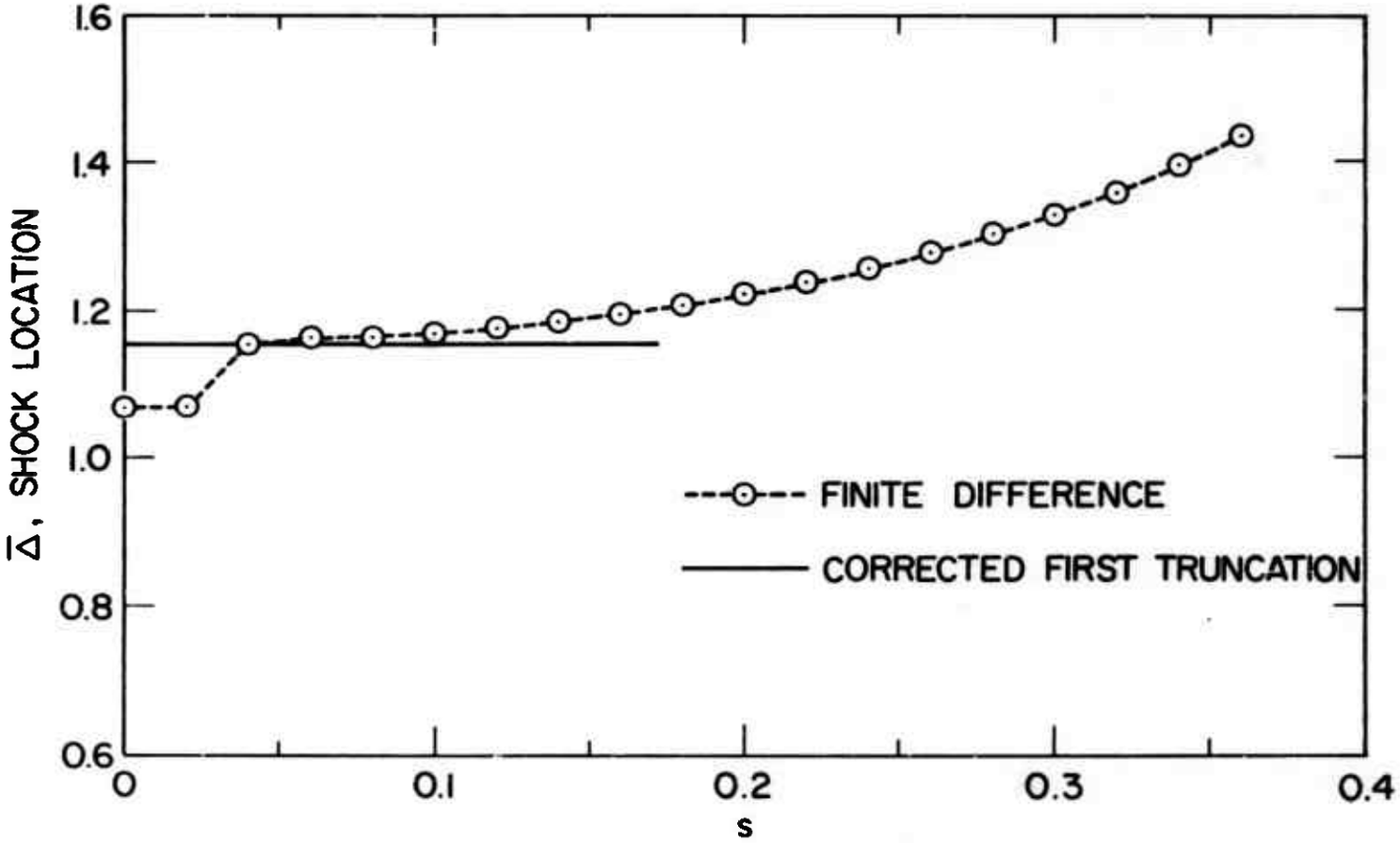

Figure 4.2

Shock standoff distance computed from method I using the thin-shock-layer approximation for the tangential pressure gradient and the density: $\gamma = 1.4$, $M_\infty = 10$, $Re_s = 100$, $b = 0.6$, $\sigma = 0.7$, and $\omega = 1/2$.

at the first computation step is of particular interest. It was found after these computations were made that the initial data were incorrect. The correct first-truncation value of $\bar{\Delta}$ has also been shown in figure 4.?. It can be seen that the finite-difference scheme yields the correct value of $\bar{\Delta}$ even when started from an incorrect value. As s increases, the number of iterations that are required to obtain "convergence" of the pressure increases. In addition, the computed values of $\bar{\Delta}$ become less consistent with the assumption that $\phi = \theta$; at $s = 0.34$, the application of equation (2.19) yields $\theta - \phi = 11°$. Thus there is little point in continuing the calculations to larger values of s. This inconsistency in the computation would no doubt be removed by the specification of the mass flow in the shock layer (as is done in the thin-shock-layer computation). If this were done, the resulting problem would represent an extension of the results of H.K. Cheng to a more uniform treatment of the second-order boundary-layer effects.

It should be noted that if the shock angle is allowed to vary in the shock conditions and if equation (2.19) is used to relate $\bar{\Delta}$ and ϕ in the above calculations, the computed value of $\bar{\Delta}$ very slowly decreases. A similar result had been obtained earlier when considering the complete normal momentum equation. This is typical of the difficulties associated with attempting to compute the shock shape.

We now consider the second treatment of the normal momentum equation. The calculations include the effect of the terms uv_s and vv_n in the computation of the density in order to improve the description of the density field. In addition, these computations use an

improved means of calculating the shock position. Instead of using the iterative method described earlier, the shock position is obtained simultaneously with the solution of the finite-difference equations for u and T as described in the following paragraph.

Earlier in this chapter, it was stated that the calculation of $w(N_s+1)$ was achieved by combining the equation $w(N_s) = H(N_s)+K(N_s)w(N_s+1)$ with the boundary condition (4.5b). Later, it was observed that interpolation formulas (equations (4.10)) were used to obtain the boundary condition (4.5b). This led to the appearance of $\bar{\Delta}$ and ϕ in the coefficients of equation (4.5b). This was previously handled by using extrapolated data for the shock parameters. However, if one additional equation could be obtained that related $w(N_s)$, $w(N_s+1)$, and $\bar{\Delta}$, then $\bar{\Delta}$ could be computed simultaneously with $w(N_s+1)$, and the necessity of iterating on the shock position would be eliminated. Such an equation can be obtained from the integral form of mass conservation, equation (2.18). Let

$$I(N) = 2^j \epsilon \int_0^{N\Delta n} \rho u (r+\epsilon n \sin\theta)^j \, dn \qquad (4.14a)$$

It is shown in Appendix B, for the case of $i = 2$, that

$$I(N) = A_I(N) + B_I(N)u(N) + C_I(N)T(N) \qquad (4.14b)$$

where $A_I(N)$, $B_I(N)$, and $C_I(N)$ are scalar quantities that can be numerically evaluated along with $H(N)$ and $K(N)$; i.e., $A_I(N)$, $B_I(N)$, and $C_I(N)$ can be evaluated from recursive relations starting at $N = 0$. Thus equation (2.18) can be written as

$$(r+\epsilon\bar{\Delta}\, n(N_s+\alpha_s)\sin\theta)^{j+1} = (1-\alpha_s)(A_I(N_s) +$$

$$B_I(N_s)\, w(N_s)) + \alpha_s(A_I(N_s+1) + B_I(N_s+1)\, w(N_s+1)) \qquad (4.15)$$

where the linear interpolation formula (equation (4.10a)) has been used to evaluate the integral at the shock. Equation (4.15) is the additional equation that permits the solution of $\bar{\Delta}$. The three equations are non-linear and thus must be solved by some appropriate numerical technique. Once the values of $\bar{\Delta}$, $w(N_s)$, and $w(N_s+1)$ have been obtained, the solution proceeds as described before.

With the computation of $\bar{\Delta}$ handled in this manner, the Rankine-Hugoniot condition on the normal velocity, v, should become superfluous. As noted in the preceding chapter, equation (2.18) is not an independent condition; it can be used only to replace one of the boundary conditions which describe the mass flux across the boundar, Hence the integrated value of v (equation (4.11)) should now automatically satisfy the Rankine-Hugoniot condition. In practice, of course, the linearization of the finite-difference equations and the use of an extrapolated value of ρ in equations (4.11) and (4.14a) prevent this from being exact -- there will always be a small difference between the integrated and the Rankine-Hugoniot values of v.

After the pressure is determined from equation (4.13b), iterations on the values of all the variables can be obtained. It was found that for these calculations, the iterations did not significantly alter the results, but did tend to smooth the results somewhat near the axis.

The computed value of $\bar{\Delta}$ is again used as an indication of the stability of the scheme. However, it is convenient to make use of equation (2.19) and to present the results in the form of the shock angle. It should be noted that a small oscillation in the value of $\bar{\Delta}$ results in a rather substantial oscillation in the value of ϕ. Figure 4.3 illustrates the results for a variety of assumptions.

1) First, consider the cases for which the computations were started from initial data obtained from the first-truncation results. As before, it was found that the computation of the shock angle lead to instabilities. Hence, the results shown in figure 4.3 are based on an assumed value of $\phi = \theta$ (the solution of the equations provides a computed value of ϕ which is the value shown in figure 4.3).

a) When the pressure gradient $\frac{\partial p_T}{\partial s}$ is computed at each step, instabilities appear immediately. This is illustrated by one curve in figure 4.3. Thus the procedure is less stable than it was when the influence of the terms uv_s and vv_n was eliminated entirely. This must be a consequence of the inclusion of the influence of uv_s and vv_n in the computation of the density.

b) The strength of this influence is evaluated by considering the pressure gradient to be a specified function (equal to the series-truncation results). Hence the only source of instability due to the terms uv_s and vv_n is in the computation of the density. The calculations now proceed to about $s = 0.2$ before instabilities cause the computation to break down (see figure 4.3).

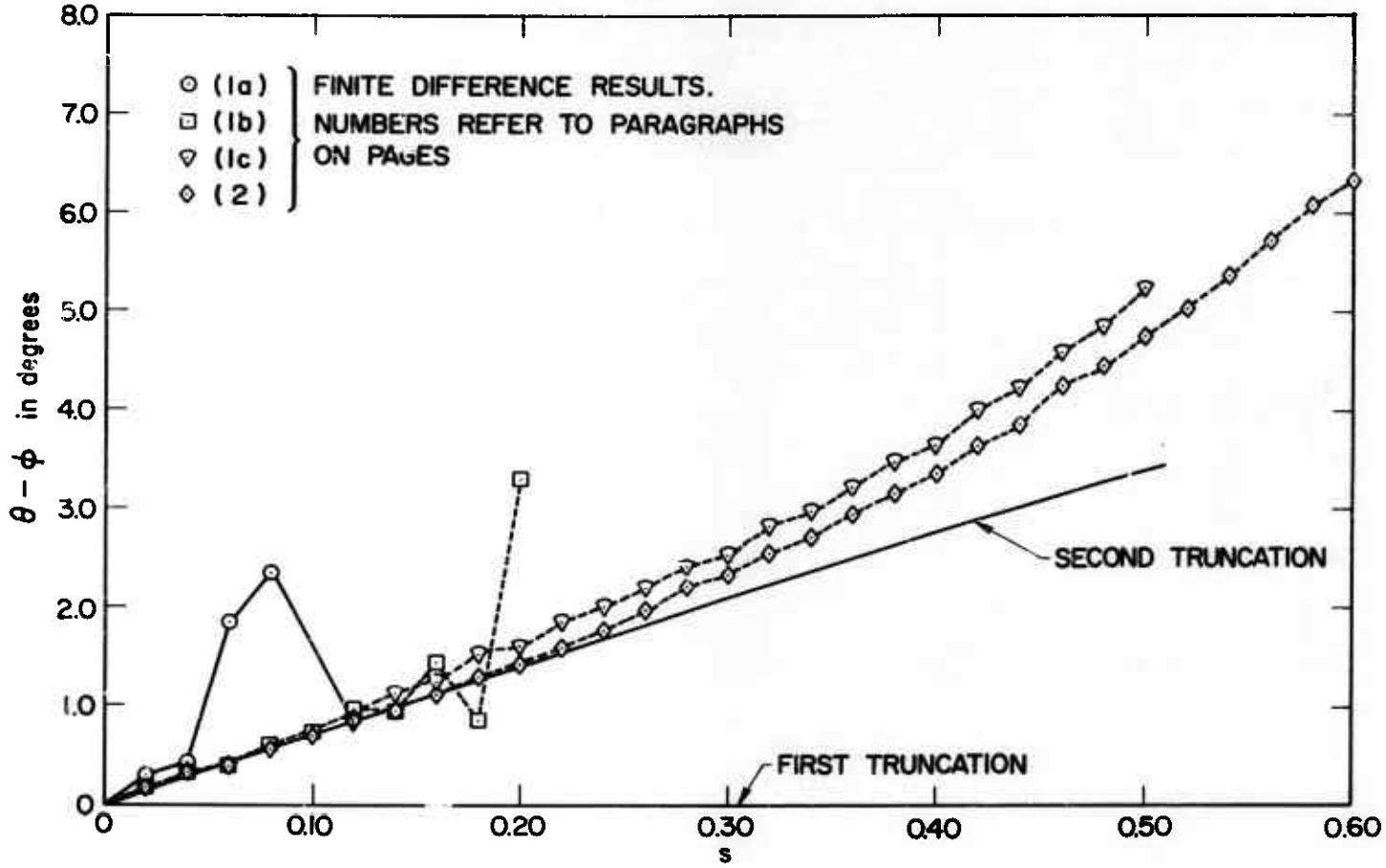

Figure 4.3

Shock angle computed from method I under the approximations explained in paragraphs 1a, 1b, 1c, and 2 on pages 125 and 127; $\gamma = 1.4$, $M_\infty = 10$, $Re_s = 100$, $b = 0.6$, $\sigma = 0.7$, and $\omega = 1/2$.

c) The onset of these instabilities can be delayed by averaging the computed and the extrapolated values of the pressure:

$$p = (1-h)\, p_{extrapolated} + h\, p_{calculated} \qquad (4.16)$$

At $s = 0$, h is taken to be unity. The computations proceed for increasing s until they become unstable. The value of h is then decreased, and the calculations are started at a point just before the onset of the instability. By repeating this process whenever necessary, the calculations have been carried to $s = 0.50$, and this result is also shown in figure 4.3. The final value of h is 0.10. The instabilities which appear at intervals along the curve are not shown but are quite similar to the one that has been shown at $s = 0.2$ in the figure.

It would seem that at best these numerical computations could only reproduce the truncation results since a large number of constraints have been placed on the numerical procedure. However, the computed values of ϕ closely match the second-truncation result for ϕ even though the computed values are based on initial dats and a pressure gradient that are obtained from the first truncation and the first-truncation assumption that $\phi = \theta$ has been used in the evaluation of the shock conditions. Hence, in this one respect, the finite-difference scheme is yielding "new"information.

2) Also shown in figure 4.3 are the results of using the second-truncation computations for initial data, for the pressure gradient,

and for the shock angle. These computations have been carried out to $s = 0.62$ by averaging the pressure as described in paragraph (1c) above. Again, the value of h was gradually reduced to a final value of 0.10. No attempt has been made to determine how far the calculations can be carried in this manner. At the largest value of s, most of the "inviscid", outer flow has become supersonic. This is illustrated in figure 4.4 where the shock and the sonic line have been depicted. Shown for comparison is the sonic point on the body as computed from an inviscid theory (this value was obtained from reference 12 and is the result of an analysis by H. Lomax of NASA). Due to the presence of the viscous layer, the sonic line will turn and roughly parallel the body as s increases further. The extent of the viscous layer has been illustrated by showing the tangential velocity profile at $s = 0.4$.

Returning to a consideration of figure 4.3, we can see that the computed value of ϕ deviates only slightly from the assumed, second-truncation value. It was previously noted that the finite-difference result for ϕ was obviously more accurate than the first-truncation value on which the computations were based. Whether this is true of the present results can be determined in the following manner.

In Chapter III, it was seen that an inability to adequately determine the shock shape was the major cause of inaccuracy in the series-truncation analysis. We now use the finite-difference result found here to determine the value of ϕ_3, which in Chapter III was arbitrarily set to zero. That is, we determine ϕ_3 such that $\phi_1 \sin s + \phi_3 \sin^3 s$ (see equation (3.3b)) provides a least-squares fit to the finite-difference

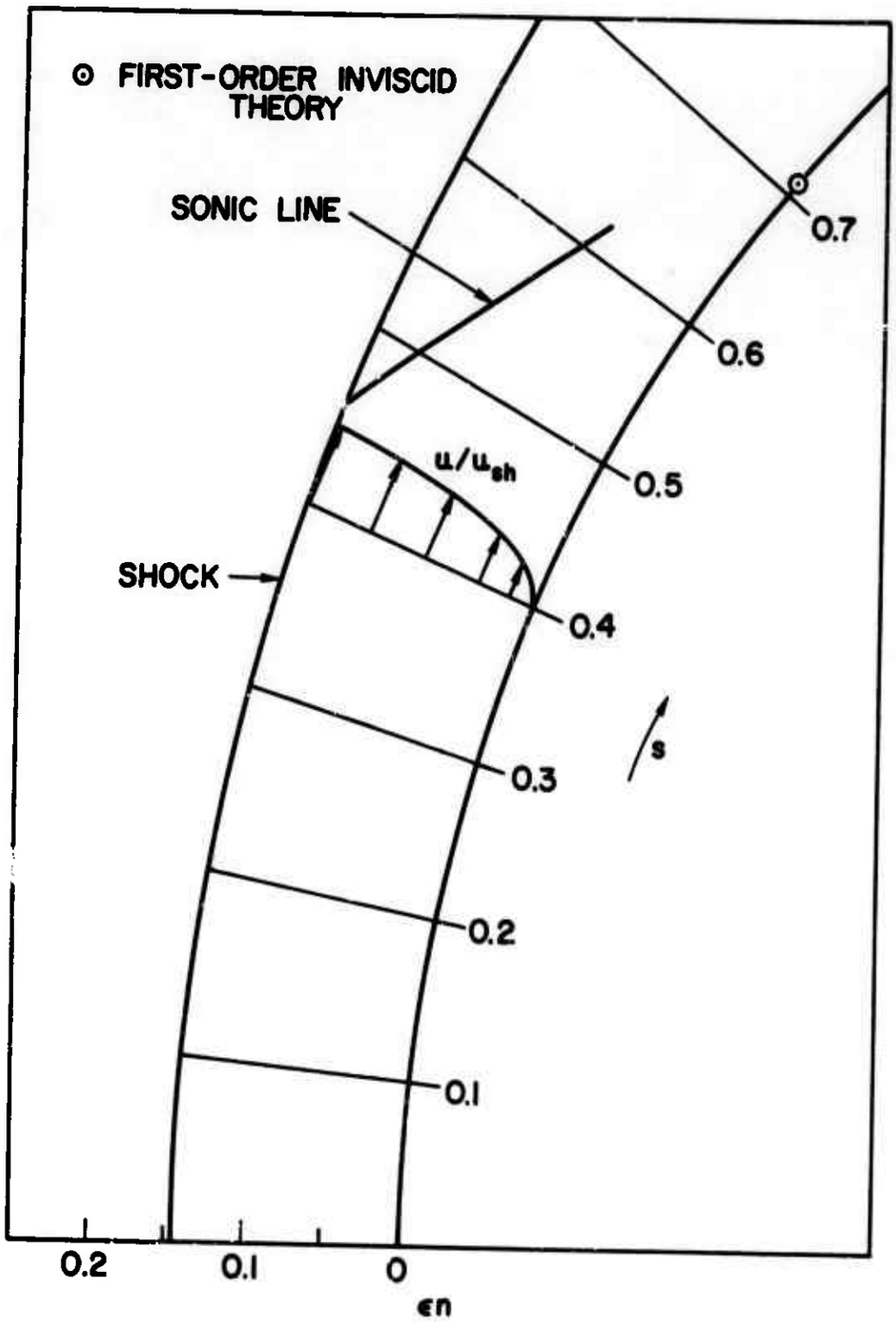

Figure 4.4

The shock and the sonic line computed from method I; $\gamma = 1.4$, $M_\infty = 10$, $Re_s = 100$, $b = 0.6$, $\sigma = 0.7$, and $\omega = 1/2$.

result for $\theta-\phi$. We are not free to choose the value of ϕ_1 as it is entirely dictated by the solution of the second-truncation problem as described in Chapter III. Further, the values of ϕ_1 and ϕ_3 are mutually dependent: $\phi_1 \sin s$ increases above the value shown in figure 4.3 as the value of ϕ_3 is increased. Hence the least-squares fit of $\phi_1 \sin s + \phi_3 \sin^3 s$ is not as accurate as might be expected: $\theta-\phi = 0.152 \sin s + 0.112 \sin^3 s$, and the root-mean-square error is approximately 0.006 compared with $\theta-\phi = 0.111$ at $s = 0.6$. However, the shear stress result is now

$$\tau/\epsilon = 1.23 \sin s - 0.74 \sin^3 s ,$$

which is considerably better than the previous second-truncation result given by equation (3.24b) and illustrated in figure 3.1. It is certainly not recommended that the finite-difference solutions be used to improve the series truncation solutions in this manner; but the above result does show that the finite-difference solution for ϕ is more accurate than the second-truncation result on which the finite-difference computations were based.

Despite this one positive result, it is quite clear that the compressible-flow computations are far more unstable than were the constant-density computations of reference 11. In fact, it appears that this method of computation is not suitable for the computation of the flow in the shock layer; a better means of handling the computation of the normal velocity and the pressure is needed.

D. Method II

One such possible method for an improved calculation of the pressure and normal velocity makes use of the method of characteristics. This method has several advantages over the one described previously. It was developed by Weinbaum and Garvine [40] for use in the laminar wake flow. Its application to the blunt-body problem is now considered.

In Chapter II it was noted that there are two "non-parabolic" characteristic surfaces of the partial differential equations (2.2)-(2.5). These surfaces are described by equation (2.9):

$$\frac{1}{1+\epsilon\kappa n}\,\frac{dn}{ds} = \frac{v}{u} \pm \sqrt{\frac{p}{\rho}}\,\frac{1}{\epsilon u} = \lambda_{1,2} \qquad (4.17)$$

These two characteristics can be traced to the continuity equation and the normal momentum equation, and they are the characteristics which are associated with the determination of the derivatives of pressure and normal velocity. Hence we now consider equations (2.3) and (2.5).

First, introduce two new coordinates $\xi = \xi(s,n)$ and $\eta = \eta(s,n)$. In general,

$$\frac{\partial}{\partial s} = \frac{\partial \xi}{\partial s}\,\frac{\partial}{\partial \xi} + \frac{\partial \eta}{\partial s}\,\frac{\partial}{\partial \eta}$$

and

$$\frac{\partial}{\partial n} = \frac{\partial \xi}{\partial n}\,\frac{\partial}{\partial \xi} + \frac{\partial \eta}{\partial n}\,\frac{\partial}{\partial \eta}$$

These relations need to be substituted into equations (2.3) and (2.5) only for the derivatives of p and v since the other variables are

not associated with the two characteristic surfaces described by equation (4.17). We now specify that the curves ξ = const. be tangent to one family of characteristic surfaces and that the curves η = const. be tangent to the other. Hence, the slopes of the curves ξ = const. and η = const. are given by λ_1 and λ_2, respectively. Therefore, on ξ = const.

$$\frac{\xi_s}{\xi_n} = -\frac{dn}{ds} = -\lambda_1(1+\epsilon\kappa n) \tag{4.18a}$$

and on η = const.

$$\frac{\eta_s}{\eta_n} = -\frac{dn}{ds} = -\lambda_2(1+\epsilon\kappa n) \tag{4.18b}$$

If the two equations are applied along the curve ξ = const. and equation (4.18a) is introduced, they can be combined so that only η-derivatives of p and v appear:

$$p_\eta + \epsilon\sqrt{p\rho}\, v_\eta = [\kappa\sqrt{p\rho}\, u - \frac{pT}{\alpha u}((\frac{\alpha u}{T})_s + v(\frac{\beta\alpha}{T})_n)]\frac{ds}{d\eta} \quad \text{on } \xi = \text{const.}$$

where $\alpha(s,n) = (r+\epsilon n\sin\theta)^j$ and $\beta(n) = 1+\epsilon\kappa n$. This equation can be re-written in the form

$$p_\eta + \epsilon\sqrt{p\rho}\, v_\eta = -\frac{pT}{\alpha u}(\frac{\alpha u}{T})_\eta + [\kappa\sqrt{p\rho}\, u + \frac{pT}{\alpha u}[\lambda_1\beta(\frac{\alpha u}{T})_n - v(\frac{\beta\alpha}{T})_n])\frac{ds}{d\eta} \quad \text{on } \xi = \text{const.} \tag{4.19a}$$

which is the form given in reference 40. Similarly, if the equations are applied along the curve η = const. and equation (4.18b) is used, they can be combined to form

$$p_\xi - \epsilon\sqrt{p\rho}\, v_\xi = -\frac{pT}{\alpha u}\left(\frac{\alpha u}{T}\right)_\xi + \{-\kappa\sqrt{p\rho}\, u + \frac{pT}{\alpha u}\left[\lambda_2\beta\left(\frac{\alpha u}{T}\right)_n - v\left(\frac{\beta\alpha}{T}\right)_n\right]\}\frac{ds}{d\xi} \quad \text{on} \quad \eta = \text{const.} \tag{4.19b}$$

The value of the method of characteristics (and of equations (4.19)) is that the equations are reduced to ordinary differential equations along the characteristic curves (in equations (4.19) this is achieved only with the derivatives of p and v -- the variables u and T remain as partial derivatives). The characteristic curves themselves are functions of the variables, however, and must be determined as part of the solution. The standard means of handling this is by iterative methods: an approximation to the characteristics yields a solution to the variables that can be used to obtain a better description of the characteristics, etc.

We now consider the manner in which equations (4.19) can be incorporated into the basic finite-difference scheme. Consider an arbitrary mesh point, $(m+1,N)$, of the grid that was depicted in figure 4.1, and denote it with the subscript 3. The two characteristic curves, ξ = const. and η = const., which pass through this point 3 intersect the line $s = m\Delta s$ at points that are denoted by the subscripts 1 and 2, respectively (see figure 4.5). The data which are used to linearize the finite-difference equations can be used to determine the locations of points 1 and 2 (if desired, subsequent iterations can be used to improve these values). Points 1 and 2, of course, will generally not be grid points, and evaluation of the variables there

will require the use of interpolation formulas.

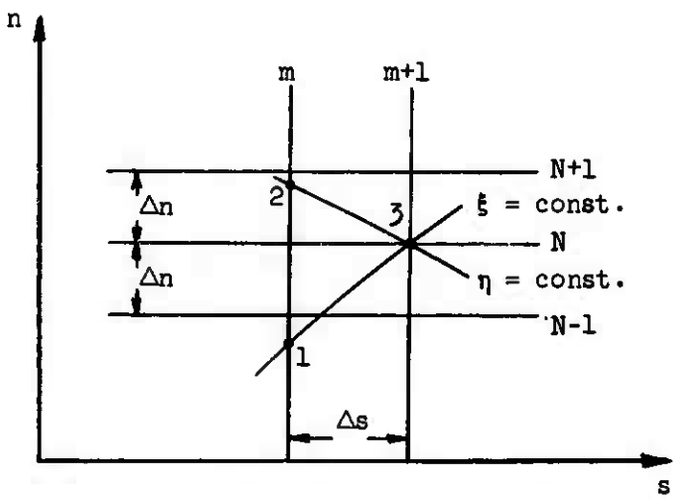

Figure 4.5. Finite-difference grid for the characteristic curves.

If we replace the derivatives with respect to ξ and η with the difference quotients

$$\left.\frac{\partial F}{\partial \xi}\right|_{\eta = \text{const.}} = \frac{F_3 - F_2}{\Delta \xi}$$

and

$$\left.\frac{\partial F}{\partial \eta}\right|_{\xi = \text{const.}} = \frac{F_3 - F_1}{\Delta \eta}$$

and if we replace the functions $\sqrt{p\rho}$, $\frac{pT}{\alpha u}$, etc. with suitable averages over the intervals 3-1 and 3-2, then equations (4.19) can be used to obtain relations of the form

$$p_{m+1,N} = A_p + B_p\, u_{m+1,N} + D_p\, T_{m+1,N} \qquad (4.20a)$$

and

$$v_{m+1,N} = A_v + B_v\, u_{m+1,N} + D_v\, T_{m+1,N} \qquad (4.20b)$$

The coefficients of these equations are functions of the variables at points 1 and 2 and/or functions of average values over the arcs 3-1 and 3-2. Hence, they can be assigned numerical values which are consistent with the linearization of the finite-difference scheme. Note also that the values of $\Delta\xi$ and $\Delta\eta$ need not be known; only Δs remains in the equations.

When the tangential momentum equation and the energy equation were replaced with the difference equations (4.3), the variable $p_{m+1,N}$ entered into the coefficients of the equations through the term $\frac{\partial p}{\partial s}$. In method I, an extrapolated value of p was used, and it was seen that this was one of the contributing factors to the occurrence of instabilities. Now, however, equation (4.20a) can be used to eliminate $p_{m+1,N}$ in favor of $u_{m+1,N}$ and $T_{m+1,N}$; this will, of course, redefine the values of the coefficients of equations (4.3). Once u and T are obtained from the finite-difference solution, p and v are available from equations (4.20). However, by making use of the characteristic coordinates for p and v, the solution of all the variables is simultaneous, whereas in method I there was a sequential ordering to the solution of the various variables.

Unfortunately, for the blunt-body problem the reduction of the differential equations (4.19) to the algebraic equations (4.20) cannot be accomplished as easily as indicated above. Since the slope of the characteristics is proportional to $\frac{1}{u}$, the slopes are rather large

near the axis of symmetry of the flow and near the body surface. Figure 4.6 illustrates the situation by depicting the two characteristics which pass through the point $(s,n) = (0.10, 0.60)$ for flow around a sphere with $\gamma = 1.4$, $M_\infty = 10$, $Re_s = 100$, $b = 0.6$, etc. The computation of the location of the characteristics is based on the second-truncation results. Also shown in figure 4.6 are the characteristics which intersect the boundaries at $s = 0.10$. If the reduction of equations (4.19) as described above is to be valid, the length of the arcs 3-1 and 3-2 must be small. It can be seen that this will require an extremely small step size in the s-direction, even if the truncations were accurate enough that the finite-difference scheme could be started at $s = 0.10$. A step size of $\Delta s = 0.001$ could probably be used but would result in rather large computation times. If a more reasonable value of Δs is to be used, a more elaborate means of integrating equations (4.19) along the characteristics must be used. This would tend to destroy the simplicity of the method and lead to rather complicated computational procedures. Hence, the scheme has not been further investigated although it is at least theoretically feasible.

However, the fact that the pressure and the normal velocity can be treated by the method of characteristics is quite important in itself, irrespective of whether the method is practical. The existence of the characteristic relations for p and v is verification of the feasibility of solving the shock-layer equations, (2.2)-(2.7), as an initial-boundary-value problem with the axis of symmetry for the initial station. In addition, the characteristics may be useful for the

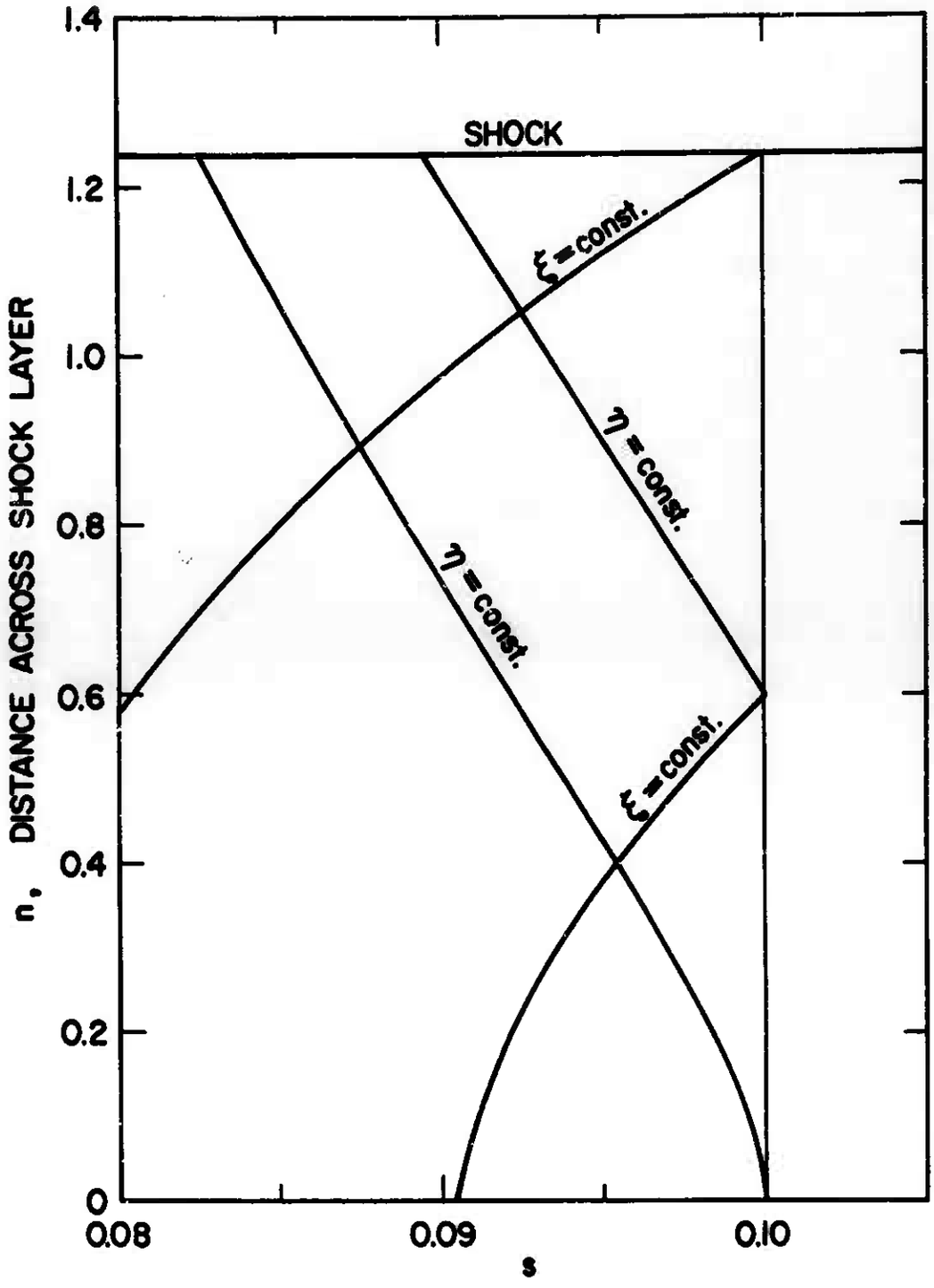

Figure 4.6

Typical characteristic curves originating at $s = 0.10$ on a sphere at $\gamma = 1.4$, $M_\infty = 10$, $Re_s = 100$, $b = 0.6$, $\sigma = 0.7$, and $\omega = 1/2$.

application of the boundary conditions. In section C, it was seen that the application of the shock conditions led to complications. The shock conditions provide values of each of the four variables at $n = \bar{\Delta}$ as functions of the shock angle ϕ. This angle is, of course, an unknown, and it might appear that the problem is underdetermined. However, there is one characteristic curve that originates in the "known" flow field (i.e., $s < (m+1)\Delta s$ and $0 \leq n \leq \bar{\Delta}$) and that intersects the shock at $s = (m+1)\Delta s$. The differential equation that applies along this characteristic provides an additional constraint on the values of the variables and permits the determination of ϕ. At the body surface there are boundary conditions on u (equation (2.10)), T (equation (2.11)), and v (equation (2.12)), but none on the pressure (or density). The fact that one of the characteristic curves that originates in the "known" flow field intersects the wall and provides an additional constraint indicates that no boundary condition is needed.[1] It has, of course, been tacitly assumed throughout this investigation that the physical boundary conditions were mathematically adequate for a solution of the type that has been sought. One can interprete the above discussion as an indication that the boundary conditions are of sufficient number to yield a well posed initial-boundary-value problem.

[1] A discussion of the use of characteristics to determine the number of boundary conditions and initial conditions for partial differential equations of various types is contained in reference 23.

In addition, the use of the characteristic curves that intersect the boundaries may be a practical means of evaluating some of the boundary values although this point has not been investigated.

E. Method III

Since it is somewhat inconvenient to make explicit use of the characteristic equations, we now consider whether the basic finite-difference scheme itself is capable of handling the characteristics implicitly. The use of explicit finite-difference schemes to solve simple partial differential equations of the hyperbolic type is discussed in most texts on numerical methods. The well-known result is that the domain of dependence of the numerical scheme must contain the domain of dependence of the differential equations. Thus, for explicit finite-difference methods, a strict requirement is placed on the ratio of the step sizes, $\frac{\Delta s}{\Delta n}$, if the computations are to be stable. However, for implicit finite-difference schemes, no such requirement on $\frac{\Delta s}{\Delta n}$ is needed since the numerical domain of dependence extends across the entire flow field. This does not mean that an implicit finite-difference method will necessarily work, but it does mean that the scheme at least meets the minimum requirements for stability. Hence we now consider a computational method in which all the flow variables are programmed into the implicit finite-difference scheme.

This method was briefly examined at an early stage of the present investigation, and a rather peculiar type of instability was encountered.

Although this method was then dropped in favor of method I, the analysis of the previous sections has indicated that this method may offer the best chance of success. Hence, the method is described in this section in order to determine the nature of the instability that was previously encountered. It will be found that the instability is not related to the instabilities encountered in section C and that it can be eliminated in a simple manner. This method is in many respects the simplest and most straightforward of the three methods considered in this chapter since the entire solution is given by the difference relations (4.6)-(4.8). However, there are certain features of the computation that require close examination, and these details are explained below.

The partial differential equations (2.2)-(2.5) are reduced to the difference equations (4.4) by introducing the difference quotients given in equations (4.2). Either the density or the pressure may be considered to be the fourth dependent variable in addition to u, v and T. The coefficients (A, B, C, and D) of the difference equation (4.4) now contain a total of fifty-two components.

The determination of the boundary conditions (4.5) requires some explanation. Equation (4.5a) contains boundary conditions on all the variables, and, of course, these constraints are required by the numerical method. Two of these constraints are provided by the slip and temperature-jump conditions, (2.10) and (2.11), and a third is obtained quite simply from the boundary condition on the normal velocity, equation (2.12). Although required by the numerical method, there is no physical boundary condition on the density (or pressure) at the wall.

Further, it was seen in the preceding section that the differential equations do not mathematically need such a constraint. Hence, the necessary numerical condition must be obtained from the differential equations themselves. It was noted in the preceding section that this could be obtained from the differential equation that applies along the characteristic intersecting the wall. A simpler means is to evaluate the continuity equation (2.2) at $n = 0$ (note that the differential equations had been previously reduced to difference equations only at $N = 1,2,\ldots,N_s$ -- hence this condition will be an independent equation). The central-difference formulas of equation (4.2) cannot be used for this purpose, but a forward-difference relation such as

$$\left.\frac{\partial F}{\partial n}\right|_{m+1,N} = -\frac{3F(0) - 4F(1) + F(2)}{2\Delta n} + O(\Delta n^2)$$

must be used. The resulting three-point equation is reduced to the required two-point form as described in section C.

A similar situation arises at the shock. Although the Rankine-Hugoniot conditions supply all the necessary conditions in equation (4.5b), it does so in terms of an additional unknown, $\bar{\Delta}$. Hence, an additional condition, which must be supplied by the equations themselves, is needed. The use of the characteristic curve that intersects the shock was described in section D as one possibility. The use of the integral form of mass conservation as described in section C is another possibility although it is not known whether this will result in a numerically independent condition. Or one of the differential equations can be

evaluated in such a way that a numerically independent condition is obtained, as was done at the wall.

As noted earlier, some rough calculations based on this method led to a rather strange instability. At the first computational step, the values of the variables at the even-numbered grid points appeared to become uncoupled from the values at the odd-numbered grid points. This is illustrated in figure 4.7 by a plot of the tangential velocity, u, at $s = 0.006$. Other variables show a similar effect. Unlike the case of method I, this instability does not become progressively worse as s increases but is inherent to the solution at each step. It should be emphasized that these results are accurate solutions of the difference equations (4.4), and thus the source of this problem should be sought in the formulation of the difference equations (and not in the boundary conditions or the method of solution).

It has now been recognized that the probable source of this difficulty is in the use of the central difference quotient (4.2b) for the normal derivatives of ρ and v. This equation does not contain the central point $(m+1,N)$, and this will obviously have a tendency to uncouple the variables at adjacent grid points. When considering the variables u and T, this is no problem since the principle terms involving u and T are second derivatives and equation (4.2c) contains the variables evaluated at $N-1$, N, and $N+1$. However, for ρ and v, the first derivatives are the principle terms, and the central difference of equation (4.2b) is not appropriate. It should be noted that, due to the influence of other terms, the

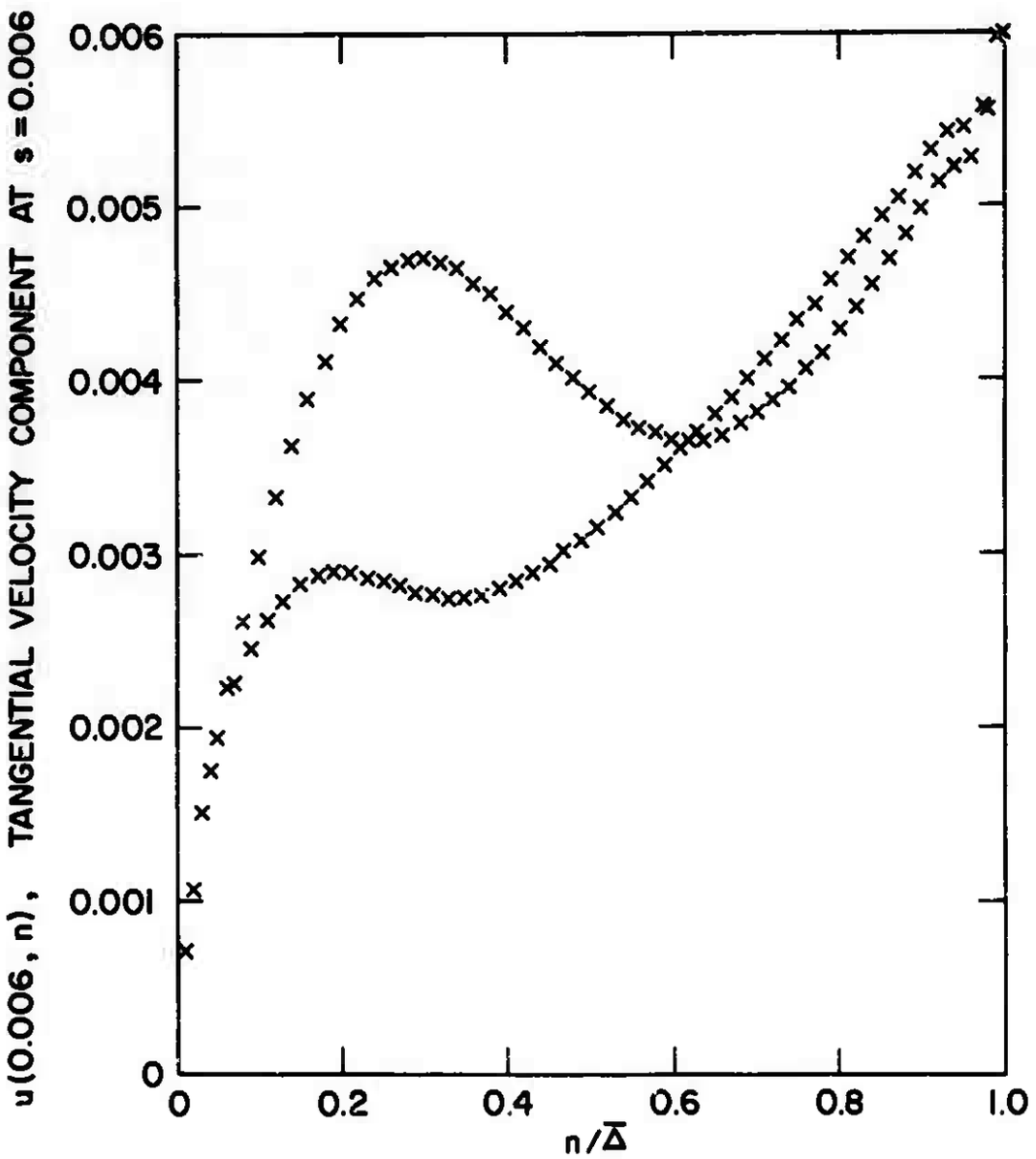

Figure 4.7

Example of the instability encountered with method III.

coefficients of $\rho(N)$ and $v(N)$ in the difference equations are not zero; nevertheless, the use of the central-difference quotient for the principle terms, $\frac{\partial \rho}{\partial n}$ and $\frac{\partial v}{\partial n}$, is the probable source of the instability illustrated in figure 4.7.

This conclusion is reinforced by a consideration of the order of the differential equations and the order of the difference equations. The use of the central difference quotients, (4.2b) and (4.2c), results in the difference equations (4.4) being second-order difference equations. We have seen that this worked well for the tangential momentum equation and the energy equation, which are second-order differential equations; but when the continuity and normal momentum equations, which are first order, are included, the instability of figure 4.7 occurred. In reference 15, it is pointed out that the use of difference equations to approximate differential equations can lead to what the authors call "computational instabilities" if the difference equations are of higher order than the differential equations. These "computational" instabilities are of a different nature than the more common instabilities that usually result in the catastrophic breakdown of the computational procedure.

Fortunately, in the present case, it would appear to be a simple matter to remove this instability by using

$$\left.\frac{\partial F}{\partial n}\right|_{m+1,N} = \frac{F_{m+1,N+1} - F_{m+1,N}}{\Delta n} + O(\Delta n)$$

for the normal derivatives of ρ and v, although this point has not been checked. It is clear, however, that a successful application

of this method must consider the type of difference quotients that are to be used.

F. Summary and Concluding Remarks

In their present state of development, the computational procedures that have been presented in this chapter are clearly not capable of yielding accurate solutions to the blunt-body problem. However, several of the results of this investigation did indicate that the methods might be adequate if properly formulated. The major difficulties were traced to two factors: the determination of the shock location and the handling of the terms ρuv_s and ρvv_n, which appear in the normal momentum equation. In reference 11, two approximations were introduced for the constant-density flow in order to overcome these difficulties. In the present investigation (method I), it was found that these approximations were less satisfactory for the variable-density case:

1. The assumption of a concentric shock and body was one of the approximations that permitted the solution of the constant-density flow. The shock location was then found to be consistent with the assumption. However, it is known from the series-truncation analysis that such an assumption is not generally valid for a flow of variable density. Hence, to specify the shock angle in the present investigation, it was necessary to rely on the truncation results despite the fact that the description of the shock angle appears to be among the least reliable of the results of the series-truncation analysis.

Near the axis, the finite-difference computations did lead to results that were consistent with the assumed shock angle, but this could not be expected to be true over an extended range in s. Furthermore, the fact that the results are consistent with the assumption does not in inself prove that the assumption is correct. The ability to compute the shock position and angle as a part of the finite-difference solution is a critical factor, and considerable attention must be given this point in any further analysis of the type that was considered in this chapter.[1] It was noted that this difficulty can be circumvented by the use of the thin-shock-layer model, but this must necessarily influence the accuracy of the results.

2. The second approximation that was used to obtain the solution of the constant-density equations was to make use of the thin-shock-layer pressure to evaluate the tangential pressure gradient, $\frac{\partial p}{\partial s}$. That is, the influence of the terms $\rho u v_s$ and $\rho v v_n$ was omitted. Since these two terms could influence the flow variables, other than p, only through the $\frac{\partial p}{\partial s}$ term of the tangential momentum equation, this approximation was equivalent

[1] It has recently been suggested by Davis [9] that the problem should be formulated in variables which are defined by $\tilde{n} = n/\Delta$, $\tilde{u} = u/u(\Delta)$, etc. With these variables, the shock location and the values of the variables at the shock all become unity. The unknown quantities such as Δ and $u(\Delta)$, etc. now appear only in the differential equations. According to Davis, the difficulties associated with the computation of the shock position, Δ, can be removed in this manner.

to the thin-shock-layer approximation, in which these terms are omitted entirely. The resulting equations are parabolic in nature and hence are easily treated by finite-difference methods. For the variable-density case, the complete omission of the terms $\rho u v_s$ and $\rho v v_n$ leads to somewhat unrealistic values of density and pressure across the shock layer for certain body shapes (including spheres). Hence, a second approximation, which was analogous to the approximation used in reference 11 but which would not encounter the density distributions of thin-shock-layer theory, was considered. It was found that the influence of the terms $\rho u v_s$ and $\rho v v_n$ through the density was sufficiently large to cause instabilities.

These two terms are the source of the two characteristics of equations (2.2)-(2.5) that are of the hyperbolic type. Hence, a method was examined that used the method of characteristics to handle the computation of the pressure and the normal velocity (method II). It was found that the method of characteristics was somewhat inconvenient to apply due to large slopes of the characteristic curves. Finally, a method in which all the variables were programmed into the finite-difference scheme was considered (method III). It was found that with this method care must be taken to choose difference quotients that are compatible with the differential equations. Neither of these last two methods was investigated in detail. The last method in particular appears to be worthy of further investigation.

Despite the general lack of success with these methods, there were several results that indicated that the methods might yield valid results if they were properly formulated. In particular, method I was able to compute values of $\bar{\Delta}$ and ϕ that were considerably more accurate that the assumptions and data that formed the basis of the computations, and the analysis of method II indicates that the formulation of the blunt-body problem as an initial-boundary-value problem is justified.

There is, however, one important problem concerning this last point that has not yet been discussed in detail: it is not clear what effect an upstream influence has on the finite-difference procedure. The series-truncation analysis has clearly shown that there is an upstream influence in the flow despite the "parabolic-hyperbolic" nature of the equations. This was exhibited by the strong influence of the downstream wall temperature on the flow variables at the axis. (For non-spherical bodies, the coefficient κ_2 of an expansion $\kappa(\theta) = 1 + \kappa_2 \sin^2\theta + \cdots$ would have a similar, though less pronounced, effect). Thus, as a result of the upstream influence, the initial data will be, to some extent, incompatible with some of the downstream boundary parameters, especially the wall temperature. We have seen that this incompatibility may be fairly large if the first-truncation results are used as initial data; with higher truncations, the initial data will more closely approximate the data which are correct for the desired wall temperature. Due to this incompatibility, it is necessary to inquire whether the problem can be formulated with a specified wall temperature. If this formulation is to be valid, the

finite-difference results must be able to quickly adjust to the imposed conditions irrespective of the possibly erroneous initial data. This is true of boundary-layer computations -- the influence of the initial data diminishes rapidly as the computations proceed away from the initial station -- but is less likely to be true of the shock-layer equations because the equations have some hyperbolic characteristics. That is, it is likely that the effect of the "erroneous" initial data will be propagated downstream. Since the initial data may not be valid for the particular temperature that is desired, it is possible that a solution cannot be found from the finite-difference procedure unless the downstream wall temperature is adjusted to be compatible with the initial data. The manner in which the compatible wall temperature would be determined, as well as the manner by which the incompatibility would be manifested, is unknown since this discussion is somewhat speculative.

An example of how it might be determined can be seen in an examination of method I. It was there noted that the use of the integral equation expressing the overall mass conservation should automatically insure that the Rankine-Hugoniot condition on the normal velocity is satisfied. In practice, it was found that this was not always the case. Normally, the error was less than one percent, but as instabilities developed, the error grew, becoming 5-10 percent just before the computational procedure had to terminate. This error possibly could

have been removed by adjusting the value of the wall temperature at each s-step.

The effectiveness of any such computation procedure can be evaluated by using the first truncation results as initial data. The wall temperature that would be calculated by the finite-difference scheme should then agree to $O(\sin^2 s)$ with the second-truncation temperature distribution that produced a concentric shock and body (Chapter III, section D.3). Alternatively, if a constant wall temperature is specified together with the first-truncation initial data, the results must make some rather obvious and abrupt adjustments (in $\bar{\Delta}$ and τ, for example) if they are to be meaningful. If either of these two cases can be realized, an evaluation of the reliability of the results of a computation scheme of the type that was considered in this chapter will not be difficult.

Chapter V

SUMMARY

A simplified form of the Navier-Stokes equations has been used to describe the flow in the shock layer of a blunt body. These equations are uniformly valid to $O(\epsilon)$ throughout the entire shock layer and thus are valid in the same flow re ime as the second-order boundary-layer theory.

The nature of these shock-layer equations has led to the treatment of the problem as an initial-boundary-value problem -- with the axis of symmetry as the initial station. Solutions at the axis of symmetry have been obtained for a wide range of flow conditions by use of the method of series truncation. The second-truncation solutions have been found to yield excellent results for the heat transfer at the wall and results for wall shear that contain only moderate errors. The first- and second-truncation results have been compared to the results of several previous investigations of the flow in the stagnation region. These comparisons have shown

1) that the basic flow model is adequate for values of the shock Reynolds number down to the order of 10^2 and

2) that, contrary to the conclusion of a previous investigation, the method of local similarity may lead to substantial errors at the axis.

With regard to this second result, the le of the wall temperature in

determining the relative geometry of the body and shock has been clearly pointed out.

Several methods based on the use of finite-differences have been examined as means of extending the solutions beyond the stagnation region. A method that was previously used to solve the constant-density shock layer was found to be less adequate for the variable-density case. Although several interesting results were obtained, the method encountered serious instabilities. Two additional methods, which should avoid these instabilities, have been described. Exploratory computations have illustrated the features of each that require further attention. Finally, the results of this investigation indicated that the formulation of the problem as an initial-boundary-value problem is valid but that special attention must be given to a possible incompatibility between the initial data and the wall temperature downstream of the axis of symmetry.

APPENDIX A

Coefficients of the finite-difference equations (method I)

Equations (4.3a) and (4.3b) are the difference equations that are used in method I (section B, Chapter IV). The coefficients of these equations are determined by substituting the difference quotients given by equations (4.2) into the differential equations (2.3) and (2.5). We introduce the following notation. A subscript e indicates that a quantity is evaluated at the point $(s,n) = ((m+1)\Delta s, N\Delta n)$ but is obtained either from the extrapolation formula (4.2e) or from a previous iteration. Multiplying the two equations by $4\Delta n$ and letting $L = \frac{2\Delta n}{\Delta s}$, we obtain the following relations.

$$Al_N = -2\left[\epsilon\mu\left(\kappa + j\,\frac{\sin\theta}{r}\right) - (\rho v)_e\right] - \mu'\left(\frac{T_{m,N+1} - T_{m,N-1}}{\Delta n}\right) - \frac{4\mu}{\Delta n} \qquad (A\text{-}1)$$

$$Bl_N = \frac{3L}{1+\kappa\epsilon\,\Delta n N}\,(\rho u)_e + \frac{4\epsilon\kappa\Delta n}{1+\kappa\epsilon\,\Delta n N}\,(\rho v)_e + \frac{8\mu}{\Delta n} \qquad (A\text{-}2)$$

$$Cl_N = -Al_N - \frac{8\mu}{\Delta n} \qquad (A\text{-}3)$$

$$Dl_N = -\mu'\left(\frac{u_{m,N+1} - u_{m,N-1}}{\Delta n} - 2c\kappa u_e\right) \qquad (A\text{-}4)$$

$$El_N = 0 \qquad (A\text{-}5)$$

$$Fl_N = -Dl_N \qquad (A\text{-}6)$$

$$G1_N = \frac{L(\rho u)_e}{1+\kappa\epsilon N\Delta n}\left(4u_{m,N} - u_{m-1,N}\right) - \frac{4\Delta n}{1+\kappa\epsilon N\Delta n}\left(\frac{\partial p}{\partial s}\right)_e$$

$$- \frac{\mu'}{\Delta n}\left(T_{m,N+1} - T_{m,N-1}\right)\left(u_{m,N+1} - u_{m,N-1}\right) \qquad \text{(A-7)}$$

and

$$A2_N = -2\mu\left(\frac{u_{m,N+1} - u_{m,N-1}}{\Delta n} - 2\epsilon\kappa u_e\right) \qquad \text{(A-8)}$$

$$B2_N = -\frac{4\Delta n}{1+\kappa\epsilon N\Delta n}\left(\frac{\partial p}{\partial s}\right)_e \qquad \text{(A-9)}$$

$$C2_N = -A2_N \qquad \text{(A-10)}$$

$$D2_N = \frac{-2\mu'}{\sigma\Delta n}\left(T_{m,N+1} - T_{m,N-1}\right) - 2\frac{\epsilon\mu}{\sigma}\left(\kappa + j\frac{\sin\theta}{r}\right)$$

$$+ 2(\rho v)_e - \frac{4\mu}{\sigma\Delta n} \qquad \text{(A-11)}$$

$$E2_N = \frac{3L}{1+\kappa\epsilon N\Delta n}(\rho u)_e + \frac{8\mu}{\sigma\Delta n} \qquad \text{(A-12)}$$

$$F2_N = -D2_N - \frac{8\mu}{\sigma\Delta n} \qquad \text{(A-13)}$$

$$G2_N = \frac{L(\rho u)_e}{1+\kappa\epsilon N\Delta n}\left(4\,T_{m,N} - T_{m-1,N}\right) + 4\Delta n\left(v\frac{\partial p}{\partial n}\right)_e$$

$$- \frac{\mu'}{\sigma\Delta n}\left(T_{m,N+1} - T_{m,N-1}\right)^2 - \frac{\mu}{\Delta n}\left(u_{m,N+1} - u_{m,N-1}\right)^2 \qquad \text{(A-14)}$$

The quantities r, κ, and θ are evaluated at $s = (m+1)\Delta s$. The quantities μ and μ' are functions of the temperature, T, and must be evaluated either from an extrapolated value of T or from a value of T from a previous iteration.

APPENDIX B

Derivation of the difference equations for the mass-flow integral

We wish to show that the integral given by equation (4.14a),

$$I(N) = 2^{j}\epsilon \int_{o}^{N\Delta n} \rho u(r+\epsilon n \sin\theta)^{j} dn \,, \qquad \text{(B-1)}$$

can be evaluated from the simple algebraic equation

$$I(N) = A_I(N) + B_I(N)u(N) + C_I(N)T(N) \qquad \text{(B-2)}$$

where the coefficients A_I, B_I, and C_I can be computed along with $H(N)$ and $K(N)$ (i.e., they can be obtained from recursive relations starting at $N = 0$, prior to the calculation of u and T). We consider only the case of $i = 2$ here, but the more general case of $i = 4$ can be handled in an analogous manner.

For $i = 2$, the difference equation (4.6) may be written out explicitly as

$$u(N) = H_1(N) + K_{11}(N)u(N+1) + K_{12}(N)T(N+1) \qquad \text{(B-3a)}$$

and

$$T(N) = H_2(N) + K_{21}(N)u(N+1) + K_{22}(N)T(N+1) \qquad \text{(B-3b)}$$

where H_1, H_2, K_{11}, K_{12}, K_{21}, K_{22} are the components of $H(N)$ and $K(N)$.

The integral I is evaluated by using the trapezoidal integration formula:

$$I(N+1) - I(N) = 2^{j-1}\Delta n\epsilon \{\rho(N+1)u(N+1)[r + \epsilon\Delta n\,(N+..)\sin\theta]^j$$

$$+ \rho(N)u(N)[r+\epsilon\Delta n\, N \sin\theta]^j\} \qquad (B\text{-}4)$$

Let $R(N) = 2^{j-1}\Delta n\,\epsilon\,\rho(N)(r+\epsilon\Delta n\, N \sin\theta)^j$. If ρ is evaluated by extrapolation, which is consistent with the linearization of the difference equations, then $R(N)$ can immediately be evaluated at each value of N. Equation (B-4) can be written as

$$I(N+1) = I(N) + R(N+1)u(N+1) + R(N)u(N) \qquad (B\text{-}5)$$

At the wall, $I(0) = 0$. Note that by recursive application of equation (B-5) for $N = 1,2,\ldots$ and by using equations (B-3) to eliminate the undesired values of u and T, the integral $I(N+1)$ can be expressed as a linear function of $u(N+1)$ and $T(N+1)$, equation (B-2). The coefficients of (B-2) are evaluated as follows.

Substitute (B-2) into (B-5):

$$I(N+1) = A_I(N) + R(N+1)u(N+1) + [B_I(N) + R(N)]u(N)$$

$$+ C_I(N)T(N)$$

Use equations (B-3) to eliminate $u(N)$ and $T(N)$:

$$I(N+1) = A_I(N) + [B_I(N) + R(N)]H_1(N) + C_I(N)H_2(N) + \{R(N+1)$$

$$+ [B_I(N) + R(N)]K_{11}(N) + C_I(N)K_{21}(N)\}u(N+1)$$

$$+ \{[B_I(N) + R(N)]K_{12}(N) + C_I(N)K_{22}(N)\}T(N+1)$$

This result now gives

$$A_I(N+1) = A_I(N) + [B_I(N) + R(N)]\, H_1(N) + C_I(N)H_2(N) \qquad \text{(B-6a)}$$

$$B_I(N+1) = R(N+1) + [B_I(N) + R(N)]\, K_{11}(N) + C_I(N)K_{21}(N) \qquad \text{(B-6b)}$$

and

$$C_I(N+1) = [B_I(N) + R(N)]K_{12}(N) + C_I(N)K_{22}(N) \qquad \text{(B-6c)}$$

Since $A_I(0) = B_I(0) = C_I(0) = 0$, the coefficients A_I, B_I, and C_I can be evaluated at each value of N by recursive application of equations (B-6) for $N = 0,1,2,\ldots,N_s$.

REFERENCES

1. Cheng, H.K. "Hypersonic shock-layer theory of the stagnation region at low Reynolds number," Proc. 1961 Heat Transfer and Fluid Mech. Inst., Univ. So. Calif., ed. Binder, Epstein, Mannes, and Yang, Stanford Univ. Press, pp. 161-175, June 1961.

2. Cheng, H.K. "The blunt-body problem in hypersonic flow at low Reynolds number," Cornell Aero. Lab. Rep. no. AF-1285-A-10, June 1963, revision of: IAS Paper No. 63-92.

3. Cheng, H.K. "Viscous hypersonic blunt-body problems snd the Newtonian theory," in Fundamental Phenomena in Hypersonic Flow, Proc. International Symposium Sponsored by Cornell Aero. Lab., ed. J. Gordon Hall, Cornell Univ. Press, 1966.

4. Cheng, P., and Vincenti, W.G. "Inviscid radiating flow over a blunt body," J. Fluid Mech., vol. 27 part 4, pp. 625-646, 1967.

5. Clutter, D.W., and Smith, A.M.O. "Solution of the general boundary-layer equations for compressable laminar flow, including transverse curvature," Douglas Aircraft Div. Report No. LB 31088, 1963.

6. Conti, R.J. "Stagnation equilibrium layer in nonequilibrium blunt-body flows," AIAA J., vol. 2, no. 11, pp. 2044-2046, 1964.

7. Conti, R.J. "A theoretical study of non-equilibrium blunt-body flows," J. Fluid Mech., vol. 24, part 1, pp. 65-88, 1966.

8. Davis, R.T. "Laminar incompressible flow past a semi-infinite flat plate," J. Fluid Mech., vol. 27, part 4, pp. 691-704, 1967.

9. Davis, R.T. "The hypersonic fully viscous shock layer problem," AGARD Seminar on Numerical Methods for Viscous Flows, Nat. Physical Lab., Teddington, England, Sept. 1967.

10. Davis, R.T. "Boundary layers on parabolas and paraboloids by methods of local truncation," to be published.

11. Davis, R.T., and Chyu, W.J. "Laminar flow past a sphere at high Mach number," J. Fluid Mech., vol. 24, part 3, pp. 481-495, 1966.

12. Davis, R.T., and Flügge-Lotz, I. "Second-order boundary-layer effects in hypersonic flow past axisymmetric blunt bodies," J. Fluid Mech., vol. 20, part 4, pp. 593-623, 1964. Abbrev. version of "Laminar compressible flow past axisymmetric blunt bodies (results of a second-order theory)," Tech. Report No. 143, Div. Engineering Mech., Stanford Univ., Dec. 1963.

13. Fannelöp, T.K., and Flügge-Lotz, I. "Viscous hypersonic flow over simple blunt bodies including second-ord effects," Tech. Report No. 144, Div. of Engineering Mech., Stanford Univ., June 1964 abbreviated version: J. de Mécanique, vol. 5, no. 1, pp. 69-100, 1966.

14. Flügge-Lotz, I., and Blottner, F.G. "Computation of the compressible laminar boundary-layer flow including displacement-thickness interaction using finite-difference methods," Tech. Report No. 131, Div. Engineering Mech., Stanford Univ., Jan. 1962 abbreviated version: "Finite-difference computation of the boundary layer with displacement thickness interaction," J. de Mécanique, vol. 2, no. 4, pp. 397-423, 1963.

15. Forsythe, G.E., and Wasow, W.R. Finite-Difference Methods for Partial Differential Equations, John Wiley and Sons, Inc., New York, 1960.

16. Garabedian, P.R. Partial Differential Equations, John Wiley and Sons, Inc., New York, 1964.

17. Goldberg, L. "The structure of the viscous hypersonic shock layer," General Electric Co., MSD, TIS R65SD50, Dec. 1965.

18. Hayes, W.D., and Probstein, R.F. Hypersonic Flow Theory, Academic Press, New York, 1959.

19. Ho, H.T., and Probstein, R.F. "The compressible viscous layer in rarefied hypersonic flow," Brown Univ. ARL TN 60-132, Aug. 1960 also in: Rarefied Gas Dynamics, Proc. 2nd Int. Symp. on Rarefied Gas Dynamics, ed. L. Talbot, Academic Press, New York, pp. 525-552, 1961.

20. Inouye, M., and Lomax, H. "Comparison of experimental and numerical results for the flow of a perfect gas about blunt-nosed bodies," NASA TN D-1426, 1962.

21. Kao, H.C. "Hypersonic viscous flow near the stagnation streamline of a blunt body: I. A test of local similarity," AIAA J., vol. 2, no. 11, pp. 1892-1897, 1964.

22. Krause, E. "Numerical solution of the boundary-layer equations," AIAA J., vol. 5, no. 7, pp. 1231-1237, 1967.

23. Lee, E.H., and Fayers, F.J. "The use of the method of characteristics in determining boundary conditions for problems in reservoir analysis," Petroleum Trans., AIME, vol. 216, pp. 284-298, 1959.

24. Levinsky, E.S., and Yoshihara, H. "Rarefied hypersonic flow over a sphere," in Hypersonic Flow Research, ed. F.R. Riddell, Academic Press, New York, pp. 81-106, 1962.

25. Perry, J.C., and Pasiuk, L. "A comparison of solutions to a blunt body problem," AIAA J., vol. 4, no. 8, pp. 1425-1426, 1966.

26. Petrovsky, I.G. Lectures on Partial Differential Equations, Interscience Publishers, Inc., New York, 1954.

27. Probstein, R.F. "Shock wave and flow field development in hypersonic re-entry," ARS J., vol. 31, no. 2, pp. 185-194, 1961.

28. Probstein, R.F., and Kemp, N.H. "Viscous aerodynamic characteristics in hypersonic rarefied gas flow," J. Aero/Space Sci., vol. 27, pp. 174-192, 1960.

29. Sedov, L.I., Michailova, M.P., and Chernyi, C.G. "On the influence of viscosity and heat conduction on the gas flow behind a strong shock wavc," Vestnik Moskovskovo Universiteta, No. 3, p. 95, 1953.

30. Shih, W.C.L., and Krupp, R.S. "Viscous nonequilibrium blunt body flows," M.I.T. Aerophysics Lab., Tech. Report 100, Nov. 1964 also: AIAA J., vol. 5, no. 1, pp. 16-25, 1967.

31. Swigart, R.J. "A theory of asymmetric hypersonic blunt-body flows," AIAA J., vol. 1, no. 5, pp. 1034-1042, 1963.

32. Van Dyke, M. "Second-order compressible boundary-layer theory with application to blunt bodies in hypersonic flow," in Hypersonic Flow Research, ed. F.R. Riddell, Academic Press, New York, pp. 37-76, 1962.

33. Van Dyke, M. "A review and extension of second-order hypersonic boundary-layer theory," in Rarefied Gas Dynamics, Proc. 3rd Int. Symp. on Rarefied Gas Dynamics, ed. J.A. Laurman, vol. II, Academic Press, New York, 1963.

34. Van Dyke, M. "The circle at low Reynolds number as a test of the method of series truncation," Proc. 11th International Congress of Applied Mech., Springer, Berlin, also: Dept. Aero. and Astro., Stanford Univ., SUDAER No. 211, Oct. 1964.

35. Van Dyke, M. "A method of series truncation applied to some problems in fluid mechanics," VII Symposium on Advanced Problems and Methods in Fluid Mechanics, Jurata, Poland, Sept. 1965 also: Dept. Aero. and Astro., Stanford Univ., SUDAER No. 247, Oct. 1965.

36. Van Dyke, M. "Hypersonic flow behind a paraboloidal shock wave," J. de Mécanique, vol. 4, no. 4, pp. 477-493, 1965.

37. Van Dyke, M. "The blunt-body problem revisited," in Fundamental Phenomena in Hypersonic Flow, Proc. International Symposium Sponsored by Cornell Aero. Lab., ed. J. Gordon Hall, Cornell Univ. Press, 1966.

38. Van Dyke, M. "A survey of higher-order boundary-layer theory," AGARD Seminar on Numerical Methods for Viscous Flows, Nat. Physical Lab., Teddington, England, Sept. 1967.

39. Weinbaum, S. "Near wake uniqueness and a re-examination of the throat concept in laminar mixing theory," AIAA Paper 67-65, Jan. 1967.

40. Weinbaum, S., and Garvine, R.W. "The pressure field in compressible boundary layer theory--a critical re-examination and treatment," General Electric Co., MSD, TIS R66SD13, March 1966.

Security Classification

DOCUMENT CONTROL DATA - R & D

(Security classification of title, body of abstract and indexing annotation must be entered when the overall report is classified)

1. ORIGINATING ACTIVITY (Corporate author)
Stanford University
Division of Engineering Mechanics
Stanford, California 94305

2a. REPORT SECURITY CLASSIFICATION
UNCLASSIFIED

2b. GROUP

3. REPORT TITLE

VISCOUS, HYPERSONIC FLOW AROUND A BLUNT BODY

4. DESCRIPTIVE NOTES (Type of report and inclusive dates)
Scientific Interim

5. AUTHOR(S) (First name, middle initial, last name)
John E. Kaiser
I. Flügge-Lotz

6. REPORT DATE	7a. TOTAL NO. OF PAGES	7b. NO. OF REFS
January 1968	161	40

8a. CONTRACT OR GRANT NO.	9a. ORIGINATOR'S REPORT NUMBER(S)
AF 49(638)-1385	178
b. PROJECT NO. 9749-01	
c. 6144501F	9b. OTHER REPORT NO(S) (Any other numbers that may be assigned this report) AFOSR 68-0988
d. 681304	

10. DISTRIBUTION STATEMENT

1. This document has been approved for public release and sale; its distribution is unlimited.

11. SUPPLEMENTARY NOTES	12. SPONSORING MILITARY ACTIVITY
TECH, OTHER	Air Force Office of Scientific Research (SRMA) 1400 Wilson Boulevard Arlington, Virginia 22209

13. ABSTRACT

A simplified form of the Navier-Stokes equations has been used to describe the flow in the shock layer of a blunt body. The equations are solved near the axis of the body by using the method of series truncation. The main method of solution is a finite difference method, which in prinicple allows to handle sxisymmetric bodies of arbitrary shape. The body shape is assumed to be given and the bow shock shape is determined step by step.

DD FORM 1 NOV 65 1473

Security Classification

Security Classification

14 KEY WORDS	LINK A		LINK B		LINK C	
	ROLE	WT	ROLE	WT	ROLE	WT
Navier-Stokes Equations Flow in shock layer						